

# A new geological map of the Island of Syros (Aegean Sea, Greece): Implications for lithostratigraphy and structural history of the Cycladic Blueschist Unit

by Mark Keiter, Chris Ballhaus, and Frank Tomaschek



THE GEOLOGICAL SOCIETY  
OF AMERICA®

**Special Paper 481**

by Mark Keiter, Chris Ballhaus,  
and Frank Tomaschek

A new geological map of the Island of Syros (Aegean Sea, Greece):  
Implications for lithostratigraphy and structural history of the Cycladic Blueschist Unit

Special Paper 481



Copyright © 2011, The Geological Society of America (GSA), Inc. All rights reserved. GSA grants permission to individual scientists to make unlimited photocopies of one or more items from this volume for noncommercial purposes advancing science or education, including classroom use. In addition, an author has the right to use his or her article or a portion of the article in a thesis or dissertation without requesting permission from GSA, provided the bibliographic citation and the GSA copyright credit line are given on the appropriate pages. For permission to make photocopies of any item in this volume for other noncommercial, nonprofit purposes, contact The Geological Society of America. Written permission is required from GSA for all other forms of capture or reproduction of any item in the volume including, but not limited to, all types of electronic or digital scanning or other digital or manual transformation of articles or any portion thereof, such as abstracts, into computer-readable and/or transmittable form for personal or corporate use, either noncommercial or commercial, for-profit or otherwise. Send permission requests to GSA Copyright Permissions, 3300 Penrose Place, P.O. Box 9140, Boulder, Colorado 80301-9140, USA. GSA provides this and other forums for the presentation of diverse opinions and positions by scientists worldwide, regardless of their race, citizenship, gender, religion, sexual orientation, or political viewpoint. Opinions presented in this publication do not reflect official positions of the Society.

Copyright is not claimed on any material prepared wholly by government employees within the scope of their employment.

Published by The Geological Society of America, Inc.  
3300 Penrose Place, P.O. Box 9140, Boulder, Colorado 80301-9140, USA  
[www.geosociety.org](http://www.geosociety.org)

Printed in U.S.A.

GSA Books Science Editors: Marion E. Bickford and Donald I. Siegel

Library of Congress Cataloging-in-Publication Data

Keiter, Mark.

A new geological map of the Island of Syros (Aegean Sea, Greece) : implications for lithostratigraphy and structural history of the Cycladic blueschist unit / Mark Keiter, Chris Ballhaus, Frank Tomaschek.

p. cm. -- (Special paper ; 481)

Includes bibliographical references.

ISBN 978-0-8137-2481-2 (pbk.)

1. Geology--Greece--Syros Island--Maps. 2. Geology, Structural--Greece--Syros Island--Maps. 3. Lithofacies--Greece--Syros Island--Maps. I. Ballhaus, Chris. II. Tomaschek, Frank. III. Title.

G2002.S9C5K4 2011

554.9495'85--dc22

2011016084

Cover image: Folded marbles near Kastri, northeast Syros. Photograph by Mark Keiter.

# Contents

|   |    |
|---|----|
| <i>Acknowledgments</i> .....  | iv |
| <i>Abstract</i> .....   | 1  |
| <i>Chapter 1: Introduction</i> .....  | 3  |
| <i>Chapter 2: General Petrography of Mapped Lithological Units</i> .....  | 9  |
| <i>Chapter 3: Lithostratigraphy and Indications for Primary Associations in<br/>the Cycladic Blueschist Unit on Syros</i> ..... | 21 |
| <i>Chapter 4: Structural Evolution of the Cycladic Blueschist Unit—The Example of Syros</i> .....                               | 25 |
| <i>Chapter 5: Concluding Remarks</i> .....  | 39 |
| <i>References Cited</i> .....   | 40 |

## ***Acknowledgments***

Thanks are due to Karsten Piepjohn, Michael Bode, Markus Lagos, and countless students—without their work, this project would have been impossible. We thank the Münster workshop crew for sample preparation, and the team in Bonn for whole-rock analyses. Thanks to Christine Putnis, Timm John, and Ralf Hetzel for comments on early versions of this manuscript. Manfred Schliestedt, Alexander Krohe, Douwe van Hinsbergen, and Michael Bröcker are owed for discussions about various aspects of the Cycladic geology. Reviews of Aral Okay, Uwe Ring, and an anonymous referee have helped to improve the manuscript. M.E. Bickford (science) and Bridgette Moore (technical) are thanked for their dedicated editorial work. The field campaign was supported by the Deutsche Forschungsgemeinschaft (DFG) grant Ba 964/10-2. MK expresses his deepest gratitude to K.B. Petersen for delivering inspiration whenever it was needed.

# ***A new geological map of the Island of Syros (Aegean Sea, Greece): Implications for lithostratigraphy and structural history of the Cycladic Blueschist Unit***

**Mark Keiter**

*Institut für Mineralogie, Westfälische Wilhelms-Universität Münster, Corrensstrasse 24, 48149 Münster, Germany*

**Chris Ballhaus**

*Steinmann-Institut für Geologie, Mineralogie, Paläontologie, Universität Bonn, Poppelsdorfer Schloss, 53115 Bonn, Germany*

**Frank Tomaschek**

*Institut für Mineralogie, Westfälische Wilhelms-Universität Münster, Corrensstrasse 24, 48149, Münster, Germany*

*Arguably the most efficient, effective way to increase one's understanding of the architecture of Earth, or at least the nature of the near-surface geologic environment, is to conduct mapping as a necessary step to subsequent investigations....If we hope to understand the detailed architecture of Earth as it now exists, and the evolution of our home planet, our first step must therefore include geologic mapping. This is truly where the rubber meets the road.*

—W.G. Ernst, *GSA Special Paper 413*

## **ABSTRACT**

**The Island of Syros (Cyclades, Greece) is a prime locality for the study of processes active in deep levels of orogens and is world famous for its exceptionally well preserved blueschist- to eclogite-facies lithologies. Syros Island was completely remapped at a scale of 1:25,000. Detailed lithostratigraphical observations and area-wide, closely spaced structural measurements allowed a much more detailed depiction of the highly variable lithological assemblage, as well as of the complex structural evolution.**

**Lithostratigraphical indications, such as the distribution of Mn-mineralization and sequential repetition of characteristic marker successions, suggest that the whole-rock pile of the Cycladic Blueschist Unit on Syros, including meta-ophiolites and metasediments, retains numerous primary depositional features. Magmatic activity in an Upper Cretaceous backarc environment was likely to be contemporaneous with the deposition of the sedimentary protoliths comprising the main lithological succession on Syros.**

The structural evolution of the Cycladic Blueschist Unit on Syros comprises multiphase isoclinal intrafolial folding and ductile thrusting, regarded as essentially burial related and terminating close to peak metamorphic conditions, either prograde or very early on the retrograde path. Especially in areas where blueschist- to eclogite-facies metamorphism is undisturbed, high-pressure fabrics are well preserved. The retrograde evolution was accompanied by heterogeneously distributed, weakly developed extensional tectonics and episodic, contractional deformation, followed by intense brittle transpressional and transtensional tectonics, disrupting the rock sequence since Miocene to subrecent times.

## Introduction

The Cycladic archipelago is a key area to study all kinds of orogeny-related processes. The island of Syros, which is located in the heart of the Cycladic blueschist terrane, is one of few localities in Europe where remnants of blueschist- and eclogite-facies metamorphism are exceptionally well preserved. Syros features a wide range of spectacular high-pressure lithologies, including metabasites, meta-acidites, former hydrothermal Mn-Fe-rich ocean-floor precipitations, metagraywackes, and metacarbonates. Parts of the succession can be related to an oceanic crust that was subducted to ~50 km depths during the Eocene and then exhumed. As a result, the sequence recrystallized under blueschist- to eclogite-facies conditions and was deformed by at least two prograde, penetrative deformation events. Except for the south of the island, greenschist overprint over the high-pressure assemblages and structures is minimal. These facts render Syros a prime location for the study of metamorphic, tectonic, and chemical processes in fossil collision zones (e.g., Ridley and Dixon, 1984; Putlitz et al., 2000; Marschall et al. 2007; Schumacher et al., 2008).

In order to provide meaningful interpretations of field-related data, it is crucial to do so on the basis of an accurate geological map. The currently valid geological map of Syros was published by Hecht (1985), but is at a rather large scale of 1:50,000, and consequently much of the structural and lithological information it provides remains general. Therefore, it is not surprising that in the past several key areas of Syros were mapped in more detail in order to address specific questions (e.g., Ridley, 1982a; Melidonis and Constantinides, 1983; Rosenbaum et al., 2002; Keiter et al. 2004a; Tomaschek et al., 2008). A high-resolution geological map of Syros as a whole was previously unavailable.

The aim of this paper is to summarize the results of an extensive field campaign where the whole of the island of Syros was mapped at a scale of 1:5000 and then converted to a scale of 1:25,000. It is meant to supplement the new geological map (Map 1<sup>1</sup>) and provide lithological, stratigraphical, and structural information beyond what can be provided on the actual map sheet. Furthermore, we present an overview of the recent development of research on Syros and discuss the major disputed topics, such as paleogeography, burial and exhumation history of the Cycladic Blueschist Unit.

<sup>1</sup>Map 1. *Geological Map of Syros Island (Cyclades, Greece)* (1:25,000) is on a CD-ROM accompanying this volume. The map is also available as GSA Data Repository Item 2011259, online at [www.geosociety.org/pubs/ft2011.htm](http://www.geosociety.org/pubs/ft2011.htm), or on request from [editing@geosociety.org](mailto:editing@geosociety.org), Documents Secretary, GSA, P.O. Box 9140, Boulder, Colorado 80301, USA.

### 1.1 Regional Geological Framework

#### 1.1.1 Geology of the Hellenic Orogen and Present Plate Tectonic Situation

The Hellenic orogen comprises a series of terranes that are stacked along NE-dipping thrust faults (Fig. 1). Tectonic activity in the Hellenic orogen can be dated broadly by the onset of flysch sedimentation, which in the present geographic context migrated from the NE to the SW. In the Inner Hellenic nappes, the first flysch deposits are dated to around Dogger. In the Pelagonian and parts of the Pindos, flysch deposition is dated to Upper Cretaceous. In the Gavrovo-Tripolitza unit, flysch deposition took place during the Eocene. At the same time, the Cycladic area experienced the peak of high-pressure metamorphism. In the Ionic zone, the onset of flysch sedimentation is dated to around the Miocene. For an overview of the geology of the Hellenic orogen, see also Jacobshagen (1986), Papanikolaou et al. (2004), and Mountrakis (2006).

At the present day, the Aegean Sea, together with a large portion of Turkey and mainland Greece, forms part of the Turkish-Aegean microplate (McKenzie, 1970, see Fig. 2A). In its eastern portion, this microplate is presently being extruded westward between the Eurasian and the Arabian plate. The boundary of the Turkish-Aegean microplate is marked in the north by the prominent right-lateral North Anatolian fault zone, and in the southeast by the left-lateral East Anatolian fault zone (Fig. 2A).

Long-term global positioning system (GPS) measurements conducted during the past two decades have shown that relative motion within the Turkish-Aegean microplate has not been homogenous in direction and speed. Mainland Turkey is currently being extruded westwards at ~2 cm/yr, while in the Aegean an accelerated movement of 3.5–4 cm/yr is observed toward the southwest (McClusky et al., 2000; Hollenstein et al., 2008). This change in direction and speed is a consequence of the currently active backarc extension toward the retreating Hellenic subduction zone. As a result of backarc extension, the continental crust south of the Cyclades and in the Cretan Sea is attenuated to ~22 km. The Cycladic massif is not affected by major crustal extension and has retained a thickness of 25–30 km (e.g., Tirel et al., 2004). While in the Aegean the rollback of the Hellenic subduction zone causes crustal attenuation, western Greece (the Adriatic and Ionian area) shows crustal thickening to ~50 km, caused by active thrusting over the largely undeformed foreland represented by parts of the Ionian Islands (Makris, 1978; see Fig. 1). A seismic survey, however, has revealed the presence of deep-seated, NE-dipping reflectors west of Ionian islands,

suggesting that even the foreland is at best parautochthonous (Cocard et al., 1999).

Paleomagnetic studies have shown that during the upper Miocene and Pliocene, the Aegean area has undergone significant block rotations. Two major domains can be distinguished. On mainland Greece and the western Aegean, two

episodes of rotation have taken place, resulting in an overall clockwise rotation of  $50^\circ$  (van Hinsbergen et al., 2005), while the eastern Aegean and Turkey have rotated counterclockwise by  $\sim 20^\circ$  (van Hinsbergen et al., 2010). The border between these two domains roughly coincides with the mid-Cycladic lineament (MCL, Fig. 2B), defined by Walcott and White

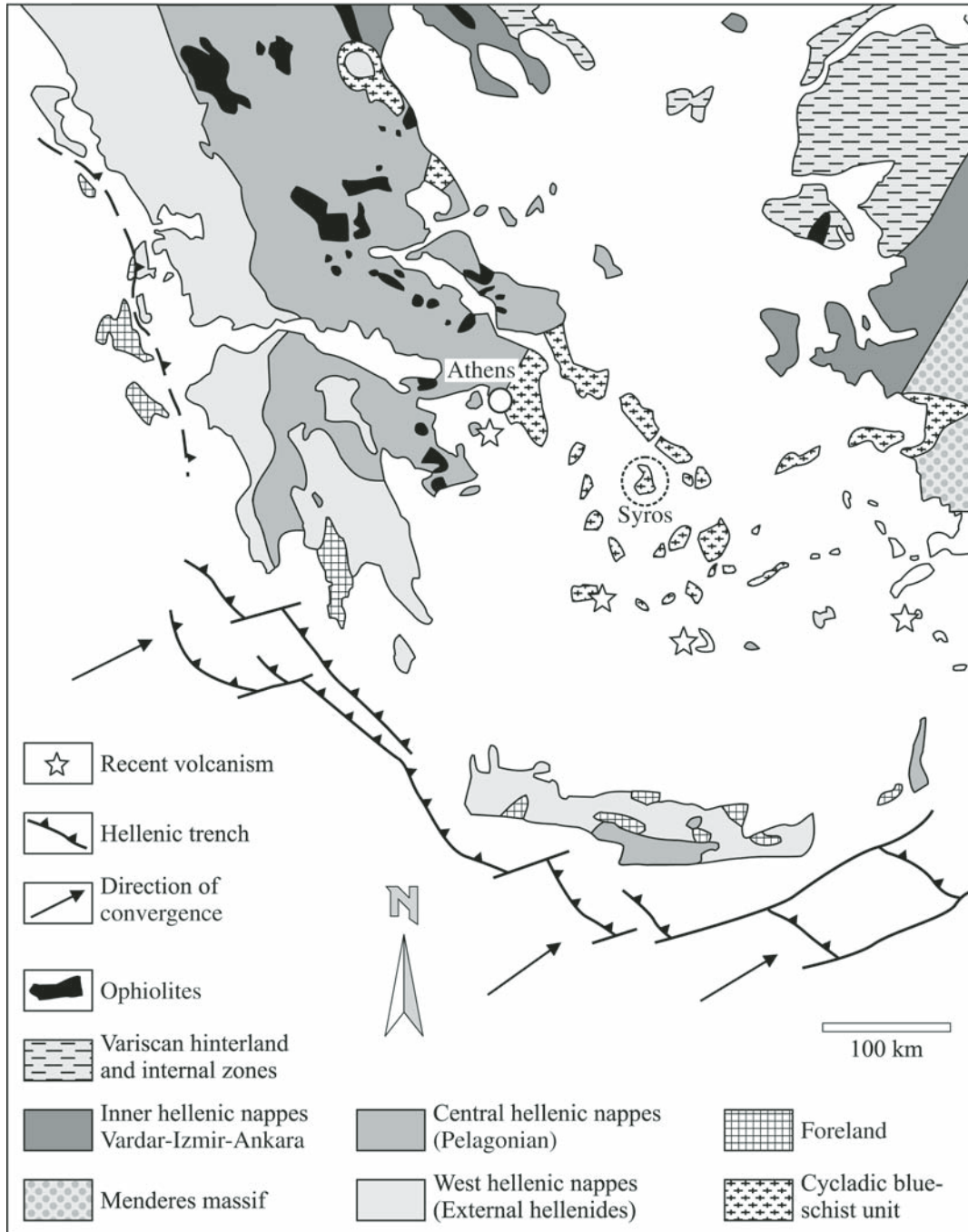


Figure 1. Simplified geological map of Greece after Jacobshagen (1986), modified after Okay (2001). Position of the Hellenic trench after Le Pichon and Angelier (1979). Basal unit on Evia, Attika, and Samos, as well as outcrops of the Cycladic Upper Unit not shown.

(1998) based on the distribution of ductile stretching lineations. Reliable paleomagnetic data from the Cycladic islands are relatively scarce, but Syros Island is inferred to lie within the western domain characterized by clockwise rotation. The current high-temperature arc of the Hellenic subduction zone is represented by the recent to subrecent volcanic activity and extends over the islands of Aegina, Milos, Santorini, and Nisyros (Fig. 1).

According to global positioning system (GPS) data and microseismicity studies (Bohnhoff et al., 2006), no major fault movement is observed within the Cyclades, apart from small clusters of microearthquakes around Santorini and in the strait between Syros and Andros/Tinos. This suggests that the Cycladic area at present acts as a tectonically more or less inactive coherent block, bounded by discrete zones of higher strain (e.g., Hollenstein et al., 2008).

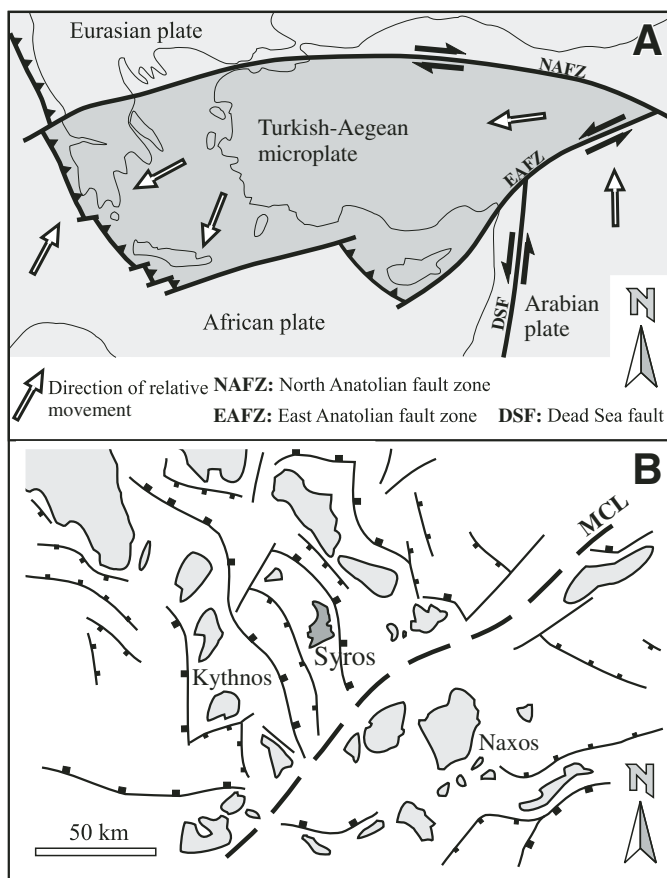


Figure 2. (A) Present-day plate tectonic situation in the eastern Mediterranean. Simplified after McKenzie (1970) and Walcott and White (1998). Position of the Hellenic trench after Le Pichon and Angelier (1979). Arrows mark the directions of movement relative to a fixed Eurasia. (B) Offshore fault pattern in the Cyclades after Walcott and White (1998) and references therein. The mid-Cycladic lineament (MCL) separates domains of postmetamorphic rotation; with clockwise rotation in the northwest, and anticlockwise rotation southeast of the MCL, respectively.

### 1.1.2 Geology of the Attic-Cycladic Crystalline Complex

Syros forms part of the Attic-Cycladic crystalline complex within the Hellenides (e.g., Dürr, 1986; Katzir et al., 2007). Two main tectonic units are distinguished in the Attic-Cycladic crystalline complex, based on marked differences in their metamorphic history during the Alpine orogeny: the high-pressure metamorphic Cycladic Blueschist Unit, and an Upper Unit consisting of various allochthonous klippen (granitoids, high-pressure/low-temperature metamorphic rocks, and ophiolite fragments).

The Cycladic Blueschist Unit is composed of a series of stacked tectonic thrust sheets of Variscan basement, Mesozoic metasediments, and remnants of oceanic crust of Jurassic and Upper Cretaceous age (e.g., Dürr et al., 1978; Dürr, 1986; Okrusch and Bröcker, 1990; Keay, 1998; Tomaschek et al., 2003; Bulle et al., 2010). On a regional scale, the Cycladic Blueschist Unit may be correlated with the Olympos window on mainland Greece, where high-pressure units are overlain by Pelagonian nappes (e.g., Blake et al., 1981; Jacobshagen, 1986; Doutsos et al., 1993; Okay, 2001; Ring and Layer, 2003; Papanikolaou et al., 2004; Jolivet et al., 2004; Figs. 1 and 2B). Three tectonometamorphic events may be recognized in the blueschist unit—an Eocene blueschist- to eclogite-facies event (M1), a temporally and spatially heterogeneous Oligocene to Miocene medium-pressure metamorphic overprint (M2), and a contact metamorphic event of only local importance (M3), i.e., around Miocene granitoid intrusions. The medium-pressure overprint M2 reached high-grade conditions in the southern Cyclades, culminating in a migmatitic dome on Naxos (Jansen and Schuiling, 1976). The blueschist- to eclogite-facies metamorphic overprint (M1) is best recognized on the islands of Sifnos and Tinos, and especially on Syros. For a summary of the pressure-temperature-time (PTt) history in the Cyclades, see Altherr et al. (1979, 1982, 1988), Andriessen et al. (1979), Schliestedt et al. (1987), Henjes-Kunst et al. (1988), Wijbrans et al. (1990), Okrusch and Bröcker (1990), Bröcker et al. (1993), Lister and Raouzaos (1996), Keay et al. (2001), Tomaschek et al. (2003), Lagos et al. (2007), and Jolivet and Brun (2010).

The Upper Unit is a heterogeneous group of tectonically higher units overlying the Cycladic Blueschist Unit. Tertiary metamorphism is less severe or absent. The Upper Unit consists of klippen of Late Cretaceous granitoids, high-pressure/low-temperature metamorphic rocks, Jurassic ophiolite fragments, Permo-Mesozoic sediments, fragments of possible Pelagonian provenance, as well as of post-tectonic, unmetamorphosed molasse deposited along scarps of normal faults and derived from the erosion of Cycladic Blueschist Unit rocks (Reinecke et al., 1982; Altherr et al., 1994; Papanikolaou, 1987; Gautier and Brun, 1994a; Katzir et al., 1996).

### 1.1.3 Geology of Syros

For the most part, the island of Syros is dominated by rocks of the Cycladic Blueschist Unit, which is well known for its spectacular high-pressure rocks (Fig. 3). The north and the central

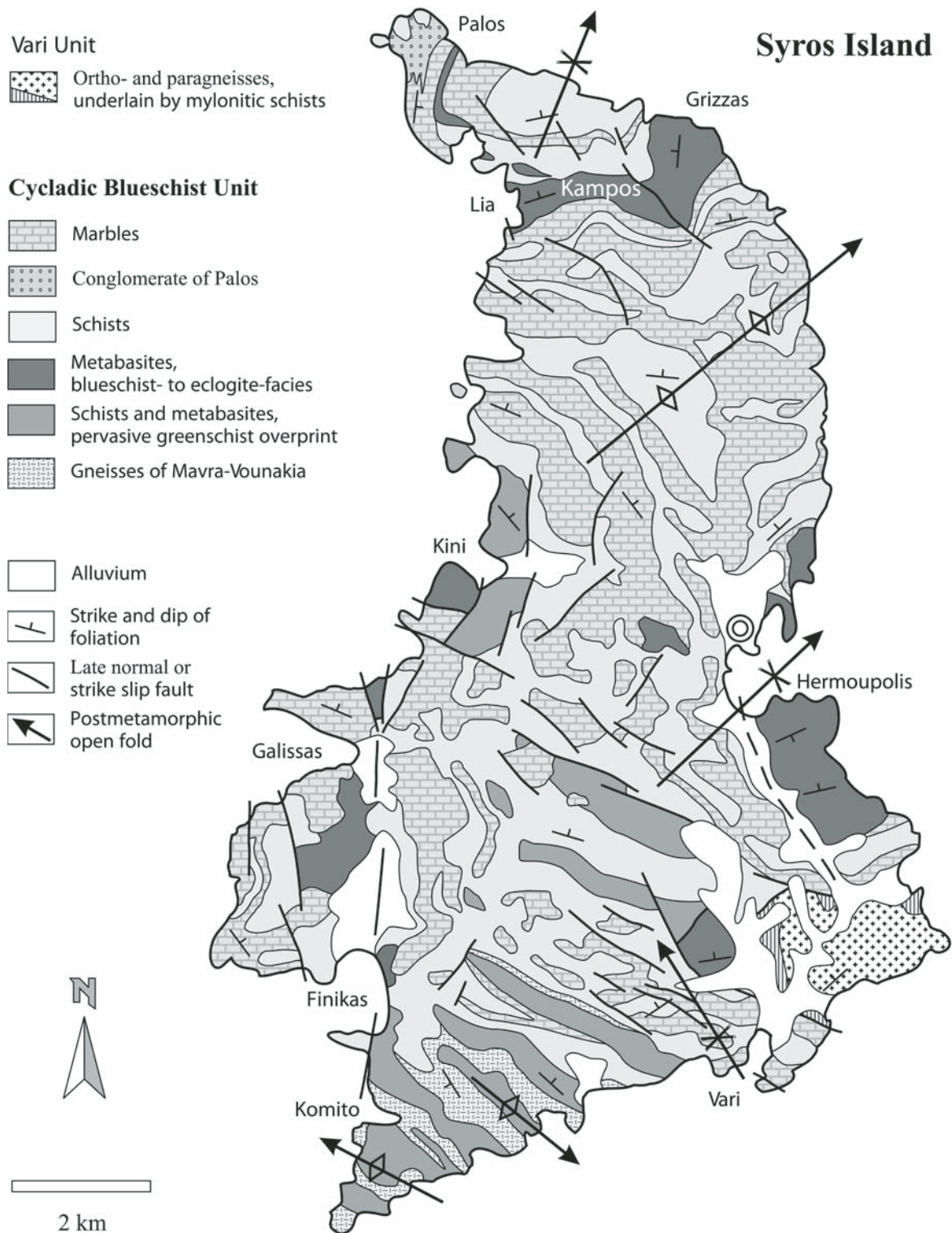


Figure 3. Generalized geological overview map of Syros Island. The main metabasite-schist-marble sequence forms part of the Cycladic Blueschist Unit; the Vari Unit, part of the allochthonous Upper Unit, is confined to the southeast of the island.

parts of the island are dominated by alternating sequences of schist and marble units, dipping around 30° to 50° to the NNE or NE. The schist-marble units were interpreted by Ridley (1982a) as thrust sheets, and indeed they are intercalated quite frequently with metabasite fragments.

In the north, the Kampos metabasite belt extends from Lia beach to Grizzas bay; in the west, metabasites crop out south of Kini and on the Charassonas peninsula. On the east coast of Syros, metabasites occur in the Ermoupolis-Mana area. Another metabasite body is exposed east of Chroussa, but here the structural relations with underlying schist-marble units are largely obscured by normal faulting and thick alluvial cover. Remnants of metabasites are occasionally found in central parts of the island.

The southwest of the island, Mavra Vounakia peninsula, is composed of predominantly greenschist-facies metabasites, mica schists, quartzo-feldspathic metasediments, and occasionally Ab-Kf-rich gneisses. Hecht (1985) discriminated these units from the high-pressure rocks of the north based on metamorphic grade, although the protoliths very likely have been the same. Marble intercalations progressively thin out and become rarer toward the south. The degree of greenschist overprint is also gradual and increases from the north (patchy and selective) to the south (pervasive). Greenschist overprint was gradual across former thrust planes, contrary to assertions by Trotet et al. (2001a). Even the most retrogressed units, such as gneisses and metabasites of Mavra Vounakia, still preserve relicts of structural and petrological elements indistinguishable from those in the north and suggest that the whole-rock sequence had a common tectonometamorphic history during the Eocene high-pressure event (Tomaschek et al., 2008 and references therein).

The protolith age of oceanic crust relicts on northern Syros provides the maximum age constraint on the onset of high-pressure metamorphism in the Cycladic Blueschist Unit. The magmatic protolith age is Upper Cretaceous (~80 Ma). This age became well established in repeated U-Pb geochronological studies on magmatic zircons from igneous-textured metabasic rocks and meta-plagiogranites (Keay, 1998; Tomaschek et al., 2003; Bröcker and Keasling, 2006). Similar zircons from metasomatic lithologies (Bröcker and Enders, 1999; Bröcker and Keasling, 2006) seem best explained as relict igneous crystals, inherited from the precursor rocks (Fu et al., 2010).

High-pressure metamorphism of the Cycladic Blueschist Unit on Syros resulted in blueschist- to eclogite-facies assemblages, for which peak conditions of ~15–16 kbar and 450–500 °C have been derived, based on univariant equilibria (e.g., Dixon, 1976; Ridley, 1984; Okrusch and Bröcker, 1990). Using multi-equilibrium calculation techniques, Trotet et al. (2001b) argued in favor of a considerably deeper burial (20 kbar and 550 °C). This high PT estimate, however, is not without ambiguity, as discussed by Putlitz et al. (2005). Recently, Schumacher et al. (2008) have studied impure marbles on Syros and used the stability of aragonite + glaucophane, as well as refined calculations of lawsonite + glaucophane to establish upper lim-

its of pressure and temperature. Their findings cast doubts on the PT estimates of Trotet et al. (2001a, 2001b) and indicate that a return to the more conservative constraints of 16 kbar and 500 °C might be in order.

Numerous studies from Syros and other Cycladic islands have attempted to constrain the age of high-pressure metamorphism (M1) in the Cycladic Blueschist Unit by K-Ar, Ar-Ar, and Rb-Sr white mica geochronology (Altherr et al., 1979; Andriessen et al., 1979; Wijbrans and McDougall, 1986; Maluski et al., 1987; Wijbrans et al., 1990; Bröcker et al., 1993; Bröcker and Enders, 2001; Putlitz et al., 2005). Well-preserved, high-pressure rocks of the Cycladic Blueschist Unit yielded a range of Eocene white mica ages, mostly between ~53 and ~40 Ma. The observed scatter of dates had been explained either by metamorphic cooling, excess argon, true heterochronicity, or mixtures of multiple mica generations, ranging from prograde to retrograde.

A detailed investigation of magmatic and metamorphic zircons from Syros yielded a U-Pb sensitive high-resolution ion microprobe (SHRIMP) age of  $52.4 \pm 0.8$  Ma for the metamorphic zircon population (Tomaschek et al., 2003). Based on intergrowth relations of texturally and chemically similar zircon with growth-zoned garnet, and concordance of U-Pb zircon with Ar-Ar white mica ages, it was argued that ~52 Ma is the best estimate for the high-pressure metamorphic event. This view accords with results from white mica geochronology obtained elsewhere on Syros (Maluski et al., 1987; Baldwin, 1996; Putlitz et al., 2005; Glodny et al., 2008). Direct dating of the rock-forming, garnet-bearing assemblages finally reduced remaining ambiguities from interpretations of white mica and accessory mineral data. Results from high-precision Lu-Hf geochronology of eclogite samples from Syros yielded a tight cluster at  $51.9 \pm 1.4$  Ma, dating the formation of the Grt + Omp assemblage (Lagos et al., 2007). This, in conjunction with the agreement among the U-Pb ages of metamorphic zircon, the maximum Rb-Sr and Ar-Ar white mica ages, and the Lu-Hf ages, strongly suggests that the ~52 Ma age dates a single, high-pressure (HP) event that affected these rocks.

The regional greenschist overprint (M2) in the Cyclades has been extensively dated with K-Ar, Ar-Ar, and Rb-Sr white mica geochronology to ~25–18 Ma (e.g., Altherr et al., 1979; Bröcker et al., 1993, 2004; Bröcker and Franz, 2006). Greenschist-facies deformation on Syros is possibly contemporaneous with shear zones on the neighboring Tinos Island where it has been constrained to ~21 Ma by Rb-Sr white mica (Bröcker and Franz, 1998). Note, though, that elsewhere in the Cyclades, along shear zones, the M2 medium-pressure overprint has continued until ~11 Ma, partially overlapping with the intrusion of the Miocene granitoids (e.g., Kumerics et al., 2005). Zircon fission-track ages of ~11 Ma, determined by Ring et al. (2003) from northern Syros, approximate the timing of the brittle-ductile transition for this part of the Cycladic Blueschist Unit.

The Vari Unit in the southeast of Syros represents a distinct allochthonous formation (Maluski et al., 1987, Fig. 3). Dominant protoliths comprise granitoids of Triassic age (244–240 Ma, U-Pb zircon, Keay, 1998; Tomaschek et al., 2000b).

The main metamorphic overprint reached epidote-amphibolite-facies conditions (Ridley, 1982a), constrained to 100–95 Ma by white mica Ar-Ar and Rb-Sr geochronology, and U-Pb on metamorphic zircon (Tomaschek et al., 2000b). White mica ages around 100 Ma have no equivalent in the blueschist unit, but are known from the Upper Unit on Tinos (Bröcker and Franz, 1998) and the Makrotandalon Unit on Andros (Bröcker and Franz, 2006). In many respects, the Vari Unit has been correlated with the Akrotiri unit on the neighboring island of Tinos (Patzak et al., 1994; Bröcker and Enders, 2001). The Vari Unit has been in a tectonically higher position at least since the Miocene, as indicated from zircon fission-track ages of 21–20 Ma. Cooling is significantly older compared to the 12–10 Ma ages from the blueschist unit on Syros (Ring et al., 2003). The Vari Unit is best considered as a klippe of an originally extensive Pelagonian-type nappe that once may have covered the Cycladic Blueschist Unit from Mount Olympus to the Cyclades (Gautier and Brun, 1994a; Sánchez-Gomez et al., 2002).

## 1.2 Previous Work and Available Geological Maps

The first geological map of Syros was presented by von Foullon and Goldschmidt (1887). Their map divides only schistose rocks and carbonates, and structural observations are scarce. Yet, they noted the high variability among the schistose rocks and provided extensive petrographic data, as well as information about weathering resistance and geomorphological characteristics. The exceptional position of the Vari Unit had not yet been recognized at that time.

Philippson (1901), in his extensive geographical study of the Greek islands, presented a small geological overview map of Syros, in which the greenschist overprint, stronger and more pervasive in the southern part, can first be discerned. He divided the schist succession into glaucophane schists in the north, and amphibolites in the south, respectively. Structural information, apart from general dip direction and a brief mention of intense folding, is again scarce and unsystematic.

A much more detailed geological map of Syros was introduced by Bonneau et al. (1980a). In addition to petrographical refinements, it also presents an overview of the complex structural inventory of Syros Island. Bonneau et al. (1980a) were the first to identify the Vari Gneiss as a regionally allochthonous unit. They originally mapped the Vari Unit as a tectonic window, emplaced along late-stage (post-Eocene) thrusts, but later reinterpreted it as a klippe in a subsequent revision (Bonneau, 1982), as depicted by Maluski et al. (1987). The gneiss-amphibolite succession of the Mavra Vounakia area in the SW of Syros was regarded as belonging to the allochthonous Vari Unit. Following the interpretations available at their time, Bonneau et al. described the various occurrences of metabasites and meta-ultrabasites, especially the Kampos melange, as olisthostromes within a flysch sequence (see also Blake et al., 1981).

Late-stage, brittle tectonics are represented by steep, mostly N-S-striking faults and, interestingly, a major horizontal tectonic

contact in the central part of the island, separating a klippe mostly made up of marbles from the main succession of Syros.

Ridley (1982a), building on the work of Dixon (1968), included in his Ph.D. thesis numerous detailed maps, lithostratigraphical information, and geological cross sections of areas of interest, e.g., of the Kampos area. Furthermore, he presented structural overview maps of island-wide foliation and lineation trends, as well as fault patterns. Ridley's work is probably the first that systematically established a deformation succession and correlated fabric development with metamorphic events. The overview map in Ridley (1982b) is broadly similar to the map of Bonneau et al. (1980a), with the difference that the rocks of the Mavra Vounakia area in the SW of the island are assigned by Ridley to the main succession of Syros, rather than to the allochthonous Vari Unit.

The highest resolution map available for Syros is the Institute of Geology and Mineral Exploration publication by Hecht (1985). Printed at a scale of 1:50,000, it allowed Hecht to refine lithostratigraphic aspects and distinguish further rock types, such as the gneisses of Mavra Vounakia in the southwest, the metaconglomerate of Palos and the schists of Kampos and Sikamia in the north. The main difference to the earlier-published maps, though, is that Hecht rigorously marked all bases of the various metabasite occurrences as thrusts, or at least as tectonic contacts. This feature marks a step away from an interpretation of the metabasitic melange units as olisthostromes, i.e., from sedimentary toward a tectonic emplacement of the metabasites. The late-stage horizontal tectonic contacts depicted in the maps of Bonneau et al. (1980a) and Ridley (1982b) are extended farther, so that in Hecht (1985) a large portion of the marble-schist sequences in the central and southwestern area of Syros is regarded as allochthonous.

## 1.3 Methods and Techniques

Geological mapping was conducted by the authors, supported by supervised student mapping projects, during several field seasons between 1999 and 2007. The complete island was mapped at a scale of 1:5000, partly aided by the use of aerial photographs. The high-resolution maps were then merged, simplified, and projected onto a 1:25,000 topographical base (purchased from Anavasi Maps and Navigation Systems, Athens) using an equal-angle Mercator projection.

Wherever possible, mapping was performed keeping potential protoliths in mind, with metamorphic grade only as a secondary priority, to emphasize constraints on primary stratigraphical features preserved in the strongly deformed lithological column. Exceptions to this guideline are the blueschist- to eclogite-facies metabasite occurrences, because they are eminent and highly typical for Syros, and—even more important—the nature of their structural boundaries toward other rock types is of special interest for the interpretation of various regional processes, such as burial and exhumation history, and the role of late-stage brittle tectonics (see Chaps. 3 and 4).

## *General Petrography of Mapped Lithological Units*

Numerous papers have been published about the various lithologies of Syros. It is beyond this work to present the vast quantity of available data in detail, so only brief descriptions of the mapped units will be given here. The reader is referred to Dixon (1968), Ridley (1982a), Dixon and Ridley (1987), Seck et al. (1996), Bröcker and Enders (2001), Putlitz et al. (2000), Bröcker and Keasling (2006), Marschall et al. (2008), Schumacher et al. (2008), Tomaschek et al. (2008), and Miller et al. (2009) for further details. All mineral abbreviations follow Whitney and Evans (2010). In general, only the main parageneses are given; common accessories are Ttn or Rt, as well as Ap ± Zrn.

### 2.1 Marbles

Calcite marbles represent one of the most abundant rock types on Syros. They are laminated to massive, medium to coarse grained, and white or light gray to blue gray in color. Intercalations of impure Ph + Gln ± Czo ± Qz-bearing marbles (recently studied in detail by Schumacher et al., 2008), and locally calc-silicate layers, are frequent. In places, matrix-supported monomict metaconglomerate horizons with calcite clasts in carbonate matrix occur, more abundantly near contacts with schist units. Frequency and thickness of marble units tend to decrease toward the south, i.e., toward the lower part of the structural pile. Intrafolial folds on the decimeter to meter scale and retrograde columnar calcites, interpreted to result from static topotactic replacement of aragonite, are also commonly preserved (Figs. 4A and 4B; see also Brady et al., 2004, Keiter et al., 2008b). Occasionally, marble layers are hydrothermally impregnated by Fe-oxide phases (Figs. 4C and 4D; Table 1). Surficial karst is common, sometimes so intense that internal fabrics and structural elements are entirely obscured.

Marble units were mapped as dolomitic where the amount of dolomite layers exceeded 20% (Plate 1A). Dolomitic layers in the marbles are usually brownish gray to yellowish in color, and are frequently alternating with calcite marble on the cm to dm scale. More massive dolomite units also occur, especially well developed in the upper part of the marble unit north of Aetou Bay in northwest Syros (see Map 1). They commonly lack internal foliation and tend to form s-parallel megaboudins in ductile calcite marble up to several hundred meters in length. Some dolomitic units can be traced across the island, and have been used by Höpfer and Schumacher (1997) in an attempt to correlate the marble units on Syros.

### 2.2 Mica Schists

Summarized under this title is a highly heterogeneous group of rocks, all of which share the common property that they originate from clastic sedimentary protoliths. Where blueschist-facies mineral assemblages are preserved, the schists are gray to bluish gray, commonly with the paragenesis Ph + Pg + Qz ± Gln ± Grt ± Cal ± Ep. Quartz segregations parallel to the dominant cleavage are very abundant. Minor intercalations of mafic Gln + white mica ± Ep ± Ttn ± Cal blueschists, interpreted to originate from volcanoclastic layers, are also frequent, locally with static Ep + Ph + Chl/Grt ± Cal ± Qz pseudomorphs after Lws. Toward the central and southern part of Syros, the degree of static, selective to pervasive greenschist-facies overprint becomes stronger, resulting in Ab + Chl-dominated assemblages.

Likely protoliths of the mica schists were graywackes and psammites, variably contaminated by, or mixed with, carbonatic and occasional mafic tuffitic intercalations. Genuine metapelite compositions appear to be rare or obscured by metamorphic overprint, as indicated by representative whole-rock geochemical data (Table 1).

### 2.3 Metaconglomerates

Metaconglomeratic layers are quite abundant and occur in or near every major marble unit on Syros, though rarely at a mappable scale. In most cases, these are monomict metaconglomerate layers with matrix-supported calcite clasts in a foliated impure calcite marble (Cal + Ph + Qz ± Gln) matrix. The clasts range in size from millimeters up to several centimeters (Plate 1B and 1C). Metaconglomerate units form laterally discontinuous layers and lenses, usually a few meters thick. They occur preferably at the base of marble units in contact with mica schists, indicating that there may be a possible primary stratigraphic relationship (to be detailed in Chap. 3).

On Palos Peninsula in northwestern Syros (see Fig. 3 and Map 1), the metaconglomerates are so prominent that Hecht (1985) distinguished them as a discrete unit. Here they reach up to several hundred meters in thickness. In addition, they are distinctly polymict, containing lithoclasts up to 5 cm in size of calcite marble, phengitic schist, metabasite, and occasional piemontite-rich aggregates (former Mn-rich hydrothermal ocean-floor sediment). Locally, metaconglomerates grade into massive, poorly foliated and highly resistant clast-poor to

clast-free Cal + Qz ± Ep ± Ph ± Gln impure marbles or calcite-rich mica schists.

The matrix-supported nature of the metaconglomerates (up to 90% matrix) renders it difficult to recognize a possible protolith. Such a texture in a primary sedimentary conglomerate would require an uncommon, high-energy depositional environment, or

possibly fluvial channel fills. However, it is possible that intense shearing during prograde deformation eradicated a large portion of clasts that may originally have been present in the sedimentary protolith, especially if they had compositional similarities to the matrix itself. The apparent matrix-supported texture of the conglomerates would in this case be of tectonic origin.

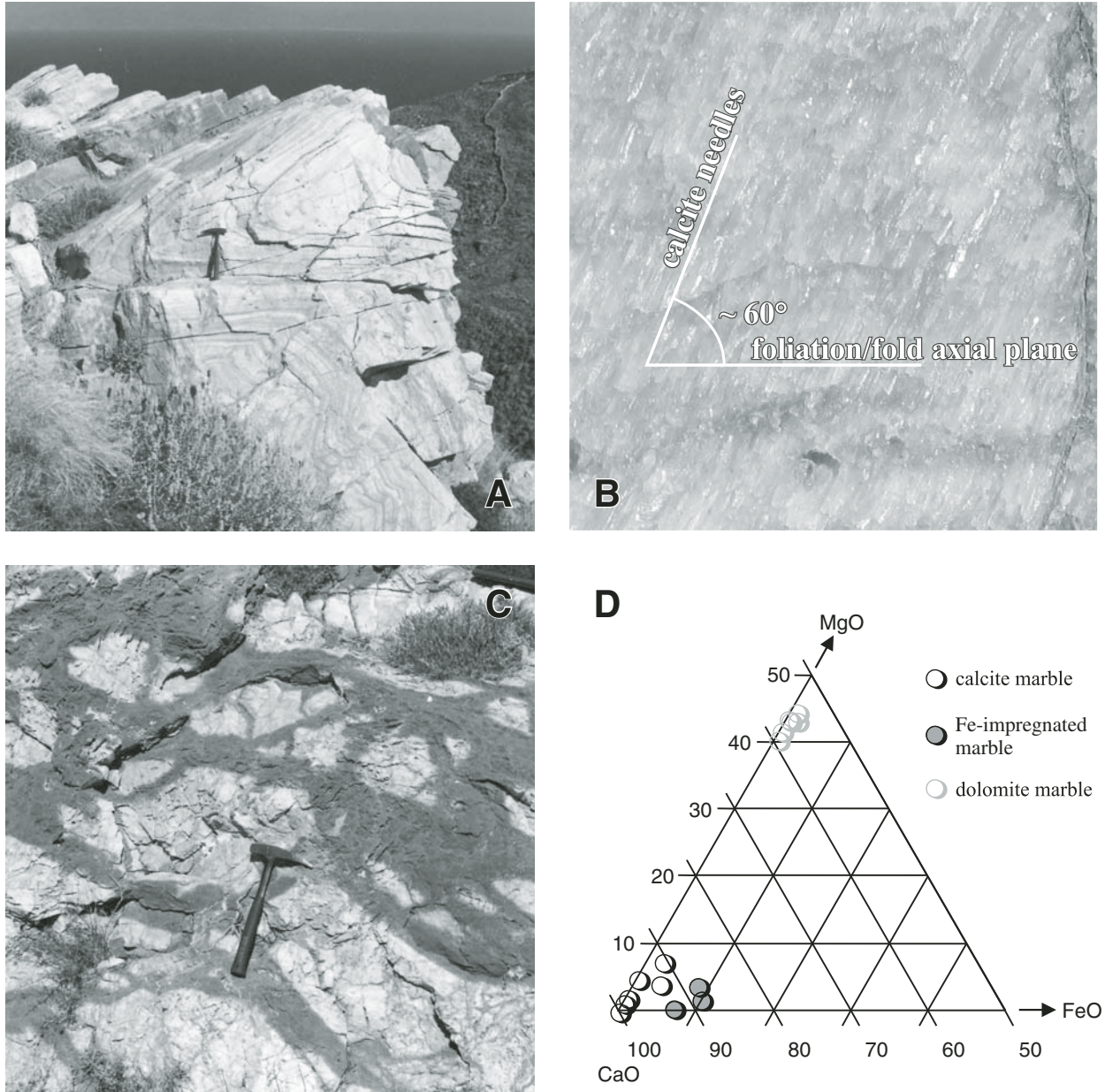


Figure 4. (A) Hinge zone of an isoclinally folded, laminated calcite marble 100 m south of the Kastri ruin, northeast Syros, looking east. (B) Calcite needles, oriented at  $60^\circ$  to the marble foliation, Katakephalos peninsula, northwest of Galissas. The foliation is in this case parallel to the fold axial plane of the main fold generation (distal to hinge zones of intrafolial folds). (C) Post-tectonic brownish Fe-oxide impregnation along irregular cracks in a calcite marble, 500 m north of Kampos. Patchy post-tectonic hydrothermal alteration is a regular phenomenon on Syros, especially abundant on the Mavra Vounakia peninsula, southwest Syros. Fe enrichment (up to  $\sim 10$  wt%) is usually confined to thin marble layers in schists or metabasites; thick pure calcite or dolomite marbles are generally unaffected. (D) MgO-CaO-FeO diagram of representative calcite and dolomite marbles of Syros. Iron-impregnated marbles are usually brown or brownish-red in color (see Table 1).

TABLE 1. WHOLE-ROCK ANALYSES FOR METAMORPHIC ROCKS AND VOLCANIC DIKES OF SYROS

| Rock type                        | Metacarbonates of the Cycladic Blueschist Unit (CBU) |        |        |        |        |                |        |        |       |        | Metasedimentary schists and metaigneous rocks, CBU |        |        |       |       |                  |        |        |        |        |        |
|----------------------------------|--|--------|--------|--------|--------|----------------|--------|--------|-------|--------|--|--------|--------|-------|-------|------------------|--------|--------|--------|--------|--------|
|                                  | Dolomite marble                                      |        |        |        |        | Calcite marble |        |        |       |        | Fe-impregnated marble                              |        |        |       |       | Metasedimentary* |        |        |        |        |        |
| Sample                           | MK4  | MK5    | MK6    | MK7    | MK9    | MK1            | MK2    | MK3    | MK15  | MK10   | MK11   | MK20   | MK12   | MK13  | MK14  | BSY314           | BSY319 | BSY320 | BSY321 | BSY322 | BSY323 |
| Major elements (wt%)             |  |        |        |        |        |                |        |        |       |        |  |        |        |       |       |                  |        |        |        |        |        |
| SiO <sub>2</sub>                 | 0.30   | 0.55   | 2.92   | 0.40   | 2.08   | 0.25           | 0.51   | 2.30   | 12.73 | 2.61   | 8.68   | 0.48   | 2.23   | 24.76 | 27.33 | 96.97            | 72.27  | 67.54  | 69.65  | 74.23  | 65.05  |
| TiO <sub>2</sub>                 | 0.01   | 0.01   | 0.01   | 0.01   | 0.03   | 0.01           | 0.01   | 0.01   | 0.02  | 0.04   | 0.05   | 0.01   | 0.01   | 0.04  | 0.01  | 0.04             | 0.58   | 0.81   | 0.24   | 0.51   | 0.65   |
| Al <sub>2</sub> O <sub>3</sub>   | 0.08   | 0.08   | 0.08   | 0.12   | 0.66   | 0.08           | 0.14   | 0.19   | 0.31  | 1.04   | 1.84   | 0.09   | 0.44   | 1.82  | 0.19  | 0.82             | 11.03  | 16.05  | 13.84  | 10.77  | 12.47  |
| Fe <sub>2</sub> O <sub>3</sub> * | 0.14   | 0.13   | 0.38   | 0.20   | 0.58   | 0.09           | 0.14   | 0.17   | 1.05  | 1.65   | 2.45   | 0.16   | 5.29   | 5.56  | 4.86  | 0.31             | 4.16   | 4.66   | 3.24   | 3.58   | 5.64   |
| MnO                              | 0.01   | 0.01   | 0.04   | 0.02   | 0.04   | 0.01           | 0.01   | 0.02   | 0.28  | 0.03   | 0.09   | 0.01   | 0.57   | 0.61  | 0.33  | 0.01             | 0.07   | 0.01   | 0.19   | 0.06   | 0.09   |
| MgO                              | 17.59  | 18.10  | 18.34  | 18.83  | 18.85  | 0.10           | 0.53   | 1.97   | 16.20 | 2.94   | 1.53   | 0.90   | 0.28   | 0.59  | 1.13  | 0.14             | 3.34   | 0.85   | 1.39   | 2.55   | 3.68   |
| CaO                              | 35.56  | 34.63  | 32.76  | 33.77  | 31.87  | 56.67          | 55.79  | 52.81  | 28.71 | 49.87  | 46.56  | 55.34  | 50.81  | 35.83 | 35.83 | 0.18             | 0.59   | 0.38   | 1.63   | 0.50   | 2.25   |
| Na <sub>2</sub> O                | 0.02   | 0.02   | 0.02   | 0.02   | 0.02   | 0.02           | 0.02   | 0.02   | 0.02  | 0.02   | 0.02   | 0.02   | 0.02   | 0.02  | 0.02  | 0.02             | 2.13   | 0.05   | 0.02   | 2.14   | 1.64   |
| K <sub>2</sub> O                 | 0.01   | 0.02   | 0.01   | 0.03   | 0.30   | 0.01           | 0.02   | 0.06   | 0.13  | 0.02   | 0.53   | 0.02   | 0.19   | 0.84  | 0.06  | 0.25             | 1.66   | 5.77   | 5.20   | 1.79   | 2.25   |
| P <sub>2</sub> O <sub>5</sub>    | 0.01   | 0.01   | 0.02   | 0.01   | 0.02   | 0.01           | 0.01   | 0.01   | 0.04  | 0.01   | 0.01   | 0.86   | 0.01   | 0.01  | 0.01  | 0.06             | 0.06   | 0.23   | 0.04   | 0.06   | 0.06   |
| L.O.I.                           | 46.87  | 46.80  | 45.68  | 46.90  | 45.80  | 43.89          | 43.90  | 43.25  | 40.43 | 42.40  | 38.49  | 43.00  | 40.63  | 29.52 | 30.21 | 0.44             | 2.72   | 2.93   | 3.42   | 2.43   | 5.55   |
| Total                            | 100.60   | 100.36 | 100.26 | 100.31 | 100.25 | 101.14         | 101.08 | 100.81 | 99.92 | 100.63 | 100.25   | 100.89 | 100.48 | 99.60 | 99.98 | 99.24            | 98.61  | 99.28  | 98.86  | 98.62  | 98.33  |
| Trace elements (ppm)             |  |        |        |        |        |                |        |        |       |        |  |        |        |       |       |                  |        |        |        |        |        |
| Sc                               | nd   | nd     | nd     | 12     | nd     | nd             | 10     | nd     | nd    | nd     | 13   | 15     | 14     | nd    | nd    | nd               | 15     | 13     | nd     | nd     | 19     |
| V                                | nd   | nd     | nd     | nd     | nd     | nd             | nd     | nd     | nd    | nd     | 20   | nd     | 12     | 14    | nd    | nd               | 94     | 34     | 11     | 89     | 112    |
| Cr                               | nd   | 10     | nd     | 12     | nd     | nd             | nd     | nd     | 22    | nd     | 19   | 11     | 10     | 47    | 39    | nd               | 303    | nd     | nd     | 236    | 253    |
| Co                               | nd   | nd     | 11     | nd     | nd     | nd             | nd     | nd     | 11    | nd     | 10   | nd     | 16     | 18    | 26    | nd               | 19     | 10     | nd     | 15     | 26     |
| Ni                               | 12   | nd     | 14     | 14     | 10     | nd             | 12     | nd     | 35    | 11     | 36   | nd     | 31     | 56    | 47    | nd               | 145    | 44     | nd     | 82     | 151    |
| Cu                               | nd   | nd     | nd     | nd     | nd     | nd             | nd     | nd     | nd    | nd     | 10   | nd     | 25     | 22    | 11    | nd               | nd     | 14     | nd     | nd     | 27     |
| Zn                               | 10   | 22     | nd     | 17     | 22     | nd             | nd     | 11     | 29    | 41     | 45   | nd     | 78     | 62    | 34    | nd               | 55     | 52     | 98     | 43     | 74     |
| Ga                               | nd   | nd     | nd     | nd     | nd     | nd             | nd     | nd     | nd    | nd     | nd   | nd     | nd     | nd    | nd    | 10               | 14     | 18     | 12     | 15     | 15     |
| As                               | nd   | nd     | nd     | nd     | nd     | nd             | nd     | nd     | nd    | nd     | nd   | nd     | 10     | 19    | nd    | nd               | nd     | nd     | nd     | nd     | nd     |
| Rb                               | nd   | nd     | nd     | nd     | nd     | nd             | nd     | nd     | nd    | nd     | 23   | nd     | nd     | 22    | nd    | nd               | 69     | 198    | 161    | 71     | 89     |
| Sr                               | 147  | 114    | 96     | 105    | 105    | 73             | 183    | 281    | 90    | 58     | 93   | 159    | 135    | 58    | 77    | nd               | 26     | 19     | 42     | 38     | 38     |
| Y                                | nd   | nd     | 12     | 13     | 18     | nd             | nd     | 17     | 32    | nd     | 12   | 14     | 38     | 51    | 18    | nd               | 21     | 29     | 21     | 12     | 17     |
| Zr                               | nd   | 14     | nd     | nd     | 13     | 10             | 12     | 17     | 10    | 15     | 20   | 10     | 14     | 33    | 10    | 12               | 133    | 225    | 176    | 145    | 138    |
| Nb                               | nd   | nd     | nd     | nd     | nd     | nd             | nd     | nd     | nd    | nd     | nd   | nd     | nd     | nd    | nd    | nd               | nd     | 38     | 15     | nd     | 12     |
| Sn                               | nd   | nd     | nd     | nd     | nd     | nd             | 10     | 23     | nd    | 32     | 29   | 15     | 23     | nd    | nd    | nd               | nd     | nd     | nd     | nd     | 24     |
| Ba                               | nd   | nd     | nd     | nd     | 21     | 16             | 6      | 29     | 88    | 40     | 169  | nd     | 378    | 530   | 92    | nd               | 289    | 1187   | 886    | 284    | 292    |
| La                               | nd   | nd     | nd     | nd     | nd     | nd             | 16     | 15     | nd    | nd     | nd   | 16     | 34     | nd    | nd    | nd               | 27     | 53     | 47     | 50     | 24     |
| Ce                               | nd   | nd     | nd     | nd     | 12     | nd             | nd     | nd     | nd    | 12     | 10   | 11     | nd     | nd    | nd    | nd               | 48     | 152    | 60     | 57     | 29     |
| Nd                               | nd   | nd     | nd     | nd     | nd     | nd             | nd     | nd     | nd    | nd     | 10   | nd     | nd     | nd    | nd    | nd               | 28     | 42     | 23     | 23     | 11     |
| Ta                               | nd   | nd     | 11     | nd     | nd     | 20             | nd     | nd     | 11    | nd     | nd   | nd     | nd     | nd    | nd    | nd               | nd     | nd     | nd     | nd     | nd     |
| Pb                               | 14   | nd     | nd     | nd     | nd     | nd             | nd     | nd     | 11    | 16     | 57   | 10     | 38     | 23    | 36    | nd               | 18     | 14     | 13     | 13     | nd     |
| Th                               | 22   | nd     | 19     | 21     | 11     | nd             | nd     | nd     | nd    | nd     | 28   | 10     | nd     | nd    | nd    | nd               | 21     | 27     | 27     | 27     | 10     |

(continued)

TABLE 1: WHOLE-ROCK ANALYSES FOR METAMORPHIC ROCKS AND VOLCANIC DIKES OF SYROS (continued)

| Rock type                        | Metasedimentary schists and metigneous rocks, ÇBU (continued) |        |        |        |        |        |        |        |        |        |            |        |        |        |        |             |        |        |        |        |        |
|----------------------------------|---|--------|--------|--------|--------|--------|--------|--------|--------|--------|------------|--------|--------|--------|--------|-------------|--------|--------|--------|--------|--------|
|                                  | Metasedimentary* (continued)                                  |        |        |        |        |        |        |        |        |        | Undefined* |        |        |        |        | Metigneous* |        |        |        |        |        |
| Sample                           | BSY324  | BSY325 | BSY326 | BSY327 | BSY328 | BSY329 | BSY330 | BSY331 | BSY333 | BSY338 | BSY343     | BSY346 | BSY352 | BSY332 | BSY334 | BSY335      | BSY349 | BSY336 | BSY337 | BSY339 | BSY340 |
| <b>Major elements (wt%)</b>      |   |        |        |        |        |        |        |        |        |        |            |        |        |        |        |             |        |        |        |        |        |
| SiO <sub>2</sub>                 | 59.99   | 62.75  | 78.10  | 49.86  | 48.59  | 51.72  | 47.75  | 46.44  | 49.04  | 63.11  | 76.20      | 47.45  | 40.82  | 70.14  | 51.85  | 50.64       | 59.92  | 39.63  | 53.90  | 47.84  | 40.62  |
| TiO <sub>2</sub>                 | 0.78  | 0.78   | 0.34   | 1.20   | 0.91   | 0.90   | 1.91   | 0.84   | 0.86   | 0.88   | 0.07       | 1.24   | 1.35   | 0.17   | 1.24   | 1.01        | 0.77   | 0.71   | 0.49   | 1.12   | 0.97   |
| Al <sub>2</sub> O <sub>3</sub>   | 14.55   | 14.84  | 10.65  | 17.97  | 14.83  | 23.47  | 15.63  | 14.00  | 14.68  | 14.73  | 12.20      | 19.89  | 13.97  | 3.86   | 13.92  | 16.17       | 16.31  | 14.98  | 15.28  | 16.72  | 14.37  |
| Fe <sub>2</sub> O <sub>3</sub> * | 6.19  | 6.91   | 2.58   | 9.88   | 11.06  | 8.27   | 10.09  | 8.73   | 10.48  | 5.64   | 1.38       | 10.98  | 11.40  | 14.21  | 9.64   | 8.68        | 7.74   | 8.96   | 9.41   | 10.86  | 9.10   |
| MnO                              | 0.11  | 0.09   | 0.04   | 0.16   | 0.23   | 0.07   | 0.18   | 0.21   | 0.14   | 0.05   | 0.03       | 0.08   | 0.16   | 0.22   | 0.14   | 0.11        | 0.19   | 0.14   | 0.13   | 0.18   | 0.18   |
| MgO                              | 3.94  | 3.86   | 0.79   | 5.01   | 7.91   | 1.20   | 6.00   | 5.17   | 6.70   | 2.06   | 0.45       | 3.03   | 7.54   | 2.50   | 5.07   | 7.02        | 4.63   | 4.05   | 8.88   | 4.25   | 5.02   |
| CaO                              | 2.96  | 0.46   | 0.14   | 5.43   | 4.75   | 0.08   | 9.51   | 10.19  | 5.95   | 2.84   | 0.58       | 9.37   | 12.36  | 4.43   | 7.49   | 6.15        | 0.60   | 17.15  | 2.70   | 9.71   | 12.12  |
| Na <sub>2</sub> O                | 1.93  | 2.89   | 2.23   | 3.11   | 3.84   | 0.48   | 3.66   | 3.53   | 2.58   | 2.05   | 2.57       | 3.08   | 2.88   | 1.51   | 4.06   | 4.12        | 1.04   | 1.72   | 3.12   | 2.81   | 2.21   |
| K <sub>2</sub> O                 | 2.84  | 2.33   | 2.01   | 3.14   | 1.48   | 7.29   | 0.76   | 0.40   | 2.69   | 2.79   | 3.21       | 0.38   | 0.66   | 0.23   | 1.02   | 0.90        | 3.44   | 0.73   | 0.61   | 1.91   | 3.38   |
| P <sub>2</sub> O <sub>5</sub>    | 0.08  | 0.09   | 0.04   | 0.31   | 0.10   | 0.04   | 0.22   | 0.11   | 0.15   | 0.13   | 0.01       | 0.24   | 0.14   | 0.03   | 0.24   | 0.06        | 0.07   | 0.11   | 0.03   | 0.04   | 0.17   |
| L.O.I.                           | 5.62  | 3.87   | 1.78   | 3.05   | 5.31   | 4.83   | 2.98   | 9.19   | 5.66   | 4.89   | 1.75       | 3.06   | 7.59   | 2.11   | 4.11   | 3.89        | 3.96   | 10.79  | 4.54   | 3.47   | 10.33  |
| Total                            | 98.99   | 98.67  | 98.70  | 99.12  | 99.01  | 98.35  | 98.69  | 98.81  | 98.93  | 98.77  | 98.45      | 98.80  | 98.87  | 98.41  | 98.78  | 98.75       | 98.67  | 98.97  | 99.09  | 98.91  | 98.47  |
| <b>Trace elements (ppm)</b>      |   |        |        |        |        |        |        |        |        |        |            |        |        |        |        |             |        |        |        |        |        |
| Sc                               | 15  | 19     | nd     | 34     | 42     | 18     | 29     | 26     | 40     | 13     | nd         | 41     | 46     | 10     | 25     | 44          | nd     | 33     | 30     | 44     | 27     |
| V                                | 135   | 133    | 45     | 270    | 233    | 168    | 256    | 234    | 234    | 101    | 12         | 159    | 308    | 64     | 222    | 229         | 171    | 159    | 239    | 263    | 222    |
| Cr                               | 318   | 312    | 24     | 156    | 300    | 107    | 215    | 236    | 197    | 85     | 19         | 277    | 298    | 45     | 162    | 208         | 331    | 265    | 256    | 265    | 290    |
| Co                               | 29  | 30     | 12     | 31     | 48     | 16     | 38     | 34     | 52     | 16     | nd         | 49     | 46     | 22     | 40     | 39          | 38     | 38     | 38     | 46     | 40     |
| Ni                               | 157   | 194    | 25     | 66     | 158    | 40     | 57     | 86     | 156    | 39     | 13         | 150    | 214    | 51     | 59     | 101         | 263    | 103    | 94     | 94     | 132    |
| Cu                               | 43  | 34     | nd     | 13     | 30     | 33     | 47     | 22     | 39     | 26     | nd         | 17     | 69     | 27     | 36     | 65          | 31     | 29     | 29     | 64     | 35     |
| Zn                               | 84  | 96     | 43     | 87     | 110    | 79     | 72     | 78     | 132    | 81     | 18         | 145    | 74     | 51     | 81     | 76          | 120    | 55     | 69     | 87     | 76     |
| Ga                               | 19  | 17     | 14     | 17     | 22     | 32     | 18     | 16     | 17     | 17     | 10         | 21     | 17     | 10     | 17     | 11          | 22     | 24     | 14     | 14     | 15     |
| As                               | 26  | nd     | nd     | nd     | nd     | 56     | nd     | nd     | nd     | 22     | nd         | nd     | nd     | nd     | nd     | nd          | nd     | nd     | nd     | nd     | nd     |
| Rb                               | 103   | 107    | 74     | 67     | 38     | 272    | 23     | 13     | 65     | 115    | 121        | nd     | nd     | 18     | 21     | 44          | 143    | 22     | 21     | 35     | 63     |
| Sr                               | 62  | 20     | 20     | 185    | 80     | 28     | 319    | 208    | 123    | 57     | 25         | 487    | 264    | 286    | 147    | 184         | 18     | 307    | 104    | 237    | 197    |
| Y                                | 21  | 25     | 17     | 30     | 27     | 45     | 37     | 23     | 21     | 30     | 15         | 42     | 22     | nd     | 43     | 23          | 24     | 20     | 15     | 31     | 18     |
| Zr                               | 170   | 146    | 110    | 114    | 79     | 220    | 169    | 71     | 85     | 186    | 116        | 117    | 109    | 51     | 154    | 76          | 136    | 54     | 34     | 78     | 83     |
| Nb                               | 13  | 11     | nd     | nd     | nd     | 17     | nd     | nd     | nd     | nd     | 25         | nd     | nd     | nd     | nd     | nd          | 11     | nd     | nd     | nd     | nd     |
| Sn                               | nd  | 15     | nd         | nd     | nd     | nd     | nd     | nd          | nd     | nd     | nd     | nd     | nd     |
| Ba                               | 383   | 361    | 271    | 183    | 87     | 914    | 50     | 47     | 161    | 419    | 206        | 21     | 30     | nd     | 108    | 37          | 262    | 68     | 26     | 85     | 233    |
| La                               | 23  | 32     | 19     | 29     | 35     | 43     | 10     | 25     | 32     | 36     | 55         | 12     | 15     | nd     | 14     | nd          | 20     | 42     | nd     | 39     | 13     |
| Ce                               | 46  | 60     | 52     | 67     | 15     | 112    | 41     | nd     | nd     | nd     | 89         | 46     | nd     | 27     | 76     | 20          | 64     | 33     | 37     | nd     | nd     |
| Nd                               | 27  | 11     | 17     | 23     | nd     | 38     | 15     | 23     | 10     | 17     | 31         | 48     | 14     | nd     | 31     | nd          | 26     | nd     | 20     | nd     | nd     |
| Ta                               | nd  | nd     | nd     | nd     | nd     | nd     | nd     | nd     | nd     | nd     | nd         | 10     | nd     | nd     | nd     | 11          | nd     | nd     | nd     | nd     | nd     |
| Pb                               | 18  | 18     | nd     | 13     | nd     | 16     | 19     | 27     | 18     | 28     | nd         | 14     | nd     | 15     | 16     | 12          | 17     | 12     | nd     | nd     | 17     |
| Th                               | 25  | 16     | 17     | nd     | 10     | 19     | nd     | nd     | 12     | 21     | 23         | nd     | nd     | nd     | nd     | nd          | 18     | nd     | 14     | nd     | nd     |

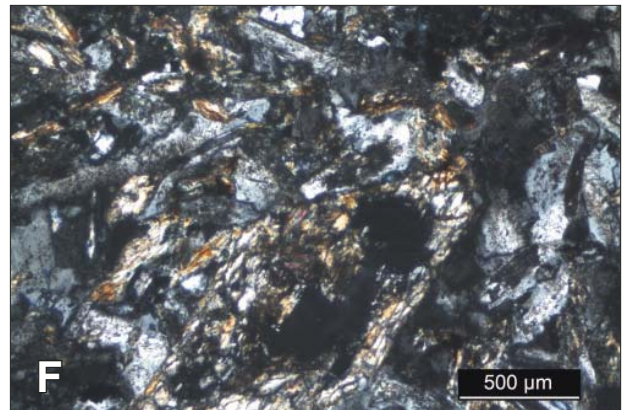
(continued)

TABLE 1. WHOLE-ROCK ANALYSES FOR METAMORPHIC ROCKS AND VOLCANIC DIKES OF SYROS (continued)

| Rock type                        | Metasedimentary schists and metaigneous rocks, CBU (continued) |        | Banded tuffitic schists, CBU |        | Hermoupolis locality  |        | Volcanic dikes from south Syros |        | Orthogneisses of the Vari Unit |        |        |        |        |        |        |        |        |       |       |
|----------------------------------|--|--------|------------------------------|--------|-----------------------|--------|---------------------------------|--------|--------------------------------|--------|--------|--------|--------|--------|--------|--------|--------|-------|-------|
|                                  | Metigneous* (continued)  |        | Azolimnos locality           |        | Chalandriani locality |        |                                 |        |                                |        |        |        |        |        |        |        |        |       |       |
| Sample                           | BSY341   | BSY342 | BSY344                       | BSY345 | BSY347                | BSY348 | BSY351                          | BSY372 | BSY373                         | BSY374 | BSY375 | BSY376 | BSY377 | BSY378 | BSY379 | BSY317 | BSY318 | VA61  | VA77  |
| Major elements (wt%)             | 34.72  | 44.73  | 38.83                        | 41.95  | 45.77                 | 53.25  | 40.29                           | 69.55  | 53.23                          | 75.65  | 48.58  | 53.48  | 73.65  | 72.34  | 53.72  | 58.78  | 51.55  | 77.09 | 64.19 |
| SiO <sub>2</sub>                 | 0.14   | 1.23   | 0.94                         | 1.00   | 1.18                  | 0.73   | 0.04                            | 0.41   | 0.55                           | 0.26   | 0.69   | 0.57   | 0.30   | 0.39   | 0.63   | 0.54   | 0.76   | 0.19  | 0.54  |
| TiO <sub>2</sub>                 | 19.46  | 16.53  | 13.79                        | 15.86  | 15.97                 | 16.65  | 2.64                            | 13.72  | 15.44                          | 12.41  | 18.55  | 16.45  | 13.34  | 13.70  | 14.52  | 15.64  | 14.15  | 12.15 | 13.41 |
| Al <sub>2</sub> O <sub>3</sub>   | 12.71  | 10.67  | 8.57                         | 9.42   | 9.80                  | 9.96   | 8.95                            | 5.61   | 12.96                          | 3.13   | 11.35  | 12.71  | 3.04   | 3.75   | 12.95  | 5.20   | 6.02   | 1.58  | 5.65  |
| Fe <sub>2</sub> O <sub>3</sub> * | 0.14   | 0.22   | 0.12                         | 0.13   | 0.15                  | 0.12   | 0.13                            | 0.13   | 0.18                           | 0.04   | 0.18   | 0.39   | 0.03   | 0.03   | 0.36   | 0.09   | 0.12   | 0.02  | 0.09  |
| MnO                              | 0.39   | 2.71   | 3.39                         | 2.79   | 10.11                 | 5.55   | 33.10                           | 1.62   | 6.13                           | 0.90   | 4.93   | 6.54   | 1.01   | 1.72   | 7.26   | 5.58   | 5.37   | 0.39  | 3.70  |
| MgO                              | 22.28  | 13.75  | 16.76                        | 14.83  | 9.21                  | 3.14   | 1.82                            | 1.92   | 2.86                           | 1.88   | 7.19   | 0.85   | 1.55   | 2.11   | 2.03   | 3.90   | 7.08   | 1.67  | 5.18  |
| CaO                              | 0.77   | 3.05   | 3.61                         | 1.04   | 1.96                  | 6.29   | 0.02                            | 5.28   | 6.24                           | 4.14   | 3.65   | 4.87   | 3.79   | 1.92   | 5.56   | 4.11   | 2.17   | 4.84  | 2.58  |
| Na <sub>2</sub> O                | 0.68   | 1.38   | 0.17                         | 2.32   | 0.98                  | 0.28   | 0.01                            | 0.22   | 0.27                           | 0.31   | 0.15   | 0.79   | 1.49   | 2.22   | 1.18   | 3.10   | 2.77   | 0.33  | 1.73  |
| K <sub>2</sub> O                 | 0.01   | 0.11   | 0.15                         | 0.13   | 0.11                  | 0.05   | 0.01                            | 0.04   | 0.03                           | 0.04   | 0.02   | 0.03   | 0.02   | 0.07   | 0.09   | 0.11   | 0.28   | 0.05  | 0.10  |
| P <sub>2</sub> O <sub>5</sub>    | 7.34   | 4.46   | 12.60                        | 8.95   | 3.94                  | 2.62   | 11.95                           | 1.09   | 1.79                           | 1.21   | 4.48   | 3.45   | 1.59   | 1.91   | 1.84   | 2.91   | 9.83   | 0.90  | 1.97  |
| L.O.I.                           | 98.64  | 98.84  | 98.93                        | 98.42  | 99.18                 | 98.64  | 98.96                           | 99.59  | 99.68                          | 99.97  | 99.77  | 100.13 | 99.81  | 100.16 | 100.14 | 99.96  | 100.10 | 98.20 | 99.13 |
| Total                            |  |        |                              |        |                       |        |                                 |        |                                |        |        |        |        |        |        |        |        |       |       |
| Trace elements (ppm)             |  |        |                              |        |                       |        |                                 |        |                                |        |        |        |        |        |        |        |        |       |       |
| Sc                               | 49   | 32     | 13                           | 32     | 38                    | 30     | nd                              | nd     | 52                             | 16     | 49     | 57     | nd     | 18     | 43     | 18     | 15     | na    | na    |
| V                                | 285  | 175    | 235                          | 163    | 278                   | 270    | 79                              | 80     | 324                            | 32     | 316    | 238    | 25     | 34     | 221    | 106    | 126    | 14    | 145   |
| Cr                               | 212  | 282    | 243                          | 320    | 408                   | 39     | 2306                            | nd     | 18                             | nd     | 28     | 107    | 13     | nd     | 111    | 220    | 231    | 11    | 148   |
| Co                               | 12   | 35     | 38                           | 39     | 47                    | 43     | 96                              | 304    | 123                            | 289    | 129    | 142    | 156    | 137    | 71     | 64     | 33     | na    | na    |
| Ni                               | 12   | 119    | 118                          | 132    | 154                   | 48     | 1841                            | 15     | 67                             | 40     | 32     | 37     | 60     | nd     | 34     | 60     | 164    | 4     | 49    |
| Cu                               | 166  | 20     | 30                           | 54     | 33                    | 65     | 16                              | 11     | 51                             | nd     | 72     | 58     | 80     | 21     | 131    | 26     | 19     | na    | na    |
| Zn                               | nd   | 63     | 67                           | 87     | 71                    | 69     | 57                              | 58     | 102                            | 10     | 79     | 74     | 60     | 36     | 138    | 63     | 48     | 16    | 47    |
| Ga                               | 18   | 19     | 16                           | 19     | 17                    | 17     | nd                              | 14     | 15                             | 12     | 19     | 17     | 10     | 14     | 15     | 16     | 15     | na    | na    |
| As                               | nd   | nd     | nd                           | nd     | nd                    | nd     | nd                              | nd     | nd                             | nd     | nd     | nd     | nd     | nd     | nd     | nd     | nd     | na    | na    |
| Rb                               | 20   | 28     | nd                           | 57     | 15                    | nd     | nd                              | nd     | nd                             | nd     | nd     | 17     | 34     | 58     | 37     | 95     | 85     | 12    | 42    |
| Sr                               | 642  | 292    | 427                          | 472    | 197                   | 165    | 22                              | 77     | 105                            | 68     | 101    | 49     | 58     | 92     | 52     | 457    | 365    | 154   | 188   |
| Y                                | 42   | 33     | 23                           | 20     | 24                    | 20     | 10                              | 32     | 24                             | 29     | 10     | 29     | 27     | 31     | 35     | 21     | 26     | 32    | 16    |
| Zr                               | 33   | 104    | 91                           | 95     | 93                    | 52     | nd                              | 65     | 27                             | 97     | 18     | 29     | 81     | 91     | 41     | 148    | 226    | 173   | 126   |
| Nb                               | nd   | nd     | nd                           | nd     | nd                    | nd     | nd                              | nd     | nd                             | nd     | nd     | nd     | nd     | nd     | nd     | nd     | 15     | 7     | 4     |
| Sn                               | 16   | nd     | 13                           | nd     | nd                    | nd     | nd                              | nd     | nd                             | nd     | nd     | nd     | nd     | nd     | nd     | nd     | nd     | na    | na    |
| Ba                               | 59   | 94     | 28                           | 251    | 76                    | nd     | nd                              | 32     | 29                             | nd     | 23     | 126    | 249    | 256    | 122    | 773    | 439    | 52    | 176   |
| La                               | 17   | 26     | 14                           | 13     | 15                    | 34     | nd                              | nd     | 17                             | nd     | 26     | 19     | nd     | nd     | 17     | 27     | 67     | na    | na    |
| Ce                               | 28   | 19     | nd                           | 50     | 24                    | nd     | 22                              | 18     | nd                             | 24     | 10     | 28     | nd     | 15     | 48     | 24     | 87     | na    | na    |
| Nd                               | 13   | nd     | nd                           | nd     | 21                    | 10     | 10                              | 12     | nd                             | nd     | nd     | 20     | nd     | 15     | 22     | 21     | 38     | na    | na    |
| Ta                               | nd   | nd     | nd                           | nd     | nd                    | 12     | 10                              | 16     | nd                             | nd     | nd     | nd     | nd     | nd     | nd     | 11     | nd     | na    | na    |
| Pb                               | 31   | 13     | 19                           | 16     | 16                    | 14     | 14                              | nd     | 17                             | nd     | nd     | nd     | nd     | nd     | 12     | nd     | nd     | na    | na    |
| Th                               | nd   | 30     | nd                           | nd     | nd                    | 13     | nd                              | 17     | 16                             | 19     | 16     | 18     | 15     | 17     | 16     | 13     | 14     | na    | na    |

\*designating following field discrimination.

Note: Concentrations of major and trace elements for CBU and volcanic rocks were obtained on fused disks by XRF using a Philips PW-1480 spectrometer at Steinmann Institut, Universität Bonn. Vari orthogneiss data was determined using a Siemens SRS-300 spectrometer at the Institut für Mineralogie, Petrologie und Geochemie, Universität Tübingen. nd—not detected (< 10 ppm), na—sample not assayed for that element.



## 2.4 Greenschists and Epidote-Bearing Schists

A common rock type, especially in the south, is greenschist with the paragenesis  $Ab + Act + Chl \pm Qz$ . Continuous transitions to  $Ep + Cal \pm Rbk-Gln \pm Qz$  schists are frequent, depending on the degree of greenschist overprint. It is very likely that they are at least partially magmatic (basaltic) in origin. We used the epidote content in the field as a rough guide to discriminate magmatic from sedimentary protoliths, but fluid overprint associated with polyphase metamorphism renders interpretations of bulk-rock compositions rather difficult. An  $Al_2O_3 + Na_2O + K_2O$  versus  $CaO$  plot (Fig. 5; see also Table 1) of various representative schist samples, collected all over Syros, shows a tendency toward a magmatic trend in some of the samples, so intercalations of tuffs and/or tuffites are very likely.

The greenschists show strong variations in texture, ranging from fine-grained  $Chl-Ab$ -rich variants with closely spaced parallel cleavage (possibly marly protoliths) to massive calcite-bearing epidiosites, with epidote crystals in places reaching sizes of up to 2 cm. It is unclear if these textural variations suggest different protoliths or if they are a product of variations in fluid composition or deformation style during metamorphism. Thick horizons of massive epidiosites cropping out layer-parallel over large areas of Syros, as prominently depicted in the map of Hecht (1985), could not be confirmed by this study. The occurrence of such rocks is rather confined to thin layers not mappable at a scale of 1:25,000, or even patchy in places, e.g., constituting the summits of several cone-shaped hills along the south coast between Posidonia and Vari (see Map 1). It is tempting to regard such patchy and weathering-resistant outcrops of massive epidiosite as original metabasites, perhaps remnants of former basaltic feeder dikes or gabbro bodies, now overprinted in epidote-amphibolite or greenschist facies. Occasionally, dm-sized pancake or lensoid shapes can be observed in the epidiosites, which could tentatively be interpreted as pillow relicts. It is also likely, though, that the patchy appearance of the epidiosite occurrences may be just a



Plate 1. (A) Dolomite-rich layers (yellow) in calcite marble (bluish-gray) northwest of Chalandriani village. Thickness of the largest dolomite layer: ~20–30 cm. (B) Typical appearance of carbonate-dominated conglomerate, frequently found in or near marble units. (C) The matrix of the Conglomerate of Palos is usually an impure, mica-rich carbonate or calcsilicate; lithoclasts are composed mainly of marble, quartzite, schist, and metabasite. (D) Banded tuffitic schists in a road outcrop in Chalandriani village. White layer in the top left is a post-tectonic hydrothermal quartz precipitate. (E) Banded schists north of Azolimnos bay. Note the two generations of folds, indicated here by random orientation of small-scale fold axial planes. (F) Thin-section micrograph of a postmetamorphic andesite, Megas Gialos, southern Syros. (G) Fine-grained eclogite (left) and coarse, undeformed eclogitic cumulate (right), coastal outcrop south of Kini. (H) Lawsonite pseudomorphs in a sharply foliated glaucophane schist, Grammata bay, northern Syros. Lawsonite statically overgrew the blueschist-facies foliation. After lawsonite breakdown, the schists have not been affected by internal deformation. Size of pseudomorphs: ~1–2 cm.

result of disruption of a formerly stratiform coherent layer by late-stage brittle faulting, which is highly common and closely spaced in the south of Syros.

## 2.5 Banded Metatuffitic Schists of Azolimnos, Hermoupolis, Chalandriani, and Galissas

Previously summarized together with the schists of Syros (Hecht, 1985), this lithological unit was distinguished systematically for the first time during work on this project. It comprises mafic  $Gln + Grt + Omp + Czo$  layers alternating on a centimeter to decimeter scale with felsic layers composed of white mica +  $Jd + Qz \pm Czo \pm Gln \pm Grt$ , where  $Cpx$  is often replaced by  $Ab + Act \pm Hem$  pseudomorphs (Plates 1D and 1E).

The occurrences at Azolimnos and Hermoupolis show well-preserved blueschist to eclogite-facies assemblages, while near Chalandriani and Galissas retrograde overprinting is stronger (see Table 1 for bulk-rock chemistry). They are part of the main succession of Syros, forming a concordant horizon in the lithostratigraphy from Hermoupolis via Plati Vouni–Chalandriani to Syringas. Occurrences deeper in the structural pile, e.g., inland of Galissas and at Azolimnos, are interpreted as tectonic repetitions (see Chaps. 3 and 4).

## 2.6 Garnet-Bearing Albite Paragneisses

Primarily, this lithology occurs as layers in schistose units around the Pirgos massif in the central part and in the Hermoupolis-Mana area. The rocks are light-gray to whitish,

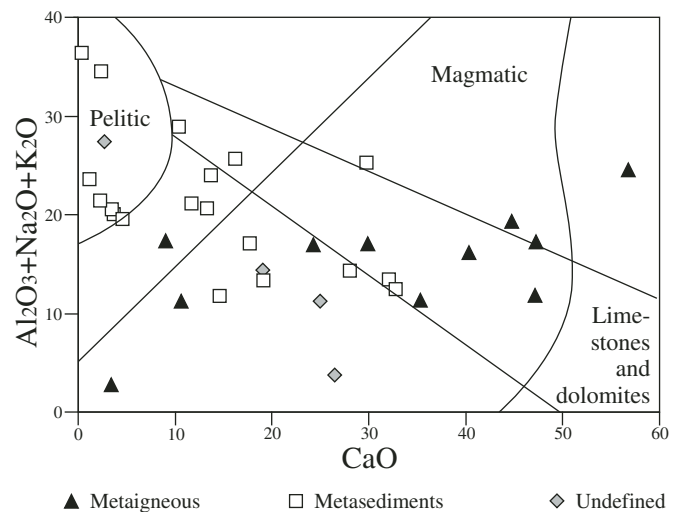


Figure 5.  $Al_2O_3 + Na_2O + K_2O$  versus  $CaO$  plot of representative metasedimentary schists and greenschists from Syros, according to classification made in the field. Schists classified as possible metabasites often contain significant amounts of epidote and minor calcite. “Undefined” are mostly calcite- and epidote-rich, fine-grained greenschists, possibly derived from marly protoliths. The flat trend of the metagneous rocks compared to the magmatic trend is possibly a result of calcite precipitation from fluids during metamorphic overprint.

coarse-grained, foliated Qz + Ab + white mica  $\pm$  Czo lithologies with gneissic fabric. In places cm-sized Grt porphyroblasts occur. Laterally and vertically, the albitic gneisses grade into albitic-bearing quartzite (see below). Likely protoliths for these rocks are arkosic layers in graywacke units.

## 2.7 Quartzites

Quartzites stick out as resistant, up to several meters thick Qz + Ab  $\pm$  white mica-bearing layers, locally with reddish-greenish coloration, cm-sized Grt porphyroblasts, and frequent, dm-sized intrafolial folds. These rocks are prominent in their appearance, but play only a minor role regarding spatial extension. Quartzite layers occur inside both schist units and albitic gneisses, and occasionally associated with metabasites.



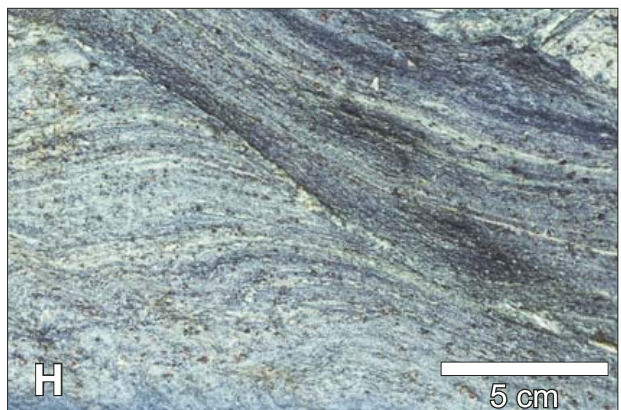
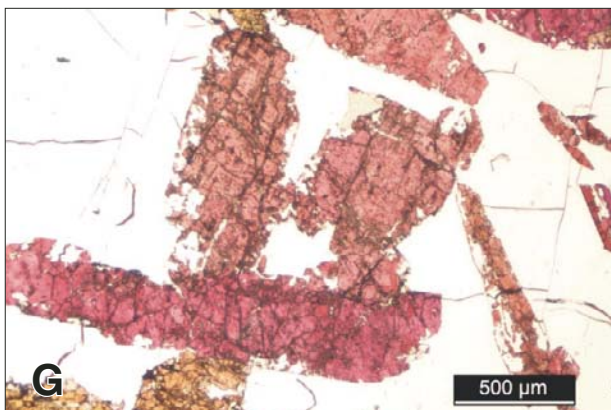
Figure 6. Relict pillow structures, now in blueschist to eclogite facies, 500 m southwest of Kalogeros Point, northern Syros. Dark rims around the pillows are caused by glaucophane enrichment, possibly a relict of a primary interaction between basalt and seawater, causing Na-enrichment in the original glass crust of the pillows.

Their lateral continuity typically does not exceed a few tens of meters, in two instances (near the village of Mytakas and southeast of Syringas) up to a few hundred meters. This is mainly due to intense disruption by late-stage faulting, but lens-shaped bodies of quartzite also occur. Partially, lens-shaped outcrops of quartzites could be attributed to boudinage or conjugate extensional shearing, but the fact that in places the quartzites laterally grade into albitic gneisses indicates that a relict primary sedimentary fabric (e.g., former psammitic channel fills) may be preserved as well.

## 2.8 Blueschist- to Eclogite-Facies Metabasite Association

This unit comprises a tectonic *mélange* of blueschist- to eclogite-facies fragments of a former oceanic crust, tectonically disrupted and juxtaposed during prograde deformation. Oceanic crust fragments include metabasalts, massive fine-grained and coarse-grained eclogites (Plate 1G) and metagabbro, as well as Gln + Czo + Omp + Pg  $\pm$  Grt blueschists (former mafic tuffs and hyaloclastites), locally with statically preserved Czo + Ph + Chl + Qz pseudomorphs after Lws (Plate 1H). Usually, the various lithologies are too limited in extent to be discriminated on a map scale. In resistant units and blocks, magmatic fabrics (e.g., relict pillows and cumulate textures) are well preserved (Fig. 6). In the past, this highly variable unit has been regarded either as an olistostrome or as a *mélange* representing remnants of a single, formerly continuous tectonic nappe overlying the marble-schist units (Hecht, 1985; Höpfer and Schumacher, 1997). Detailed mapping has shown the blueschist-eclogite lithologies are repetitive tectonic slices that are intercalated in, and structurally homogeneous with, the metasedimentary lithostratigraphy (see Chap. 3).

Plate 2. (A) Metagabbro 300 m northwest of Grizzas bay (pen for scale). Cumulate texture is well preserved in the top half of the photograph, while the lower part is dominated by a shear zone, in which omphacite is largely replaced by glaucophane. (B) Plagiogranitic dike in metagabbro west of Grizzas bay. Size of camera lid: 5 cm. (C) Bimodal metavolcanics of Kampos: felsic fragments in a glaucophane-garnet-rich matrix are interpreted as primary depositional features. Location: Grizzas bay; thickness of large felsic fragment in the top half of the photo is  $\sim$ 20 cm. (D) Bimodal metavolcanics of Kampos: strongly deformed variant. (E) Serpentinic talc schist, crenulated and sigmoidally sheared; location: between Kampos and Lia beach. (F) Manganese-rich spessartine felses showing two generations of isoclinal folds, looking roughly down the F2 fold axis. Note the refolded F1 hinges in the center of the photograph. An s2 cleavage is well developed in the mica-rich schistose matrix, parallel to the axial plane of F2 (running from top right to lower left). (G) Thin-section micrograph, showing bright-red piemontite crystals, plain-polarized light. The matrix of the piemontite-rich rock consists almost entirely of quartz, minor garnet, and very little white mica. (H) Ductile normal fault in glaucophane schists S of Kini. Assemblages indicate that faulting took place under high-pressure conditions, close to peak metamorphism.



### 2.8.1 Serpentinite and Tremolite-Chlorite-Talc $\pm$ Actinolite Schists

These rocks constitute the matrix of the various tectonic block associations, preferably inside and at the peripheries of competent metabasite, metagabbro, and metavolcanic units. The matrix itself is an incompetent pale-green, sometimes vividly blue-green mylonitic Atg + Tr/Act + Chl + Tlc schist, locally grading into serpentinite mylonite. In places, millimeter- to centimeter-sized pseudomorphs of Hem after Mag are common. Often a closely spaced crenulation cleavage and fine kink folding can be observed, as well as a disruption into lensoid slices along small-scale, low-angle, conjugate shear zones, indicating a certain amount of horizontal stretching (Plate 2E). In places (e.g., Kampos, Vari, and Finikas; see Map 1), massive serpentinite with no internal foliation is preserved. Many metabasite boudins in mylonite-serpentinite schist matrix are distinctly rounded by tectonic transport and often rimmed by highly strained, monomineralic Act and Act-Chl blackwall reaction rims, in places impregnated by static Tur and Rt. The serpentinite belts may mark shear zones active during prograde and retrograde deformation, likely to have accommodated significant strain.

### 2.8.2 Metagabbros

These are competent coarse-grained fragments in close association with metabasite units. Omphacite and Czo statically replace former magmatic augite and plagioclase. Primary cumulate textures are in places well preserved, as are Aug relicts and Act pseudomorphs after Aug in cores of Omp. The peripheries of metagabbro bodies are often intensely sheared; Omp is, in such cases, typically replaced by Gln (Plate 2A). Locally, metagabbros are truncated by metaplagiograntic dikes (Plate 2B). Metagabbro fragments are largest and most abundant in the Kampos and Kini metabasite units, in places forming continuous bodies at a scale of several hundreds of meters, but much smaller and rarer in the metabasite units at Charassonas, Chroussa, and Mana (see Map 1). Generally, smaller metagabbro units are less well preserved and more intensely sheared, and primary magmatic fabrics are often completely destroyed.

### 2.8.3 Metavolcanics of Kampos

The metavolcanics of the Kampos mafic belt comprise a bimodal suite of mafic Gln + Omp + Grt + Czo and felsic Jd + Qz  $\pm$  Pg  $\pm$  Czo rocks. In places (e.g., Grizzas and Kalogeros), proximal volcanic breccias with primary magmatic depositional features are well preserved (Plate 2C), grading laterally into a belt (north of Kampos) of highly deformed equivalents with irregularly shaped intermingled mafic and felsic bands and enclaves (Plate 2D). The latter are probably a distal, perhaps more ductile tuffitic facies of the same lithologies, but similar-looking rock types may also occur in the Kampos area, possibly representing volcanoclastics derived from a different, possibly Triassic source (Bröcker and Keasling, 2006). Highly abundant and prominent in the Kampos area,

small occurrences below the scale of our map also occur in the metabasite units of Mana, Hermoupolis, Charassonas, and east of Chroussa.

### 2.8.4 Mn-Rich Metasediments

The distribution of these lithologies is usually confined to outcrop-size, with a lateral continuity of no more than a few tens of meters. Mn-rich rocks occur as thin, extremely fine grained, chert-like layers of former hydrothermal Mn-rich ocean-floor deposits, in close proximity to metabasite and mafic tuffitic schist. In a schist matrix, manganese deposits are usually s-parallel Sps  $\pm$  Gln aggregates with no or very low content of Qz (see Plate 2F) occurring as stacked layers and rootless intrafolial fold hinges. Whole-rock geochemistry of these rocks shows an enrichment in FeO and MnO (24–33 wt% combined, with MnO reaching 20 wt%) and a low SiO<sub>2</sub> content of ~40–50 wt%. In mafic blueschists and metabasites, lenses and layers of Sps-Gln and Sps-Omp indicate manganese enrichment. Very rarely, in calcitic marbles, irregular patches of strikingly bright-red Pmt + Grt + Pg + Cal  $\pm$  Qz felses with Mn oxides can be observed (Plate 2G). The petrographical variability of the various manganese-rich rocks suggests that their chemistry is controlled by the local depositional environment. Manganese-rich spessartine felses and piemontite-rich aggregates also occasionally occur as lithoclasts in the metaconglomerate at Palos Peninsula, in the northwest of Syros.

## 2.9 Felsic Paragneisses of Mavra Vounakia

A large proportion of the lowest part of the structural pile (the Mavra Vounakia peninsula in the southwest of Syros) consists of fine- to medium-grained Ab + Qz + white mica-bearing paragneisses (Hecht, 1985) with a widely spaced, but sharply parallel foliation. Occasionally, the paragneisses bear intercalations of conglomeratic, thin carbonatic, as well as quartzitic layers. In places, small slices of Kfs megacryst orthogneiss are intercalated in the Mavra Vounakia succession. Tomaschek et al. (2008) showed that zircons in these orthogneisses yield U-Pb ages of  $315 \pm 3$  Ma and identified them as relicts of Variscan basement.

The entire southwestern peninsula of Syros is strongly affected by late-stage (post-tectonic) hydrothermal fluids. Hydrothermal activity is indicated by patchy silicification, massive, up to 3-m-thick quartz veins precipitated along faults and fracture systems, as well as crosscutting, near monomineralic Ab and/or Tur veins and impregnations. Further products of late-stage hydrothermal activity are Fe-oxide ores, which precipitated preferentially in or near the thin marble layers intercalated in the Mavra Vounakia succession (see Map 1). The strong hydrothermal activity is possibly caused by a subsurface granitoid intrusion below the south of Syros (Ballhaus et al., 2001), possibly related to the Miocene episode of granitoid intrusions in the Aegean (e.g., Altherr et al., 1982; Altherr and Siebel, 2002; Skarpelis et al., 2007).

## 2.10 Gneisses of Vari and Mylonitic Chlorite Schists of the Vari Unit

The Gneisses of Vari predominantly comprise Ab + Ph + Ep + Bt + Qz-bearing trondhjemitic orthogneisses. A granodioritic variety (e.g., on Phokia peninsula) shows the assemblage Amp (Prg-Ts) + Ab + Ep + Ph + Qz ± Ttn-Ilm (Table 1). A closely spaced mineral foliation is commonly overprinted by a widely spaced, steep foliation, superimposing on the gneiss an L-tectonite fabric. Fold axes and L-tectonite fabric generally dip to the northeast. Along its peripheries, the Vari gneisses are intercalated with slices of mica schist, amphibolite, and carbonate. We interpret these intercalations as possible relicts of original country rocks. Along the eastern coast at Azolimnos is preserved what could be interpreted as a former intrusive contact (Bonneau et al., 1980a), i.e., meta-aplitic veins interfolded with Ep-amphibolite, suggesting that gneiss and amphibolite schist selvages are part of one single tectonic unit.

Amphibole chemistry suggests that the metamorphic overprint did not exceed epidote-amphibolite-facies metamorphism (Ridley, 1982a; Tomaschek et al., 2000b). High-pressure metamorphic mineral relicts are not observed. Along fractures, faults, and toward its margins, the gneiss may be retrogressed to greenish Chl-Ep-Act-bearing varieties.

The periphery of the Vari Unit is composed of mylonitic schists and phyllites. The main assemblage is Chl, Act, Ab, Czo,

and white mica, with occasional serpentinites (e.g., on the ridge northeast of Vari Bay). The structural position of the Vari Unit in regard to the blueschist sequence is obscured by late faulting and thick alluvial cover.

## 2.11 Andesitic Volcanic Rocks

The occurrence of postmetamorphic volcanic rocks on Syros is confined to small outcrops near the south coast between Posidonia and Vari (see Map 1). Exposure of the volcanic rocks is rather poor due to thick alluvial cover and intense disruption by late-stage faults, and very little can be confirmed about their actual extent, or if there is any preferred intrusion orientation. The volcanics consist of a fine-grained matrix of mainly Pl + Hbl (as porphyroblasts) + Cpx and minor Qz, Bt, and Rt. Secondary Ser and Cal are abundant (Plate 1F). According to bulk-rock chemistry, they are andesitic to latitic in composition (Table 1). No radiometric age information is available, but there is no reason to assume that their origin markedly differs from that of other dike occurrences in the Cyclades (e.g., on Tinos and Serifos; Pe-Piper and Piper, 2002). Therefore, the intrusive rocks on Syros are considered Miocene in age, possibly similar to dacitic dikes on Tinos for which Avigad et al. (1998) determined K-Ar ages of 11.5 Ma. While common on other Cycladic islands, the existence of unmetamorphosed volcanic dikes has as yet been unknown on Syros.



## *Lithostratigraphy and Indications for Primary Associations in the Cycladic Blueschist Unit on Syros*

In a blueschist- to eclogite-facies terrane like the Cyclades, it is not easy to establish constraints on potentially primary stratigraphic features. Polyphase metamorphism and intense deformation of the rocks have largely destroyed sedimentary structures and primary magmatic fabrics. Identifiable fossils are not preserved either. Any attempt at correlation, especially of metasedimentary units, where conclusive radiometric age indications are not available, therefore invariably suffers from a high degree of uncertainty. In order to unravel possible genetic relations among the different rocks within the Cycladic Blueschist Unit on Syros, and to be able to estimate whether they have been primarily in close proximity to each other or not, we have conducted detailed stratigraphical recordings. This chapter presents an overview of our observations and their implications for the geological evolution of Syros.

### **3.1 Comparison of the High-Pressure Metabasite Occurrences**

Virtually all geochemical and geochronological information on Syros has been derived from the Kampos metabasite belt in northern Syros. There is now general agreement that U-Pb zircon ages of ~80 Ma, determined from metaigneous rocks, define the emplacement age of the magmatic protoliths within a Cretaceous oceanic crust (Keay, 1998; Tomaschek et al., 2003; Bröcker and Keasling, 2006; Fu et al., 2010). The different bodies of high-pressure metabasites on Syros show variations in their lithological assemblage. The Kampos metabasite belt differs from the other occurrences in that metagabbros, bimodal metavolcanics, and serpentinites are the most prominent rock types. In the other metabasite units, massive eclogites and mafic blueschists dominate the map picture (see Map 1). Nevertheless, all lithologies that can be found in the Kampos belt are present in the other well-preserved, high-pressure metabasite units as well, albeit in much smaller volumes. Metagabbros and bimodal metavolcanics occur as lenses and are often strongly sheared. Serpentinites and talc schists are often highly attenuated, and represent zones of weakness, along which most of the prograde and retrograde deformation probably has taken place. The different metabasite occurrences are therefore most likely genetically related, their different rock assemblages probably representing primary lateral or vertical variations along the former oceanic crust.

### **3.2 Manganese Mineralizations and Their Stratigraphical Significance**

Manganese mineralizations represent former hydrothermal deposits in an active ocean-floor environment (e.g., Neubauer et al., 1989). For Syros, this means that they are primarily linked to the magmatic activity on the Cretaceous ocean floor. As such, they occur mostly within the various metabasite units. In many cases, though, premetamorphic and predeformational manganese precipitates, now preserved in the form of spessartinites (Plate 2F), also occur within the metasedimentary sequence (e.g., north of the Kampos belt) west of Syringas or at the base of a thick marble unit northwest of Hermoupolis. Furthermore, in rare instances, manganese-rich mineralizations can be observed as reworked lithoclasts in metaconglomerates, such as in the metaconglomerates of Palos. Together with the abundant occurrence of mafic layers, manganese mineralization indicates that sedimentation and magmatic activity were at least partially contemporaneous.

The striking conclusion of the observed interleaving between primary Cretaceous ocean-floor deposits and the sedimentary stack is that large parts of the sedimentary protoliths most likely have a maximum age of ~80 Ma. Some, like the conglomerates, are perhaps even significantly younger, depending on the time assumed to rework the hydrothermal precipitates as lithoclasts in a debris flow.

Regional evidence supports our lithostratigraphic conclusion that large parts of the metasediments of the Cycladic Blueschist Unit on Syros are likely to be Upper Cretaceous in age. So far, metasediments from Syros have been regarded to be dominated by detrital zircon populations of Triassic age (Keay, 1998; Tomaschek et al., 2000a; Bröcker and Keasling, 2006). However, Keay (1998) also described evidence for detrital zircon of Upper Cretaceous age from a metaquartzite at Syringas. Extensive populations of Upper Cretaceous (~80 Ma) magmatic crystallization age have recently been documented in detrital zircons from metasediments within the Cycladic Blueschist Unit on the neighboring island of Tinos (Gärtner and Bröcker, 2007; Bulle et al., 2010).

### **3.3 Stratigraphic Elements in the Marble-Schist Sequence**

The correlation among strongly deformed and metamorphosed metasediments is especially challenging, particularly

when no conclusive geochemical or provenance information is available. In order to test if the marble-schist successions of the Cycladic Blueschist Unit forming the main part of Syros Island are to be regarded as sequential, we conducted detailed lithostratigraphical recordings. We identified a conspicuous assemblage of metasedimentary rocks that shows a combination of several notable features and thus represents a much better stratigraphical marker than any single lithology. Ridley (1982a) already postulated that the marble-schist succession in the central part of Syros represents local tectonic repetition. Detailed mapping allowed us to make similar observations on the island scale.

The base of the newly identified marker succession consists of pale calcite marble with variable proportions of dolomitic layers or boudins (Fig. 7). A very distinctive blue or blue-gray marble with resistant, centimeter-thick, chert-like quartz layers overlies the pale dolomite-bearing marble. The top of the pile

is marked by a 2–5 m thick albite-bearing quartzite, often separated from the marbles below by a thin layer of metasedimentary schists. This close association of several eye-catching lithologies gives a satisfying degree of confidence when applied as a stratigraphic marker.

The above described marker succession can best be observed at its type locality, on the southern slope of the windmill hill southeast of Syringas village. It can also be found at several other localities, such as along strike near Chalandriani, in the central part of Syros E of Kini-Delphini, on the peninsula north of Galissas, and on Charassonas (see map inlay in Fig. 7). Partly preserved, numerous outcrops can be identified all over Syros, at all structural levels, clearly indicating that considerable repetitions within the marble-schist unit occur. Furthermore, the Syringas succession is never encountered overturned but in all cases sequentially repeated, with

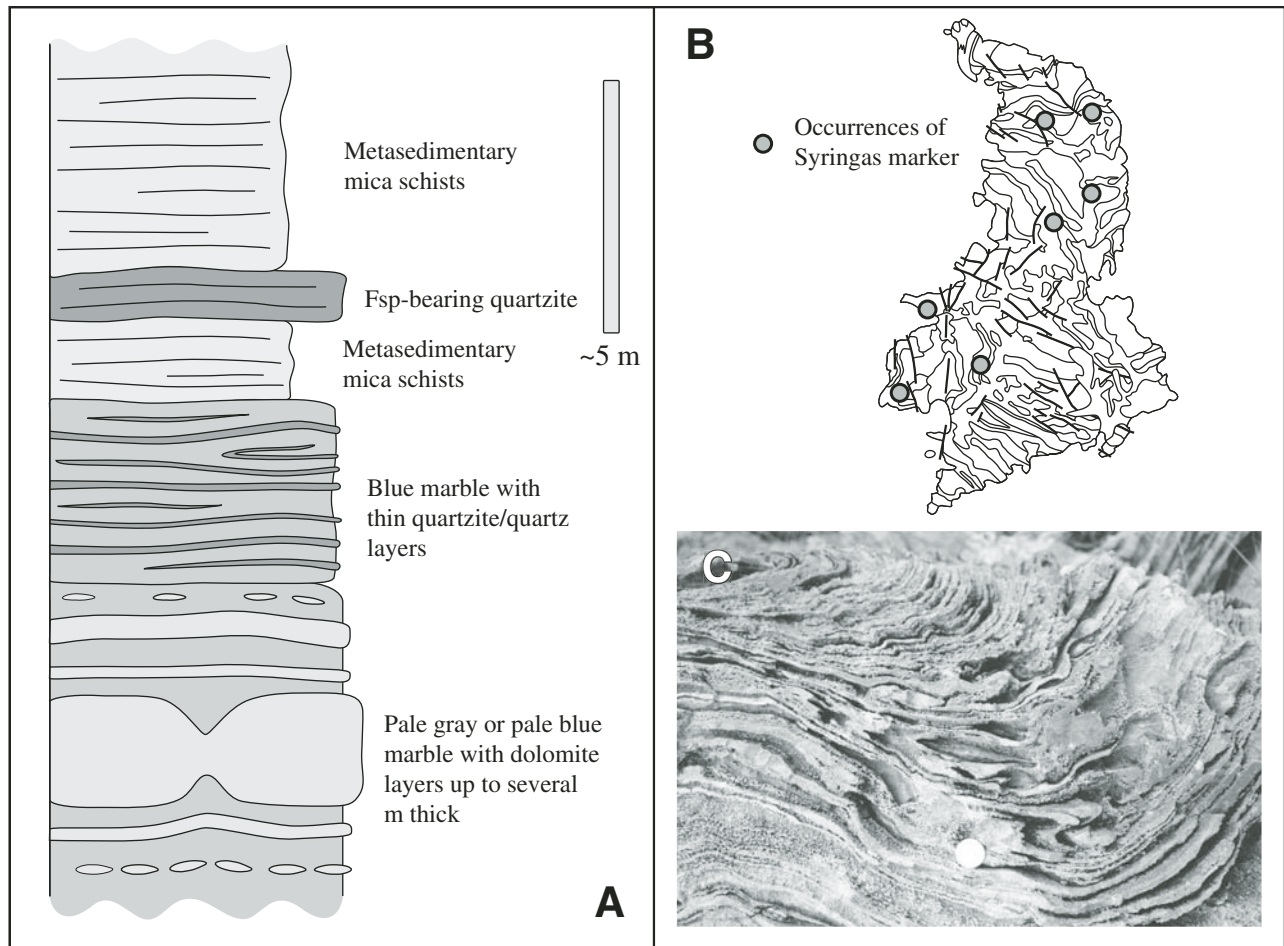


Figure 7. The Syringas marker succession. (A) Lithological characteristics of the succession. From bottom to top: dolomite-bearing pale marble, blue marble with cm-thick chert-like quartz and/or quartzite layers, feldspar-bearing quartzite. (B) Overview map of Syros. Filled circles mark occurrences where the marker lithologies are preserved complete and undisturbed. Incompletely preserved parts of this horizon can be observed in many locations throughout the whole structural pile. (C) Field photograph showing the typical appearance of chert/quartzite-bearing marble in the Syringas horizon.

dolomitic marble at the base and quartzite at the top. This has two major implications: First, the close association of the Syringas marker succession is most likely a relict of a primary sedimentary sequence, and second, a mirrored redoubling of the metasedimentary units by large km-scale folding (Bonneau, 1980b) appears unlikely. In this regard, we follow Ridley (1982a) and Dixon and Ridley (1987), who already postulated that Syros constitutes an imbricated sequence rather than a series of intact megafolds.

Originally, the sequence may have developed as a series of kilometer-scale, highly asymmetric folds, because they are present, for example, on the island of Andros (Papanikolaou, 1978; Avigad et al., 2001; Ziv et al., 2010). If megafolds existed on Syros, their short limbs and hinge zones have been widely suppressed or destroyed in the course of progressive deformation. Theoretically, it is also possible that these repetitions represent an island-scale primary sequence. Considering the intense deformation observed throughout the island, and especially the repeated inclusion of metabasites into the rock pile, we do not regard this possibility as likely and strongly favor a tectonic origin of the repeated stratigraphy.

### 3.4 Metaconglomerates and Quartzites—Their Significance as Stratigraphic Markers

Metaconglomerates preferably occur at the base of thick marble units and as such may indicate a sedimentary and/or primary stratigraphic relict. Their individual characteristics, like preferred clast composition, are too indistinct to be used as reliable markers for island-wide correlations. The conglomerate at Palos is unique in this regard, because on Palos, conglomerates show lateral gradation into almost clast-free carbonatic schists, calcisilicate felses, and marbles (see Map 1). The field relations on Palos indicate that primary sedimentary relations, such as channel fills or sequential submarine debris flows, may have in places survived the intense deformation that accompanied burial and exhumation of the rocks.

As described in the lithology section (Chap. 2), quartzites potentially show relicts of primary sedimentary features, such as lens-shaped outcrops (possible psammitic channel fills) and gradation into garnet-bearing paragneisses (lateral facies changes). As isolated stratigraphic indicators or markers, however, they are unreliable, apart from cases where they are closely associated with other distinctive lithologies (see Chap. 3.3).



In summary, all these observations indicate that despite strong deformation and metamorphic overprint, the rocks of the Cycladic Blueschist Unit on Syros have retained numerous primary relations that can provide information on the depositional environment. The base of the rock pile is represented by the Mavra Vounakia supracrustal-metabasite assemblage, in which relicts of Variscan basement are preserved, followed by a series

of metasedimentary schists and greenschists with frequent, relatively thin, marble intercalations. Above these units follows a multiply repeated assemblage of schists, thick marbles, metabasites, and meta-ultrabasites (former oceanic-crustal succession—gabbros, cumulates, dikes, pillow relicts, and hydrothermal sediments), quartzites, and banded tuffitic schists (Fig. 8). Magmatic and hydrothermal deposition is partially interleaved with the metasediments, indicating that the complete rock pile, including the gneiss-metabasite succession of Mavra Vounakia, has primarily developed in relatively close proximity during the

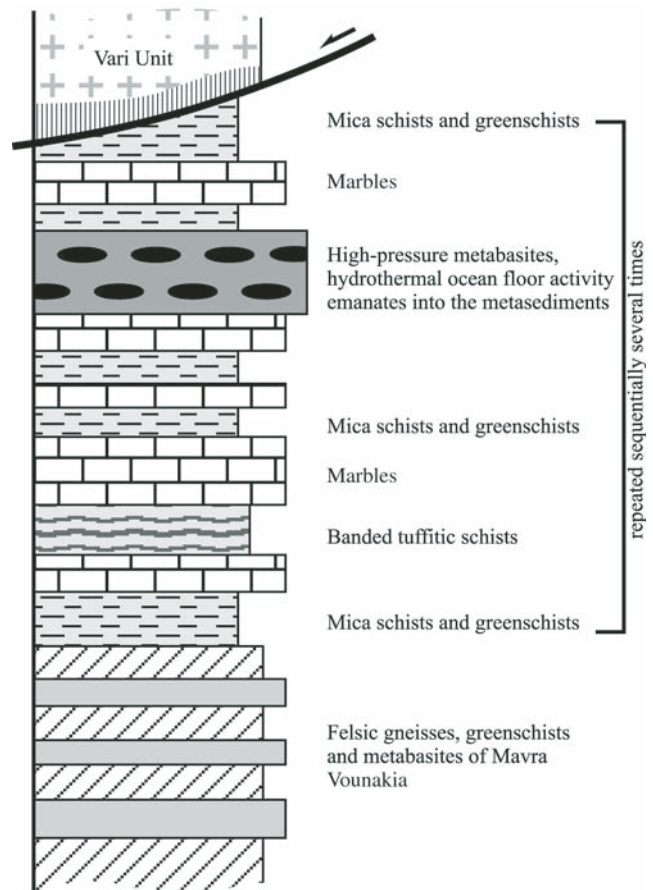


Figure 8. Condensed lithostratigraphical column of the rocks of Syros. Cycladic Blueschist Unit, from bottom to top: Felsic gneisses of Mavra Vounakia, intercalated with greenschists, small slices of Variscan basement, metabasite blocks, and thin marble layers, strongly overprinted by greenschist-facies metamorphism, but retaining relict high-pressure mineralogy. The following succession of mica schists, marbles, greenschists, banded tuffitic schists, and metabasites is repeated tectonically several times. Preservation of blueschist-facies mineralogy is abundant. Originally hydrothermal Mn and Fe precipitates can be observed in both the metabasite units and the surrounding metasediments, indicating a primarily close association. The Vari Unit is a regionally allochthonous klippe, showing Upper Cretaceous epidote-amphibolite metamorphism. It was emplaced onto the Syros lithological pile along a normal fault in the Miocene.

Late Cretaceous, most likely in a confined backarc environment at the northern margin of the Tethys (see Fig. 9).

Based on geochemical data, a backarc environment has already been proposed for the origin of the magmatic protoliths on Syros and Sifnos (Seck et al., 1996; Mocek, 2001; Lagos et al., 2002). The presence of meta-ultrabasites suggests that at least an incipient oceanic lithosphere was present, even though it may not have been fully developed.

It should be noted at this point that within the Cycladic Blueschist Unit the occurrence of distinct Jurassic oceanic crust is also documented on Andros (Bröcker and Pidgeon, 2007; Bulle et al., 2010), indicating that remnants of additional, older ocean-floor relicts may have been reworked.

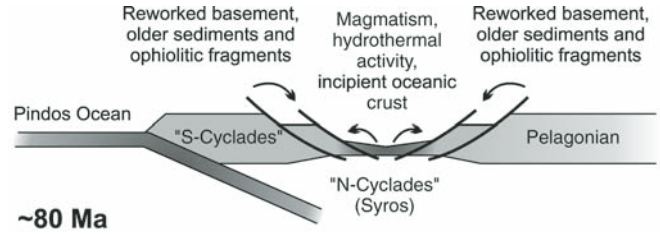


Figure 9. Paleogeographical reconstruction for the Upper Cretaceous, as suggested in this paper. The depositional environment of the protoliths comprises mostly basaltic volcanics, interleaved with clastic sediments and carbonates, as well as reworked remnants of Variscan basement rocks.

## *Structural Evolution of the Cycladic Blueschist Unit— The Example of Syros*

The mapping conducted for this work has yielded new insights into the structural development of the Cycladic Blueschist Unit. The rocks of the Cycladic Blueschist Unit on Syros were affected by several ductile deformation phases, as well as by a variety of transpressional and extensional deformation events. The latter are restricted to the late- to post-metamorphic part of the PT evolution. To deliver a framework, the following section broadly follows Keiter et al. (2004a), adding modifications where up-to-date observations from the field have become available. There are, of course, contrasting views about the structural evolution of Syros, especially concerning the timing of events and the question of whether exhumation has been accompanied by widespread deformation or not. These questions will be addressed later in this paper.

### **4.1 Prograde to Peak Metamorphic Deformation History**

#### **4.1.1 Tight to Isoclinal Prograde Folding Event D1**

The earliest discernible deformation phase on Syros, D1, is characterized by intrafolial isoclinal shear folding. Preservation of intact D1 fabrics is scarce, due to the strong overprint by a later penetrative deformation event D2 (see below), which has strongly reoriented or destroyed D1 structures. F1 fold relicts are preserved as rootless centimeter- to decimeter-sized intrafolial fold hinges in primary SiO<sub>2</sub>-rich layers such as metamorphic quartz segregations or chert-like spessartinites (regarded as s0; see Keiter et al., 2004a). In places, F1 fold relicts can be found in marbles as well, where they are identifiable as refolded “fuzzy” color banding (Fig. 10). The D1 fabrics most likely developed on the early burial path.

#### **4.1.2 Prograde Folding Event D2**

This deformation event generated the penetrative fabrics on Syros, including isoclinal intrafolial F2 shear folds and a penetrative axial plane-parallel s2 foliation (Fig. 11). Folds of the F2 generation display a distinctly different orientation than the relict F1 folds, and therefore indicate a change in the stress field during burial. Keiter et al. (2004a) have shown that the frequently observed significant spread of fold-axis orientation is the result of superposed folding—in outcrop and on a regional scale, i.e., relict F1 fold hinges reoriented systematically by S-vergent simple

shear F2 folds. A sketch of the island-wide trend of F2 fold axes is shown in Figure 12.

The largest observable F2 folds have amplitudes of several hundreds of meters (Fig. 13). The preservation of larger, intact, km-scale fold structures can be largely excluded, based on the observation that lithostratigraphical details are sequentially repeated. Progressive deformation in the course of D2 led to intense thrusting and multiple tectonic repetition of the ocean-floor sequence and the associated metasediment series in the central part of Syros (see Chap. 3). The thrust planes are oriented roughly parallel to the axial planes of the F2 folds and frequently show signs of late-stage brittle reactivation. The D2 deformation event took place on the prograde PT path and was, according to Keiter et al. (2004a), largely completed at the time of peak metamorphism. Recently though, Schumacher et al. (2008) have reported indications that the D2 deformation might have continued slightly beyond peak metamorphism into close-to-peak retrograde conditions (see Chap. 4.4.2).

**Open folding D2b.** A peculiar fabric is preserved in the high-pressure metabasite occurrence at Kini, and especially in the Mana metabasite south of Hermoupolis and in the banded tuffitic schists north of Azolimnos (see Map 1 and Fig. 14). At these localities, especially in less competent lawsonite



Figure 10. Relictic D1 fabrics in marbles 150 m east of Vari beach. Fuzzy color banding reflects an older fold generation, otherwise largely destroyed in highly ductile carbonatic lithologies.

blueschists, frequent outcrop-scale folds can be observed. Often, they show a class 1C or class 2 profile (cf. Park, 1989) and have a generally (but not always) steep fold axial plane and interlimb angles between  $100^\circ$  and  $50^\circ$  (see Plate 1E). Their fold axes generally dip gently toward the ENE ( $60^\circ$ – $70^\circ$ ). They refold the penetrative s2 cleavage, and where pseudomorphs after lawsonite are present, these are deformed on the limbs of the folds (Fig. 15). An axial plane-parallel cleavage is, if at all, only very weakly developed. No trace of dynamic greenschist-facies recrystallization can be observed, which points toward a high-pressure origin of these folds. Since lawsonite pseudomorphs are distorted by folding, but blueschist-facies parageneses are undisturbed, these folds must represent a close-to-peak deformation event, early on the retrograde path (see Schumacher et al., 2008 for a detailed discussion). To maintain consistency with the frame of deformations by Keiter et al. (2004a), this event is indexed as D2b here.

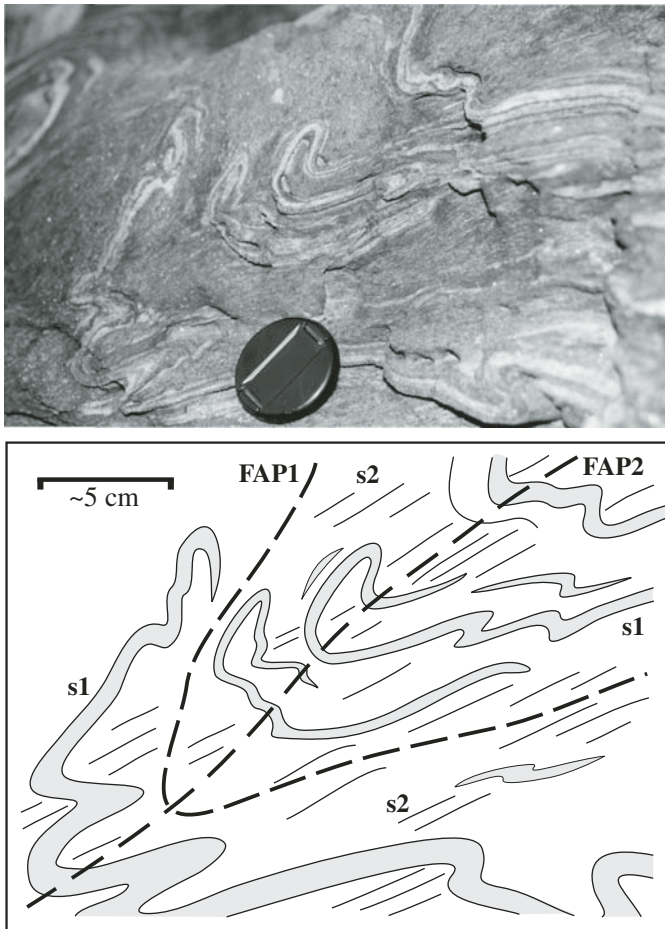


Figure 11. Spessartinites, north of Lia beach, showing two generations of isoclinal folds, looking roughly down the F2 fold axis. Note the refolded F1 fold hinges in the center of the photograph. An s2 cleavage is well developed in the mica-rich schistose matrix, parallel to the axial plane of F2 (running from top right to lower left).

## 4.2 Retrograde Deformation History

### 4.2.1 Early Retrograde Extension during Exhumation

In places, well-preserved blueschist-facies rocks on Syros show extensional fabrics most likely related to the early retrograde path close to peak metamorphism. Bröcker et al. (2010) described localized domains of shearing in schists of the Kampos mélange, yielding Rb-Sr ages of 49–42 Ma under epidote-blueschist-facies conditions. Similar conditions are inferred for rare, small-scale, ductile, high-pressure normal faults (see Plate 2H). Serpentinites and talc schists in the Kampos mélange have in places been disrupted into lensoid slices (see Chap. 2.8 and Plate 2E), although this fabric cannot unambiguously be attributed to close-to-peak deformation and may have developed later on the exhumation path. The Kampos contact was probably reactivated as normal fault (Trotet et al., 2001a), but not with lithospheric-scale displacement (see Chap. 4.5.2 below). Late, brittle overprint along the base of the Kampos metabasite belt may have obscured earlier fabrics, though subordinate, outcrop-scale imbrications along the contact indicate thrust sense of shear for the brittle overprint (Keiter et al., 2004a). For further descriptions of extensional structures, see also Bond et al. (2007).

### 4.2.2 Kink Folding and Crenulation D3

Deformation 3 was a semiductile to brittle phase of contraction that produced upright to slightly vergent kink folds F3 and locally a closely spaced crenulation cleavage s3 (Fig. 16). The crenulation cleavage is almost entirely confined to ductile lithologies like metapelites or talc schists. The D3 deformation occurred on the retrograde path. Greenschist-facies albite layers are commonly affected by crenulation and kink folding, suggesting that D3 was an episode of horizontal shortening on the retrograde exhumation path, within the stability field of albite (see also Fig. 6C in Keiter et al., 2004a).

## 4.3 Postmetamorphic Deformation History

As yet, the young brittle tectonics affecting Syros Island have received comparatively little attention. Only sporadically, detailed investigations have been conducted on the systematics of faulting on Syros (e.g., Lazarus, 2004). In this context, an important result of our mapping work is that the young brittle deformation history on Syros was much more vigorous than previously indicated (Fig. 17). Since the ductile-brittle transition, which in the Cycladic area is generally placed in the upper Miocene between  $\sim 13$  Ma and  $\sim 8$  Ma (e.g., Lee and Lister, 1992; Boronkay and Doutsos, 1994; Ring et al., 2003), the rocks of Syros were affected by several contractional deformation events. These episodes cannot easily be placed into a reasonable age succession. Clear relative relationships between certain fault and brittle fold orientations do not exist or are ambiguous. This means that the brittle deformation fabrics are either contemporaneous, or their relative age relationships have been obscured by repeated reactivation of preexisting structures. The latter is likely, because the

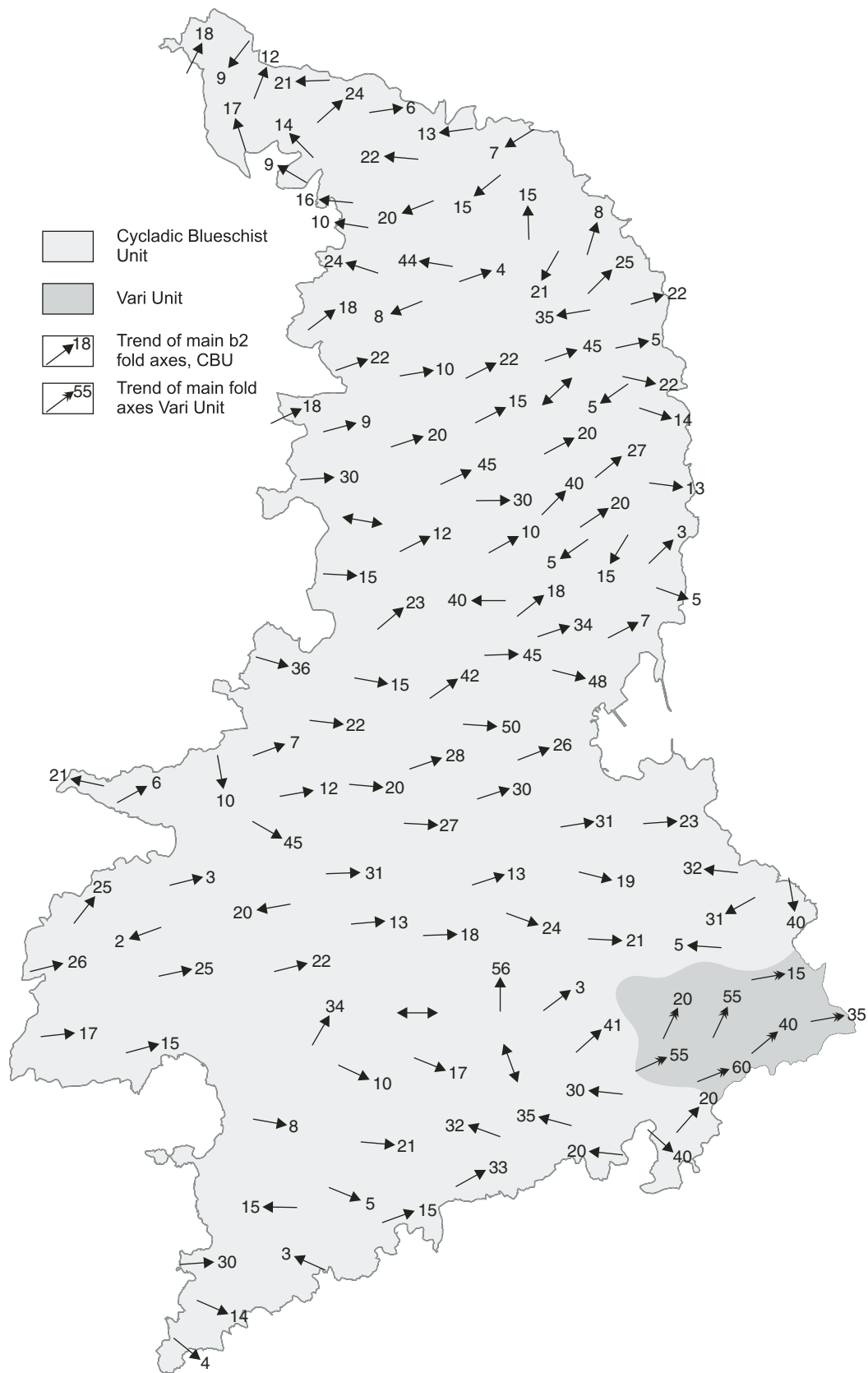


Figure 12. Overview map, showing the trend of main isoclinal intrafolial F2 fold axes on Syros. Darker gray shade indicates the approximate extent of the allochthonous Vari Unit. Folds within the Vari Unit generally show a steep axial plane and steeper dip of fold axes.

whole eastern Mediterranean has been very active tectonically in the recent geological past (Goldsworthy et al., 2002).

#### 4.3.1 Faults

Systematic mapping of fault patterns unveiled a significantly different picture of Syros compared with previously published maps. For example, we cannot confirm the large-scale nappe architecture postulated by Hecht (1985), and depicted in his geological cross sections. A large proportion of the geological boundaries on Syros are rather controlled by a complex system of late-stage steep faults that are often concentrated along domains of wrench shear (Fig. 18). Many of the fault surfaces show a significant component of horizontal strain, up to pure strike-slip movement, indicated by Riedel shears and coarse slickensides (Fig. 19).

Strike-slip faults, already postulated by Ridley (1982a) and described for the north of Syros by Keiter et al. (2004a), turned out to be a widespread feature in the late-stage structural inventory of Syros. Best observed in the southern part of Syros, en echelon arrays of strike-slip faults delineate regional zones of wrench shear, strongly influencing the geological architecture. Faults are in places so closely spaced that hardly any primary

lithological (i.e., D2 related) contacts are preserved. In the map of Hecht (1985), many lithological units are mapped in a way that suggests large-scale layering, while in fact the orientation of the regional foliation is markedly different. One striking example is shown in Figure 20. Detailed mapping of a marble unit south of Ano Mana, depicted by Hecht (1985) as a concordant ESE-WNW-striking horizon, revealed that the contacts are strongly controlled by late-stage faulting, and the regional foliation in fact dips NE to E—a discrepancy of 90°.

A good example for the possible offset along strike-slip faults can be observed at the west coast of the Mavra Vounakia peninsula in the S of Syros. The small islands offshore the Mavra Vounakia peninsula consist mainly of marble (see Map 1). Such thick and massive marbles are not found so far south on the Syros mainland, where the Nites ridge marks the southernmost outcrop of massive marble units, along a line between Finikas and Vari. Lateral offset along this prominent sinistral Finikas-Galissas fault zone (cf. Ridley, 1982a), which also displaces the Charassonas peninsula and the peninsula north of Galissas against inland Syros, would be ~2 km maximum, depending on the vertical component. Surfaces of outcrop-scale faults in close proximity to this zone often show subhorizontal striations, suggesting

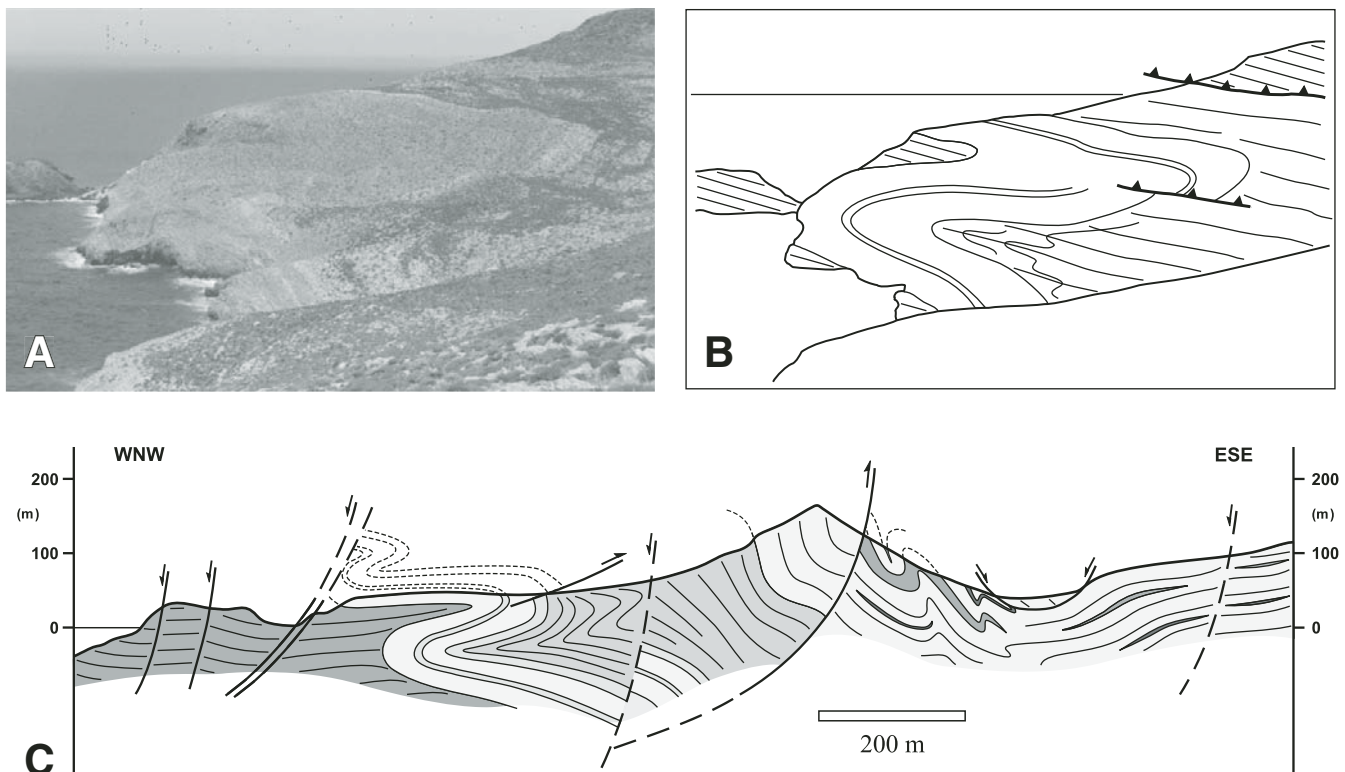


Figure 13. Palos Peninsula, looking north. (A) A laminated marble sequence, preserving the  $s_1$  foliation, is tightly to isoclinally folded. (B) Sketch of the photograph, showing the structural features observed. The schists show a strongly developed penetrative  $s_2$  cleavage. Occasionally relicts of the  $s_1$  can be found in metaconglomerates, cropping out in the core of the fold. Generally, the metaconglomerates are characterized by a spaced  $s_2$  foliation. Fold amplitude is ~300–400 m. (C) Geological cross section of the fold structure shown in (A). Profile extends a few hundred meters to the right over the edge of the photo up to a thin layer of metabasite and serpentinite in the east (see Map 1). Dark gray—schists; medium gray—metaconglomerates; light gray—marbles.

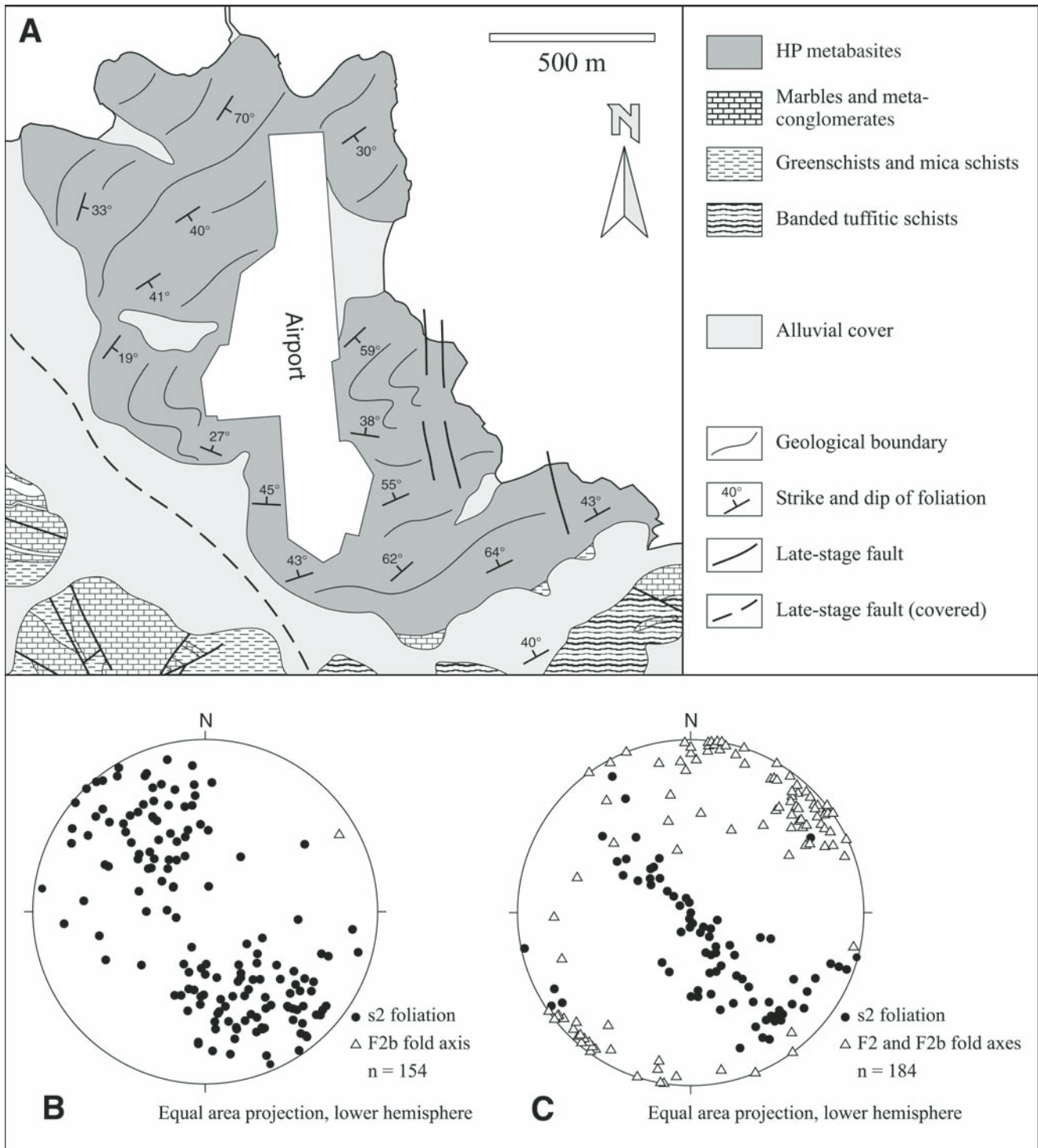


Figure 14. High-pressure (HP) D2b structures and their impact on the geology of Syros. (A) Structural map of the blueschist- to eclogite-facies metabasite body in Mana village, south of Ermoupolis. For location, see Map 1. The rocks, mainly mafic glaucophanites, form a tight, km-scale synform around a northeast-dipping axis; the fold axial plane is subvertical. (B) Stereographic plot of foliation measurements from the Mana metabasite. Interlimb angle of the major synform is  $\sim 60^{\circ}$ – $80^{\circ}$ . (C) Stereographic plot of D2b folds in banded tuffitic schists, coastal outcrop north of Azolimnos village,  $\sim 1$  km southeast of the map depicted in this figure. For location, see Map 1. At Azolimnos, the D2b folds have amplitudes of several dozen meters. The fold axial plane is steep; F2b refolds older intrafolial F2 folds. See also Plate 1E.

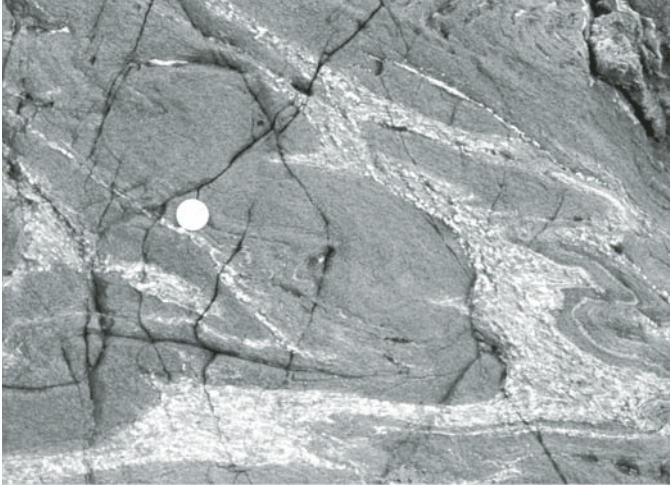


Figure 15. Concentrations of deformed lawsonite pseudomorphs in an F2b fold S of Kini, visible as coarse whitish layers in a darker matrix. Blueschist-eclogite assemblages are otherwise pristine, indicating that folding has taken place close to peak conditions shortly after lawsonite breakdown.

a pure strike-slip sense of shear. A (possibly not contemporaneous) transtensional component likely affected the faults as well, as indicated by the graben structures associated with the Finikas-Galissas fault zone (e.g., the metabasite occurrence north of Galissas; see Map 1).

#### 4.3.2 Postmetamorphic Thrust Slices

In addition to the system of strike-slip faults, locally confined, marble-dominated thrust slices occur as klippen on elevated hilltops, especially in the southern part of Syros (see Map

1). These klippen have not been described in earlier publications, and are investigated here systematically for the first time. The large-scale nappe architecture in the marble-schist sequence as depicted by Bonneau et al. (1980a) and Hecht (1985) could not be confirmed by field evidence, in so far as the actual thrust relicts are much smaller and show a significantly different spatial distribution (see Figs. 17 and 18 and Map 1).

The basal contacts of these thrust slices, if exposed, are subhorizontal to horizontal and are distinctly brittle. They are sharply discordant to the prograde  $S_2$  fabrics, and in places cut off young, steep faults (Fig. 21). Closely associated with the slices, open folds and reverse faults are observed, and schists in the immediate footwalls often show brittle drag folds and crenulation (Fig. 22). It appears that these thrust relicts are very young structures. They may have developed in shallow crustal levels during late (or after) exhumation. Therefore, on the geological map (Map 1), they are distinguished from prograde thrust contacts.

It is unclear if the rocks comprising the thrust slices are regionally allochthonous. There is no reason, though, to assume that their metamorphic history was markedly different compared to the Cycladic Blueschist Unit succession in their footwall, and lithological similarities between footwall and hanging wall point toward a more proximal origin of the slices.

The emplacement process of the marble klippen is also not clear. Keiter et al. (2004b) interpreted the contacts as thrusts. In the context of the common view about the younger deformation history of the eastern Mediterranean, this interpretation seems surprising, because usually the regional tectonic regime is regarded as widely extensional since at least the Oligocene–Miocene (e.g., Jolivet and Patriat, 1999; Jolivet et al., 2003; Ring et al., 2010). It cannot be ruled out that the basal contacts of the

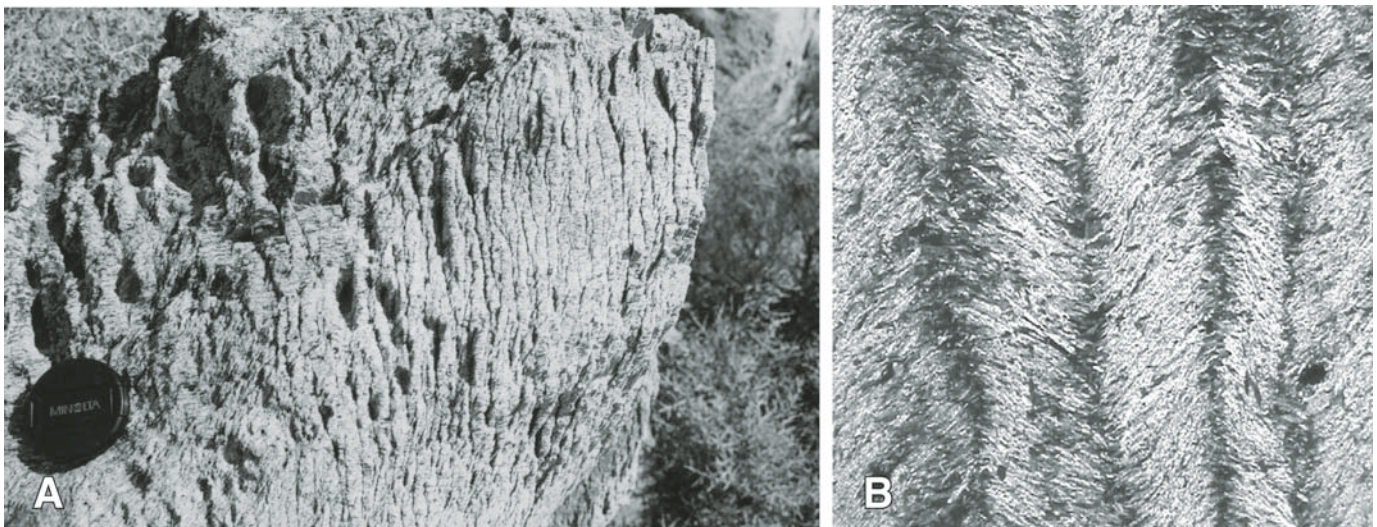


Figure 16. Greenschist facies D3 structures. (A) Albite-mica schists, showing a sharply developed vertical crenulation cleavage, 1 km WSW of Syringas. (B) Thin-section photograph (xpl) of crenulated serpentinite and/or talc schists, Mana metabasite, east of the airport. For location, see Map 1. Distance between cleavage planes:  $\sim 0.5$  cm.

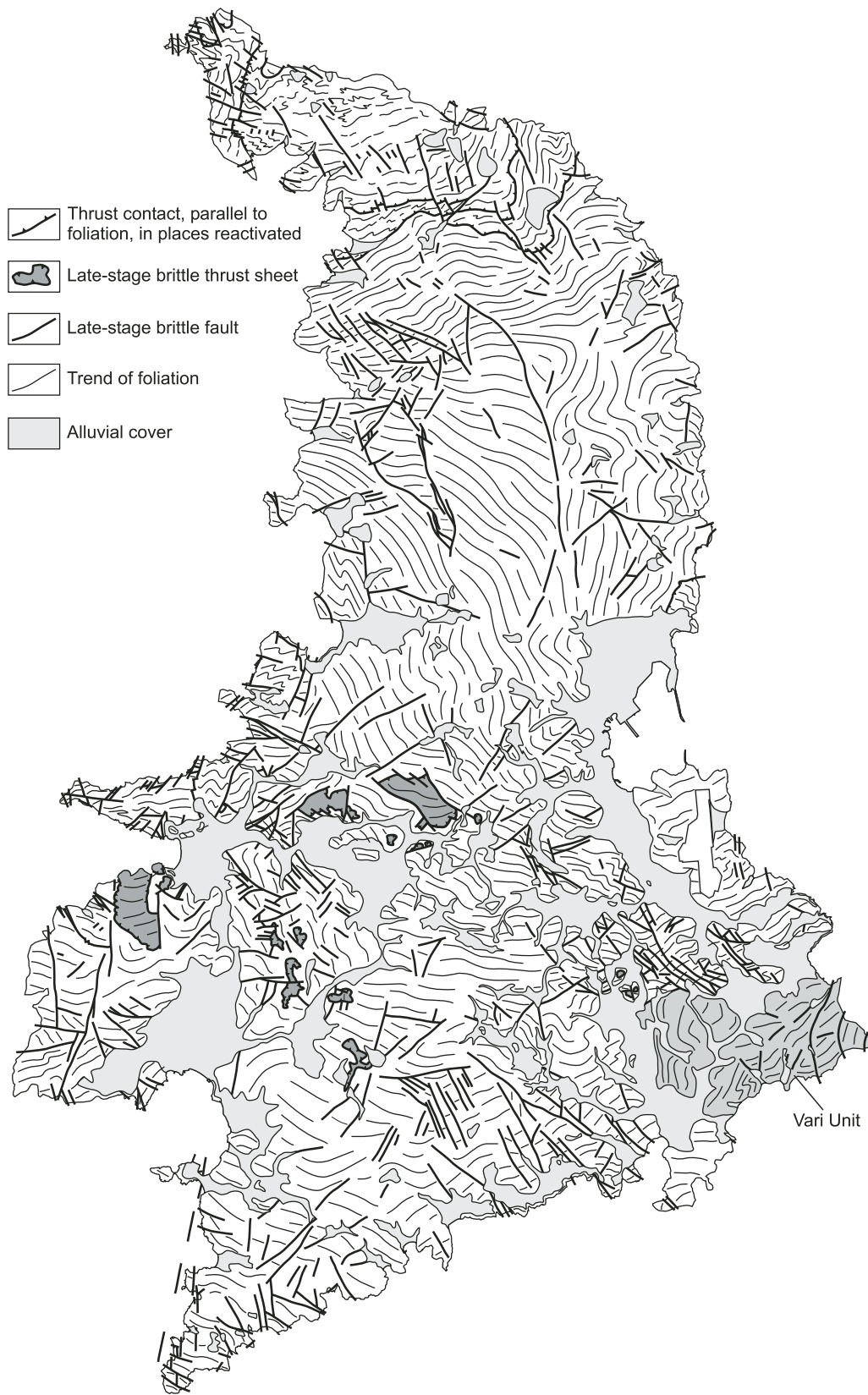


Figure 17. Overview map of Syros, showing the trend of the regional  $s_2$  foliation in the rocks of the Cycladic Blueschist Unit, as well as the penetrative foliation in the allochthonous Vari Unit (shaded in gray). Localized brittle thrust sheets are depicted in gray. The arcuate trend of the regional foliation in the north and west is a result of late-stage open folding (see Fig. 3).



Figure 18. Pattern of late-stage, high-angle faults and horizontal tectonic contacts on Syros. Dark gray—areas dominated by strike-slip wrench shear. Closely spaced, en echelon arrays of strike-slip faults synthetic to the main displacement zones can be observed especially in the WNW-ESE-striking domains enveloping the Vari Unit. Black—thrust slices. Note their close spatial association with strike-slip zones. Double-headed arrows—directions of tectonic transport, derived from striations and drag folds at the base of various thrust slices. The spatial variation in transport direction for the thrust slices is likely dependant on the locally dominating sense of wrench shear. The two dominating strike-slip systems, as well as the trend of major graben structures correspond to a regional regime of SW-NE- to WSW-ESE-directed extension.



Figure 19. Looking downwards on a right-lateral, strike-slip fault directly inland of Azolimnos village. Thick, white lines depict the fault, with remnants of a 20–30 cm thick zone of coarse brecciation in the top left of the picture. The vertical fault surface shows horizontal striations. Black lines delineate well-developed Riedel shears.

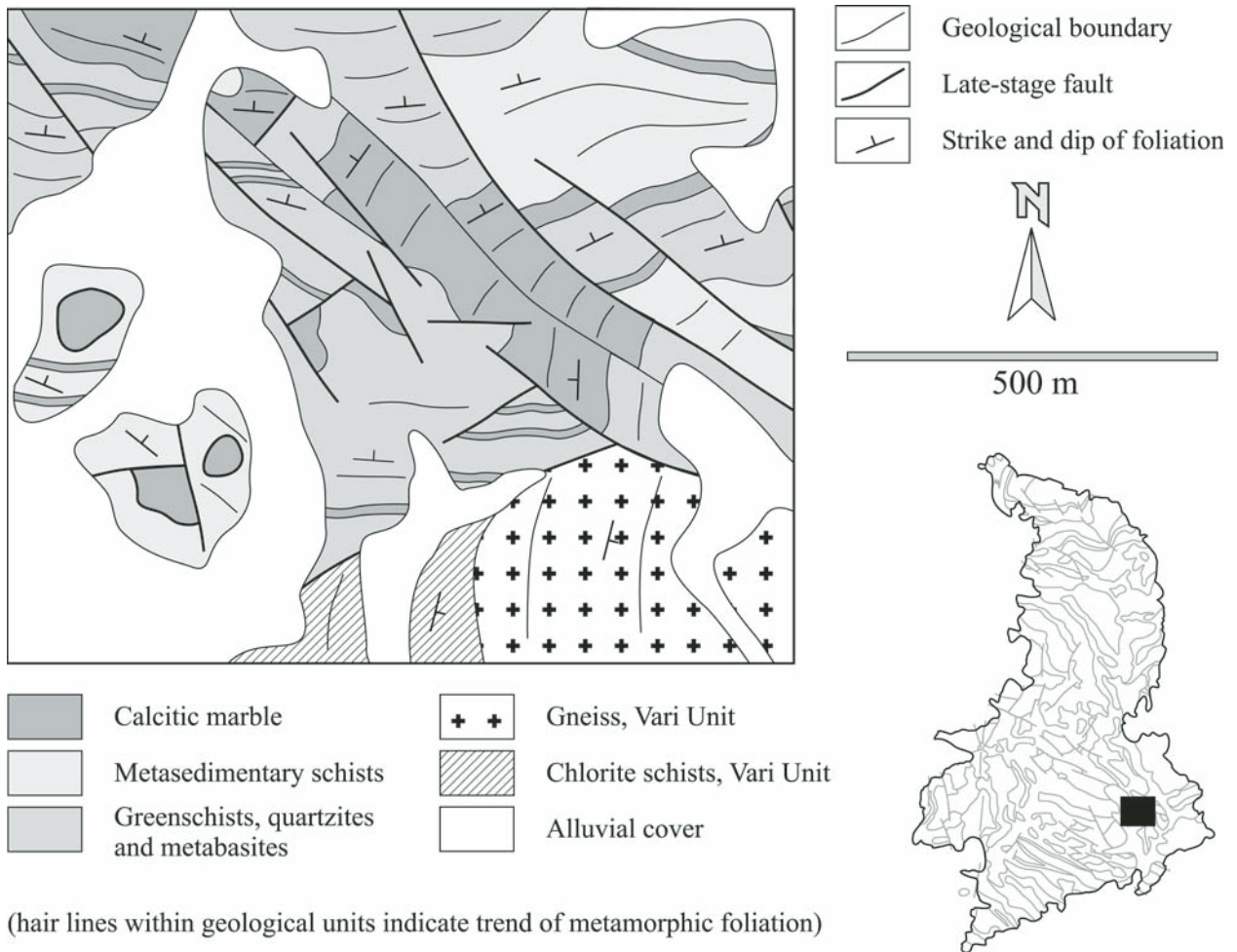


Figure 20. Magnified area from the geological map. The black square in the map inset (bottom right) marks the location. Note the closely spaced system of steep faults, controlling most of the lithological contacts. The marble unit in the center and top left of the map excerpt is depicted by Hecht (1985) as WNW-ESE-trending, layer-concordant horizon. Note also the contact to the Vari Unit, which is characterized by late-stage, high-angle faults.

marbles are low-angle normal faults. It is striking, though, that the occurrence of klippen is almost exclusively confined to the newly identified domains of strike-slip wrench shear (Fig. 18). Furthermore, the transport direction derived from structural features at their contacts (striations and drag folds), shows systematic spatial variations. At the exposed basal contact of a marble klippe in the bay of Galissas, in the vicinity of a major north-south-trending fault zone, a top-to-the-SSE transport is observed. Farther inland, where a WNW-ESE-striking wrench zone dominates, the observed direction of tectonic transport is roughly top-to-the-ESE (see Fig. 18).

As indicated above, the relative age relation between steep faults and horizontal thrust contacts is not uniform. This could point to several stages of reactivation, or to a contemporaneous development of the two fault systems. Together with the spatial and kinematic connection between marble klippen and steep strike-slip faults, we suggest that the latter is the case, and we regard the horizontal tectonic contacts as thrust faults genetically related to transpressional strike-slip zones. They may, however, be just a localized phenomenon, and as such are not in contradiction to the regional NE-SW extensional stress field, as it is established for the upper Miocene to the present (e.g., Kahle et al., 1998; Jolivet, 2001).

#### 4.3.3 Late-Stage Postmetamorphic Folding

In addition to the various brittle fold structures described, e.g., by Ridley (1982a), Hecht (1985), and Keiter et al. (2004a), and the strike-slip systems described above, further postmetamorphic shortening structures can be observed, especially in the southwestern part of Syros. The gneiss-greenschist-metabasite succession of the Mavra Vounakia peninsula is openly folded around NW-SE-striking axes, briefly mentioned by Melidonis and Constantinides (1983; see Fig. 23). Especially where layering is more closely spaced, outcrop-scale folds and reverse faults displaying NE-SW horizontal shortening are common features (Figs. 23A and 23B). The folds show distinctly straight limbs, brittle failure in their hinge zones, and are accompanied by abundant reverse accommodation faults (Fig. 23A). Static quartz veins related to the hydrothermal activity in the southwest of Syros crosscut these fabrics, indicating that the shortening event is at least Miocene in age, possibly between 10 and 15 Ma (see Chap. 2.9).

Orientation and geometry of the brittle folds do not easily fit into the general concept of continuous NE-SW extension since the Oligocene, as commonly postulated (e.g., Jolivet and Patriat, 1999; Jolivet et al., 2003; Kahle et al., 1998). It remains to be verified if they represent a localized event or if indications

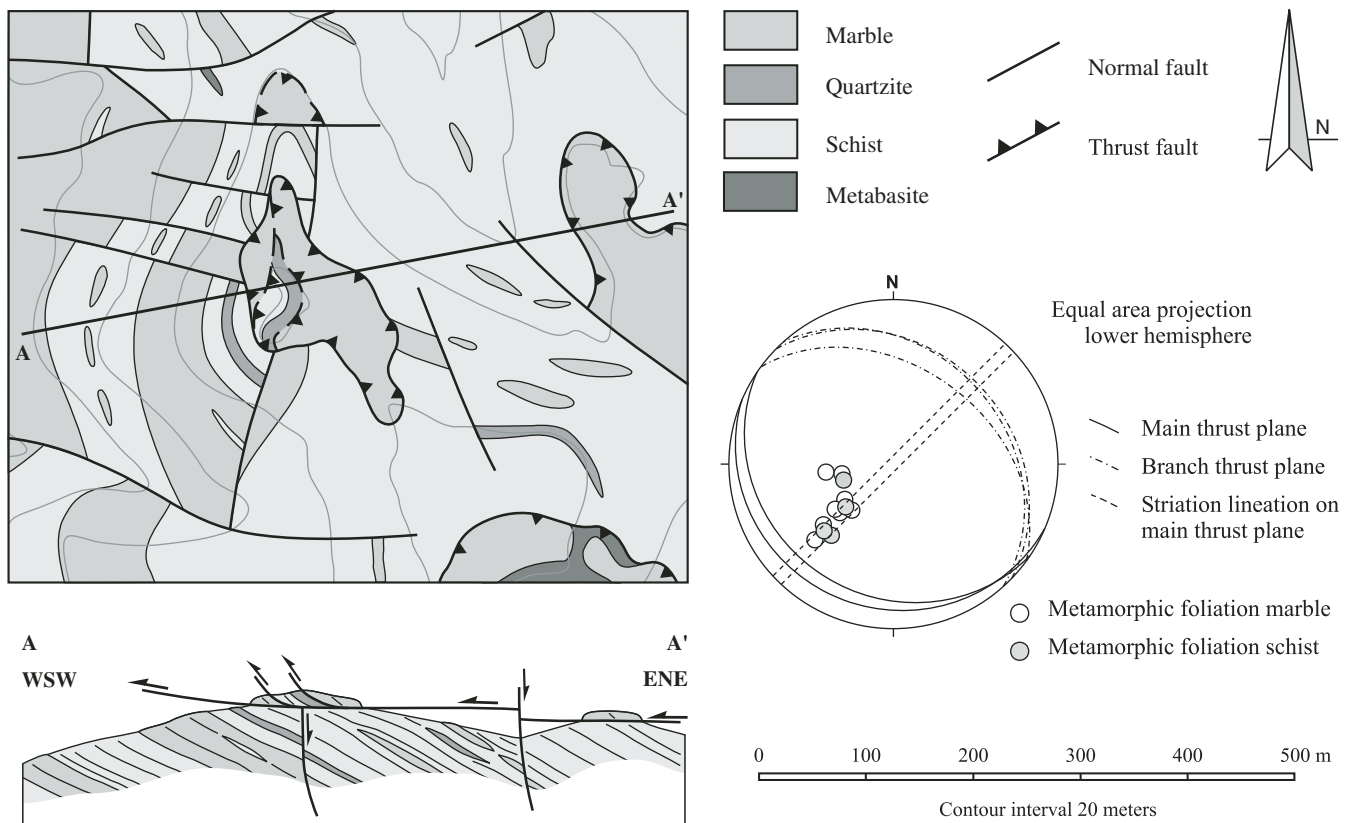


Figure 21. Map view, cross section, and measured structural data of a thrust sheet ~1.5 km southeast of Galissas (for location, see Map 1). The horizontal tectonic contact is most likely contemporaneous with the high-angle faults. Striations on the basal contact plane indicate a NE-SW-directed transport for this location.

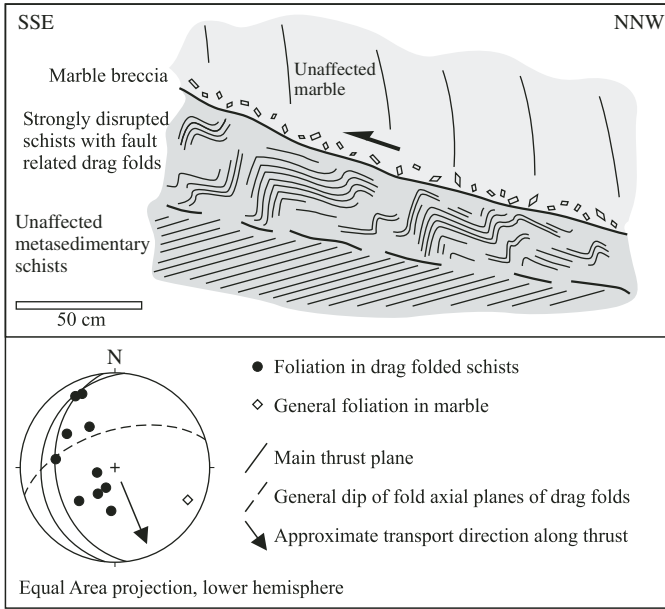


Figure 22. Basal contact of a marble-dominated thrust slice below the chapel on the southern side of Galissas bay. The base of the marble is brecciated; the mica schists in direct proximity to the contact show pronounced brittle deformation: strong fracturing and sharp, straight-limbed drag folds, indicating in this case top-to-the-SSE thrust sense of shear. Also note the general discordance between the mean foliation in the hanging-wall marble and the unaffected mica schists farther down in the footwall. The whole contact does not show a listric shape in map view. This indicates that the discordance did not result from rotation of the hanging wall and suggests that the thrust slices may have been transported onto the blueschist succession from a different structural domain.

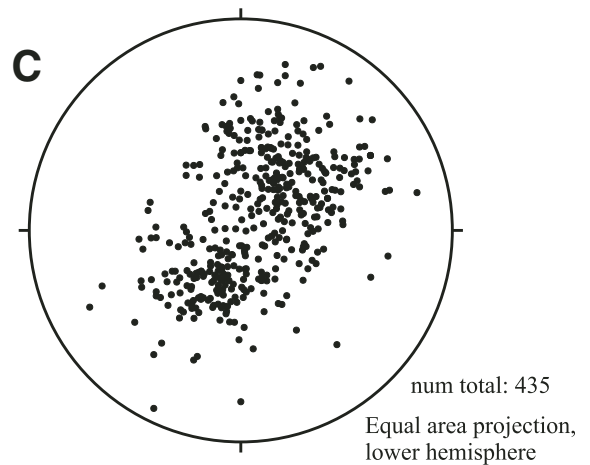
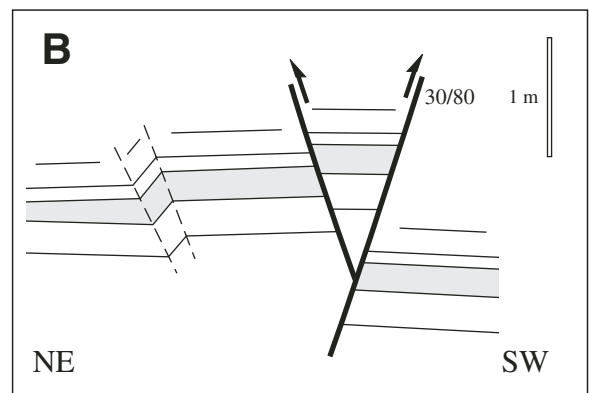
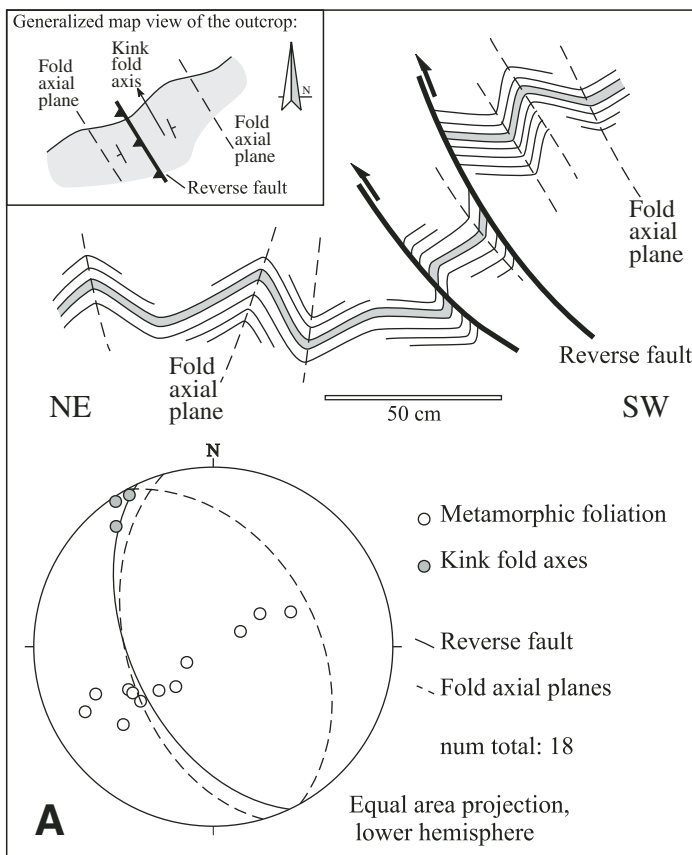


Figure 23. Brittle shortening structures in the southwest of Syros. (A) Top: chevron-style (kink) folds in a coastal outcrop of metafelsic paragneisses 150 m north of Komito beach (for location, see Map 1). The hinge zones of the folds are abundantly cut by top-to-the-NE, sharply defined reverse faults. Bottom: stereographic projection of the structural elements measured in the outcrop. (B) Pop-up structure, coastal outcrop, Komito Beach. A metabasitic layer (gray) in felsic paragneisses is sharply kinked and disrupted by NW-SE-striking steep reverse faults. (C) Stereonetic projection of metamorphic foliation s2, measured areawide over the Mavra Vounakia peninsula. The moderately developed great-circle distribution reflects open folding of the whole succession around NW-SE-trending axes.

for episodes of brittle, late-stage NE-SW shortening may be common in the Cyclades. A conservative interpretation would be that late-stage folding is a localized result of the Neogene block rotations documented in the eastern Mediterranean area. It is interesting to note that rotation in the western Aegean domain, in which Syros is inferred to be located, appears to be episodic rather than continuous (van Hinsbergen et al., 2005; van Hinsbergen et al., 2008). The older (and stronger) phase of rotation took place between 15 and 8 Ma, a period consistent with the crosscutting relationships observed on Syros. The current discussion of indications for reverse slip along the Cretan detachment, which falls roughly into the same time frame (Klein et al., 2008), may point toward a more widespread occurrence of late Miocene contractional deformation. A conclusive answer to this problem cannot be given though, as long as the late-stage brittle fold structures have not received area-wide systematic attention across the Aegean.

#### 4.4 Structural Position of the Vari Unit

Movement of the Vari Gneiss along a detachment shear zone (located within the peripheral talc and chlorite schists) has been postulated by Ring et al. (2003) to be active between ~9 and 12 Ma. Note though that a primary contact between the high-pressure succession of the Cycladic Blueschist Unit and the Vari Unit as a whole, i.e., the Gneiss of Vari plus its schistose periphery, is nowhere exposed. Either, contacts are modified by intense late-stage steep faulting, or they are covered by alluvium (see Map 1).

#### 4.5 Discussion of Available Structural Models for the Cyclades in Light of the New Detailed Map

Syros has attracted considerable attention of structural geologists, aiming to unravel its tectonometamorphic history. Excitingly, the number of opinions about how to interpret structural field data from Syros is roughly proportional to the number of working groups. The main issues currently receiving attention are: (1) the relative timing of fabric development in regard to the PTt path, (2) the degree of internal coherence of the structural pile, (3) the amount and significance of deep-crustal coaxial deformation, and (4) the process responsible for exhumation of the high-pressure rocks.

##### 4.5.1 Relative Timing of Fabric Development

Probably the most dissent in the various studies of the structural evolution of Syros exists about the processes of fabric development and their relative timing with regard to the PT evolution. In this matter, large discrepancies exist among the interpretations of different authors, and their respective deformation successions are more or less incompatible.

According to Trotet et al. (2001a) and Rosenbaum et al. (2002), hardly any prograde (i.e., burial-related) fabrics are preserved. Apart from few microscopic relicts, all penetrative struc-

tures (including the intense folding) are assigned by these authors to the retrograde PT evolution. Contrary to this interpretation, Ridley (1982a) and Keiter et al. (2004a) attributed the penetrative fabrics such as folds and pervasive foliation to the burial path, and postulated that prograde to peak metamorphic structures have been preserved largely intact during exhumation. The widespread preservation of calcite needles at a high angle to foliation, which are inferred to be a static topotactic replacement of aligned aragonite by calcite, led Brady et al. (2004) to reach the same conclusion. Bond et al. (2007) agree with Keiter et al. (2004a) in so far as many of the fold structures have been generated during burial, but argue for a strong modification of the preserved high-pressure fabrics by continuous extensional strain during exhumation, as well as for widespread penetrative greenschist-facies extensional tectonics (see also Trotet et al., 2001a and Rosenbaum et al., 2002).

It seems clear that exhumation-related extension has taken place and has left a number of traces, especially under greenschist-facies conditions (see Bond et al., 2007 for a detailed description). Based on our field observations, however, we raise questions concerning the actual significance of postcollisional, exhumation-related pervasive extension, especially in the field of glaucophane stability. A pronounced deflection of small-scale fold axis orientation proximal to assumed zones of higher strain (i.e., a progressive deformation gradient, see Bond et al., 2007) is not supported by field data. The spread in fold-axis orientation is the result of polyphase oblique folding, the younger being E-W striking, S-vergent, and tight to isoclinal (see Chap. 4.1.2 above and Fig. 4 in Keiter et al., 2004a). There is no need to postulate a significant reorientation of blueschist-facies structures by retrograde deformation. Furthermore, the concept of distributed continuous extension since peak metamorphic conditions fails to explain the apparent lack of internal deformation below the aragonite-calcite transition ( $P = 10\text{--}12$  kbar/ $450^{\circ}\text{--}500^{\circ}$ ; see Brady et al., 2004; Keiter et al., 2008b) and the abundant preservation of undeformed pseudomorphs after lawsonite, especially in lithologies that should behave highly ductilely at elevated temperatures, such as calcite marbles and, in the case of undeformed lawsonite pseudomorphs, sharply foliated blueschists (see also Philippon et al., 2010).

The conditions of lawsonite breakdown have been refined by Schumacher et al. (2008), who pointed out that the newly constrained stability of lawsonite on Syros toward higher temperatures potentially reconciles the relative deformation successions of Rosenbaum et al. (2002) and Keiter et al. (2004a) and leaves the possibility that lawsonite breakdown can be, to a certain degree, an early retrograde process. In this context, note that the lawsonite-out reaction was regarded by Keiter et al. (2004a) as prograde only in relation to pressure increase, i.e., that contractional deformation D2 consequentially ended at the time of maximum burial. The breakdown of lawsonite would in this case be a result of thermal equilibration during a static episode between burial and exhumation. Interestingly, deformed lawsonite pseudomorphs can be observed mainly in F2b folds (see Fig. 15 and

Chap. 4.1.2 for description). It cannot be ruled out that the F2b folds represent extension-parallel folds (as described, e.g., in Avigad et al., 2001), related to early exhumation. Note, though, that recently, Forster and Lister (2005), Groppo et al. (2009), and Keiter et al. (2008a) have reported indications for episodes of reburial during exhumation in the Cycladic blueschists. Similar complications on the exhumation path have also been described elsewhere (e.g., Beltrando et al., 2007). At any rate, the F2b folds at Kini, Mana, and Azolimnos clearly signify early retrograde horizontal crustal shortening and vertical thickening.

#### **4.5.2 The Degree of Internal Coherence of the Structural Pile during Exhumation**

The retrograde paths drawn for Syros are usually relatively simple and schematic (e.g., Dixon and Ridley, 1987; Rosenbaum et al., 2002; Keiter et al., 2004a), mostly because solid constraints about the retrograde PT development are scarce and ambiguous. Trotet et al. (2001a) attempted to quantify the retrograde evolution and utilized the occurrence of areas with different degrees of preservation of high-pressure assemblages. The authors postulate that crustal-scale decoupling of slices by detachments has taken place and construct different exhumation paths for different units on Syros. This interpretation is tempting, as it suggests an explanation for the juxtaposition of ocean-floor assemblages with continental sequences. The metabasites of Syros could in this case be regarded as fragments of an ophiolitic nappe, imbricated into the continental sediments.

Field observations by several authors, however, have shown that the preservation of high-pressure assemblages in the Cycladic blueschists is patchy and more likely controlled by fluid presence than by sharp, localized tectonic breaks (e.g., Schliestedt and Matthews, 1987 for Sifnos; Bröcker et al., 1993 for Tinos; Keiter et al., 2004a, Bond et al., 2007, and Schumacher et al. 2008 for Syros). Large-scale tectonic displacements are not necessary to explain different degrees of retrograde overprint. If sharp breaks in blueschist preservation are observed on Syros at all, they are along steep, late-stage brittle faults, such as, e.g., in the Chroussa area. Neither is there a discrepancy in metamorphic conditions documented in glaucophane-bearing marbles island-wide and metabasites (Schumacher et al., 2008).

Uranium-Pb dating of metamorphic zircons from metasediments near Azolimnos in the southeast of Syros and metaigneous rocks from Kampos yield, within error, the same metamorphic age of 52 Ma (Tomaschek, 2010). Therefore, we have no reason to assume that any discrepancy between the PT histories of metasediments and metovolcanics exists. Maximum Ar-Ar white-mica ages of  $53.5 \pm 1.3$  Ma from metacherts of Syros (Maluski et al., 1987) point in the same direction.

The lithostratigraphic indications discussed in Chapter 3, and the documentation of Upper Cretaceous detrital zircons in the metasediments of the Cyclades, also point toward a proximal relationship between metabasites and metasediments. Regarding the protoliths of the metabasites as an allochthonous, fully developed oceanic unit therefore seems unlikely (see also

Chap. 3.4), and it appears probable that the primary backarc association described above has not been significantly disrupted at crustal scale. Coherence of the whole structural pile on Syros may have been more or less retained during burial and exhumation (see also Brady et al., 2004), though not without smaller-scale pressure-temperature pulses, as has recently been proposed for both Syros and Sifnos (Forster and Lister, 2005; Groppo et al., 2009).

#### **4.5.3 Extent and Significance of Deep-Crustal Coaxial Deformation**

The significance of coaxial flattening, and its potential contribution to exhumation, was recently discussed using Syros as an example. A number of symmetrical structures occur, such as boudins and more or less symmetrical pressure shadows around porphyroblasts or lithoclasts in deformed metaconglomerates. While Rosenbaum et al. (2002) interpreted symmetrical fabrics to be related mostly to the earliest exhumation history, the model presented by Bond et al. (2007) went further and proposed that a continuum of broadly coaxial horizontal stretching existed throughout almost the complete retrograde history of the rocks of Syros, between 20 kbar (according to Trotet et al., 2001a) and 6 kbar. This range would comprise the whole ductile evolution, and ~70% of the total exhumation path.

Apart from the question whether a peak pressure of 20 kbar is a realistic proposition (see Chap. 4.4.1), the kinematic interpretation of coaxial layer-perpendicular shortening and its contribution to exhumation needs to be applied with care. Mesoscopic and microscopic symmetrical stretching structures such as boudins are common features, e.g., on long limbs of attenuated asymmetric folds, and need to be interpreted with the possible presence of such superordinated structures in mind (e.g., Davis and Reynolds, 1996). The regional- and map-scale structure of Syros is highly asymmetrical, with penetrative folds showing distinct vergence toward southerly directions, and sequential stacking and/or imbrication of lithological units (see Chaps. 3.3 and 4.1.2). Furthermore, a strong layer attenuation normal to thrust planes and/or fold axial planes is not a surprising feature during crustal shortening. A strong component of coaxial flattening appears to be commonplace geometry in thrusting environments (see, e.g., Ring and Kassem, 2007 and references therein). High-pressure coaxial fabrics therefore do not a priori indicate regional extension, and interpreting the oblate strain component in the blueschist units of Syros as solely exhumation related may well be an oversimplification.

#### **4.5.4 Exhumation Models and Their Applicability for Syros**

We acknowledge the findings of Trotet et al. (2001a, 2001b), Rosenbaum et al. (2002), and Bond et al. (2007) that internal extensional deformation has affected the rocks of Syros during exhumation, but we suggest that its significance for the overprint of burial-related, high-pressure fabrics and their contribution to the overall exhumation need to be evaluated carefully. But which of the different geodynamic models provides the best explanation

for the observations made on Syros, and which process of exhumation is most compatible with the field observations?

The scarcity of postorogenic sediments in the Aegean has long been recognized, and calculated exhumation rates for several islands appear to be very high, compared with common erosion rates. These observations led to the conclusion that erosion is unlikely to have been a major factor in the exhumation of the Cycladic blueschists (Lister et al., 1984; Avigad and Garfunkel, 1991; Gautier and Brun, 1994b).

The contribution of ductile vertical thinning (i.e., layer-perpendicular shortening) to exhumation has been shown by several studies to be relatively ineffective (e.g., Feehan and Brandon, 1999; Ring and Kumerics, 2008 and references therein), in so far as high values of horizontal stretching are needed for coaxial flattening to be effective for exhumation. This is due to the fact that not only the high-pressure rocks, but also their overburden need be thinned in this process. Part of the coaxial flattening preserved on Syros may well be exhumation related. But an estimate that the overall oblate strain observed on Syros contributed a major part to exhumation (70%, see Bond et al., 2007) is, the results of Feehan and Brandon (1999) qualitatively applied, potentially overestimated by a factor of 3. The exhumation effect of layer-parallel extension would be further reduced, the steeper the layering—which is overall rather steep on Syros (see profile on Map 1).

Postcollisional detachment faults have been recognized as being effective only at relatively shallow levels of the crust. Also, their potential importance for exhumation is highly dependent on their dip angle, i.e., large horizontal displacements along a low-angle fault are inherently necessary to effectively remove large quantities of overburden (Ring and Reischmann, 2002).

Since all processes described above seem to be inappropriate to achieve a major part of the exhumation from blueschist- to eclogite-facies conditions to the surface in the Cyclades, synorogenic exhumation best explains the observations. The Cycladic blueschists would then be part of one or several extrusion wedges, with geometrically necessary normal faults at their top, achieving efficient exhumation contemporaneous to crustal convergence. The process of syncollisional extrusion has been modeled by Chemenda et al. (1995), and since then been recognized by many authors to be valid in a number of orogenic settings worldwide (Grujic et al., 1996; Hetzel et al., 1998; Sölvä et al., 2001; Trotet et al., 2001a; Xypolias et al., 2003; Koukouvelas and Kokkalas, 2003; Kokkalas et al., 2006; Ring et al., 2007; Agard et al., 2009; Ring et al., 2010; Jolivet and Brun, 2010; Ring and Glodny, 2010).

In this context, recent observations that retrograde paths of many deep-crustal rocks seem to show signs of episodic reburial with temperature and pressure increase, are especially interesting (e.g., Forster and Lister, 2005; Beltrando et al., 2007; Groppo et al., 2009; Keiter et al., 2008a). An overall history of exhumation in an extrusion wedge could easily be imagined as being a temporally and spatially discontinuous process, with the roof shear zone of the wedge episodically getting stuck, and/or an increase of the regional overburden by nappe stacking in shallower levels of the converging orogen. This could result in thermal and pressure pulses during the retrograde metamorphic evolution, as well as locally significant deformation indicating crustal shortening strain, like the blueschist-facies F2b folds described in Chapter 4.1.2.

Shifting a major part of the bulk exhumation to a forearc setting, i.e., to synorogenic extrusion, might also account for the scarcity of flysch sediments in the Aegean area, since in a forearc orogenic wedge, a large volume of these sediments would have been removed or hidden from the observable system by overriding crustal slices (Malavieille, 2010).

We regard the concept of synorogenic exhumation along more or less discrete zones of high strain as the best explanation for the various field observations made on Syros. Note that it is potentially an elegant solution to the apparent contradiction between retrograde shortening and extensional fabrics described by the various authors. Recent models of orogen dynamics are taking into account the possibility of episodic tectonic mode changes during exhumation (Forster and Lister, 2005; Lister and Forster, 2009). Pressure-temperature-time quantification of such different episodes is often challenging, but the model of Lister and Forster (2009) offers a potential base for the interpretation of structures observed on Syros, because it allows mutual coexistence of contraction and extension structures. Depending on strain distribution, it also is consistent with the preservation of largely unaltered prograde fabrics throughout the whole retrograde evolution.

There is no doubt that the Cyclades are located in an extensional backarc setting active during the past 15–20 Ma, but it is not known when conditions changed from a compressional to purely extensional environment. Evaluating the timing of change from compressional to extensional also yields paleogeographical implications, such as the timing of basin formation. Generally, this change is considered to be Oligocene in age (30–35 Ma, see e.g., Jolivet et al. 2009), but may have occurred somewhat later, maybe not before middle Miocene times, as has recently been suggested by, e.g., Ring et al. (2010).

## *Concluding Remarks*

The general aim of the new geological map of Syros presented in this paper is to provide as much information as possible about primary depositional relations, regardless of the variable degrees of retrograde metamorphism. This strict guideline was loosened only in the case of blueschist- to eclogite-facies metabasite occurrences, to pay tribute to their high relevance for structural, geochemical, and petrological purposes. We like to emphasize, though, that there is no reason to assume that strongly overprinted metabasite lithologies, such as on the Mavra Vounakia peninsula in the southwest of Syros, are in any way primarily different from the well-preserved high-pressure metamorphic relicts of oceanic lithosphere elsewhere on the island.

Lithostratigraphic observations collected in the course of this mapping project confirmed the view of Dixon and Ridley (1987) that the marble-schist sequence on Syros represents a stack comprising several thrust sheets. The repetition of a distinct lithostratigraphic marker sequence (i.e., calcite marble–dolomitic marble–quartzite, see Fig. 7) indicates that tectonically lower marbles in the south of Syros are stratigraphically equivalent to tectonically higher marbles in northern Syros. The sequence was never found overturned, in accordance with the absence of intact isoclinal megafolds. The synmetamorphic structural pile is probably derived from repetition of the very same marble-schist-metabasite sequence, including metaigneous remnants of an Upper Cretaceous oceanic crust. Interpreting the blueschist-facies metabasite units as relicts of one single

discordant nappe, as indicated, e.g., by Hecht (1985) or Höpfer and Schumacher (1997), therefore appears inappropriate. The emplacement of the metabasites into the structural pile is regarded as a prograde process, with lithological contacts, where they are not disrupted by late-stage, high-angle faulting, broadly parallel to the regional foliation, and internal structural homogeneity across geological boundaries.

The synmetamorphic structural pile preserved on Syros became substantially modified by postmetamorphic tectonic processes. After the brittle-ductile transition in the late-middle to early-late Miocene, intense transpressional and transtensional tectonics disrupted the rock sequence up to subrecent times. Localized horizontal contractional deformation is likely to account for limited occurrences of postmetamorphic thrust slices and transpressional strike-slip zones on Syros, in an extensional regional setting since the late Miocene. A possible episode of localized, but significant folding around NW-SE-trending axes, falling roughly into the same time frame, marks a complication in the overall NE-SW extension setting.

The structural complexities depicted in this detailed map have demonstrated that several generalized models on the geological evolution of the Cycladic blueschists might not hold up to scrutiny in comparison with actual field relations. Because of higher lithological and structural geological resolution now available, the new geological map provides a sound basis for future studies on Syros.

## ☞ REFERENCES CITED ☞

- Agard, P., Yamato, P., Jolivet, L., and Burov, E., 2009, Exhumation of oceanic blueschists and eclogites in subduction zones: Timing and mechanisms: *Earth-Science Reviews*, v. 92, p. 53–79, doi:10.1016/j.earscirev.2008.11.002.
- Altherr, R., and Siebel, W., 2002, I-type plutonism in a continental back-arc setting: Miocene granitoids and monzonites from the Central Aegean Sea, Greece: *Contributions to Mineralogy and Petrology*, v. 143, p. 397–415, doi:10.1007/s00410-002-0352-y.
- Altherr, R., Schliestedt, M., Okrusch, M., Seidel, E., Kreuzer, H., Harre, W., Lenz, H., Wendt, I., and Wagner, G.A., 1979, Geochronology of high-pressure rocks from Sifnos (Cyclades, Greece): *Contributions to Mineralogy and Petrology*, v. 70, p. 245–255, doi:10.1007/BF00375354.
- Altherr, R., Kreuzer, H., Wendt, I., Lenz, H., Wagner, G.A., Keller, J., Harre, W., and Höhdorf, A., 1982, A late Oligocene/early Miocene high temperature belt in the Attic-Cycladic crystalline complex (SE Pelagonian, Greece): *Geologisches Jahrbuch*, v. 23, p. 97–164.
- Altherr, R., Kreuzer, H., Lenz, H., Wendt, I., Harre, W., and Dürr, S., 1994, Further evidence for a Late Cretaceous low-pressure/high-temperature terrane in the Cyclades: Petrology and geochronology of crystalline rocks from the islands of Donoussa and Ikaria: *Chemie der Erde*, v. 54, p. 319–328.
- Andriessen, P.A.M., Boelrijk, N.A.I.M., Hebeda, E.H., Priem, H.N.A., Verdummen, E.A.T., and Verschure, R.H., 1979, Dating the events of metamorphism and granitic magmatism in the Alpine orogen of Naxos (Cyclades, Greece): *Contributions to Mineralogy and Petrology*, v. 69, p. 215–255, doi:10.1007/BF00372323.
- Avigad, D., and Garfunkel, Z., 1991, Uplift and exhumation of high-pressure metamorphic terrains: The example of the Cycladic blueschist belt (Aegean Sea): *Tectonophysics*, v. 188, p. 357–372, doi:10.1016/0040-1951(91)90464-4.
- Avigad, D., Baer, G., and Heimann, A., 1998, Block rotations and continental extension in the central Aegean Sea: Palaeomagnetic and structural evidence from Tinos and Mykonos (Cyclades, Greece): *Earth and Planetary Science Letters*, v. 157, p. 23–40, doi:10.1016/S0012-821X(98)00024-7.
- Avigad, D., Ziv, A., and Garfunkel, Z., 2001, Ductile and brittle shortening, extension-parallel folds and maintenance of crustal thickness in the central Aegean (Cyclades, Greece): *Tectonics*, v. 20, p. 277–287, doi:10.1029/2000TC001190.
- Baldwin, S.L., 1996, Contrasting P-T histories for blueschists from the western Baja terrane and the Aegean: Effects of synsubduction exhumation and backarc extension, in *Bebout, G.E., Scholl, D.W., Kirby, S.H. and Platt, J.P., eds., Subduction: Top to Bottom: Geophysical Monograph*, v. 96, p. 135–141.
- Ballhaus, C., Tomaschek, F., Keiter, M., Lagos, M., Bode, M., Piepjohn, K., and Munker, C., 2001, Magmatic, metamorphic and exhumation history of Syros, Greece: *Journal of Conference Abstracts*, v. 6, no. 1, p. 345.
- Beltrando, M., Herrmann, J., Lister, G., and Compagnoni, R., 2007, On the evolution of orogens: Pressure cycles and deformation mode switches: *Earth and Planetary Science Letters*, v. 256, p. 372–388, doi:10.1016/j.epsl.2007.01.022.
- Blake, M.C., Bonneau, M., Geysant, J., Kienast, J.R., Lepvrier, C., Maluski, H., and Papanikolaou, D., 1981, A geologic reconnaissance of the Cycladic blueschist belt, Greece: *Geological Society of America Bulletin*, v. 92, p. 247–254, doi:10.1130/0016-7606(1981)92<247:AGROTC>2.0.CO;2.
- Bohnhoff, M., Rische, M., Meier, T., Becker, D., Stavrakakis, G., and Harjes, H.P., 2006, Microseismic activity in the Hellenic Volcanic Arc, Greece, with emphasis on the seismotectonic setting of the Santorini-Amorgos zone: *Tectonophysics*, v. 423, p. 17–33, doi:10.1016/j.tecto.2006.03.024.
- Bond, C.E., Butler, R.W.H., and Dixon, J.E., 2007, Co-axial horizontal stretching within extending orogens: The exhumation of HP rocks on Syros (Cyclades) revisited, in *Ries, A.C., Butler, R.W.H., and Graham, R.H., eds., Deformation of the Continental Crust: The Legacy of Mike Coward: The Geological Society of London Special Publications*, v. 272, p. 203–222.
- Bonneau, M., 1982, Évolution géodynamique de l'arc égéen depuis le Jurassique supérieur jusqu'au Miocène: *Bulletin de la Société Géologique de France, Série 7*, v. 24, p. 229–242.
- Bonneau, M., Blake, M.C., Geysant, J., Kienast, J.R., Lepvrier, C., Maluski, H., and Papanikolaou, D., 1980a, Sur la signification des séries métamorphiques (schistes bleus) des Cyclades (Héllénides, Grèce): L'exemple de l'île de Syros: *Comptes Rendus de l'Académie des Sciences de Paris, Série D*, v. 290, p. 1463–1466.
- Bonneau, M., Geysant, J., Kienast, J.R., Lepvrier, C., and Maluski, H., 1980b, Tectonique et métamorphisme haute pression d'âge éocène dans les Héllénides: Exemple de l'île de Syros (Cyclades, Grèce): *Comptes Rendus de l'Académie des Sciences de Paris, Série D*, v. 291, p. 171–174.
- Boronkay, K., and Doutsos, T., 1994, Transpression and transtension within different structural levels in the central Aegean region: *Journal of Structural Geology*, v. 16, p. 1555–1573, doi:10.1016/0191-8141(94)90033-7.
- Brady, J.B., Markley, M.J., Schumacher, J.C., Cheney, J.T., and Bianciardi, G.A., 2004, Aragonite pseudomorphs in high-pressure marbles of Syros, Greece: *Journal of Structural Geology*, v. 26, p. 3–9, doi:10.1016/S0191-8141(03)00099-3.
- Bröcker, M., and Enders, M., 1999, U-Pb zircon geochronology of unusual eclogite-facies rocks from Syros and Tinos (Cyclades, Greece): *Geological Magazine*, v. 136, p. 111–118, doi:10.1017/S0016756899002320.
- Bröcker, M., and Enders, M., 2001, Unusual bulk-rock compositions in eclogite-facies rocks from Syros and Tinos (Cyclades, Greece): Implications for U-Pb zircon geochronology: *Chemical Geology*, v. 175, p. 581–603, doi:10.1016/S0009-2541(00)00369-7.
- Bröcker, M., and Franz, L., 1998, Rb-Sr isotope studies on Tinos Island (Cyclades, Greece): Additional time constraints for metamorphism, extent of infiltration-controlled overprinting and deformational activity: *Geological Magazine*, v. 135, p. 369–382, doi:10.1017/S0016756898008681.
- Bröcker, M., and Franz, L., 2006, Dating metamorphism and tectonic juxtaposition on Andros Island (Cyclades, Greece): Results of a Rb-Sr study: *Geological Magazine*, v. 143, p. 609–620, doi:10.1017/S001675680600241X.
- Bröcker, M., and Keasling, A., 2006, Ionprobe U-Pb zircon ages from the high-pressure/low-temperature mélange of Syros, Greece: Age diversity and the importance of pre-Eocene subduction: *Journal of Metamorphic Geology*, v. 24, p. 615–631, doi:10.1111/j.1525-1314.2006.00658.x.
- Bröcker, M., and Pidgeon, R.T., 2007, Protolith ages of meta-igneous and meta-tuffaceous rocks from the Cycladic Blueschist Unit, Greece: Results of a reconnaissance U-Pb zircon study: *Journal of Geology*, v. 115, p. 83–98.
- Bröcker, M., Kreuzer, H., Matthews, A., and Okrusch, M., 1993, <sup>40</sup>Ar/<sup>39</sup>Ar and oxygen isotope studies of polymetamorphism from Tinos Island, Cycladic blueschist belt, Greece: *Journal of Metamorphic Geology*, v. 11, p. 223–240, doi:10.1111/j.1525-1314.1993.tb00144.x.
- Bröcker, M., Bieling, D., Hacker, B., and Gans, P., 2004, High-Si phengite records the time of greenschist facies overprinting: Implications for models suggesting mega-detachments in the Aegean Sea: *Journal of Metamorphic Geology*, v. 22, p. 427–442, doi:10.1111/j.1525-1314.2004.00524.x.
- Bröcker, M., Huyskens, M., and Knoblauch, S., 2010, Dating of shear zone activity in the Cyclades, Greece: Examples from the islands of Syros and Andros: Tectonic crossroads: Evolving orogens of Eurasia-Africa-Arabia: Ankara, Middle East Technical University, Abstracts with Programs, p. 64–65.
- Bulle, F., Bröcker, M., Gärtner, C., and Keasling, A., 2010, Geochemistry and geochronology of HP mélanges from Tinos and Andros, Cycladic blueschist belt, Greece: *Lithos*, v. 117, p. 61–81, doi:10.1016/j.lithos.2010.02.004.
- Chemenda, A.I., Mattauer, M., Malavieille, J., and Bokun, A.N., 1995, A mechanism for syn-collisional rock exhumation and associated normal faulting: Results from physical modelling: *Earth and Planetary Science Letters*, v. 132, p. 225–232, doi:10.1016/0012-821X(95)00042-B.
- Cocard, M., Kahle, H.-G., Peter, Y., Geiger, A., Veis, G., Felekis, S., Paradisik, D., and Billiris, H., 1999, New constraints on the rapid crustal motion of the Aegean region: Recent results inferred from GPS measurements (1993–1998) across the West Hellenic Arc, Greece: *Earth and Planetary Science Letters*, v. 172, p. 39–47, doi:10.1016/S0012-821X(99)00185-5.

- Davis, G.H., and Reynolds, S.J., 1996, *Structural Geology of Rocks and Regions*: New York, John Wiley and Sons, 776 p.
- Dixon, J.E., 1968, *The metamorphic rocks of Syros, Greece* [Ph.D. thesis]: Cambridge, St. John's College.
- Dixon J.E., 1976, Glauconite schists of Syros, Greece: *Bulletin de la Société Géologique de France, Série 7*, v. 18, p. 280.
- Dixon, J.E., and Ridley, J., 1987, Syros, in Helgeson, H.C., ed., *Chemical Transport in Metasomatic Processes*: North Atlantic Treaty Organization Advanced Science Institutes Series C, v. 218, p. 489–501.
- Doutsos, T., Pe-Piper, G., Boronkay, K., and Koukouvelas, I., 1993, Kinematics of the Central Hellenides: *Tectonics*, v. 12, p. 936–953, doi:10.1029/93TC00108.
- Dürr, S., 1986, Das Attisch-kykladische Kristallin, in Jacobshagen, V., ed., *Geologie von Griechenland*: Berlin and Stuttgart, Beiträge zur regionalen Geologie der Erde, v. 19, Borntraeger, p. 116–149.
- Dürr, S., Altherr, R., Keller, J., Okrusch, M., and Seidel, E., 1978, The median Aegean crystalline belt: Stratigraphy, structure, metamorphism, magmatism, in Cloos, H., Roeder, D., and Schmidt, H., eds., *Alps, Apennines, Hellenides*: Stuttgart, Inter-Union Commission on Geodynamics Scientific Report No. 38, Schweizerbart, p. 455–477.
- Ernst, W.G., 2006, Geologic mapping—Where the rubber meets the road, in Mazzoli, S., and Butler, R.W.H., eds., *Earth and Mind: How Geologists Think and Learn about the Earth*: Boulder, Colorado, Geological Society of America Special Paper 413, p. 13–28, doi:10.1130/2006.2413(02).
- Feehan, J.G., and Brandon, M.T., 1999, Contribution of ductile flow to exhumation of low-temperature, high-pressure metamorphic rocks: San Juan–Cascade nappes, NW Washington State: *Journal of Geophysical Research*, v. 104, p. 10,883–10,902, doi:10.1029/1998JB900054.
- Forster, M.A., and Lister, G.S., 2005, Several distinct tectono-metamorphic slices in the Cycladic eclogite-blueschist belt, Greece: *Contributions to Mineralogy and Petrology*, v. 150, p. 523–545, doi:10.1007/s00410-005-0032-9.
- Fu, B., Valley, J.W., Kita, N.T., Spicuzza, M.J., Paton, C., Tsujimori, T., Bröcker, M., and Harlow, G.E., 2010, Multiple origins of zircons in jadeite: *Contributions to Mineralogy and Petrology*, v. 159, p. 769–780, doi:10.1007/s00410-009-0453-y.
- Gärtner, C., and Bröcker, M., 2007, Depositional ages of metasediments from Tinos Island, Greece: New insights from detrital zircon geochronology: *Geological Society of America Abstracts with Programs*, v. 39, no. 6, p. 237.
- Gautier, P., and Brun, J.P., 1994a, Ductile crust exhumation and extensional detachments in the central Aegean (Cyclades and Evvia Island): *Geodynamica Acta*, v. 7, p. 57–85.
- Gautier, P., and Brun, J.P., 1994b, Crustal-scale geometry and kinematics of late-orogenic extension in the central Aegean (Cyclades and Evvia Island): *Tectonophysics*, v. 238, p. 399–424, doi:10.1016/0040-1951(94)90066-3.
- Glodny, J., Ring, U., and Will, T., 2008, Differential exhumation and fluid-rock interaction in the Cycladic blueschist belt, Greece: Constraints from Rb-Sr geochronology: Oslo, 33rd International Geological Congress, August 6–14, Abstract MPC02314P.
- Goldsworthy, M., Jackson, J., and Haines, J., 2002, The continuity of active fault systems in Greece: *Geophysical Journal International*, v. 148, p. 596–618, doi:10.1046/j.1365-246X.2002.01609.x.
- Gropo, C., Forster, M., Lister, G., and Compagnoni, R., 2009, Glauconite schists and associated rocks from Sifnos (Cyclades, Greece): New constraints on the P-T evolution from oxidized systems: *Lithos*, v. 109, p. 254–273, doi:10.1016/j.lithos.2008.10.005.
- Grujic, D., Casey, M., Davidson, C., Hollister, L.S., Kündig, R., Pavlis, T., and Schmid, S., 1996, Ductile extrusion of the Higher Himalayan Crystalline in Bhutan: Evidence from quartz microfabrics: *Tectonophysics*, v. 260, p. 21–43, doi:10.1016/0040-1951(96)00074-1.
- Hecht, J., 1985, *Geological map of Greece 1:50,000*, Syros Island: Athens, Institute of Geology and Mineral Exploration, 1 sheet.
- Henjes-Kunst, F., Altherr, R., Kreuzer, H., and Hansen, B.T., 1988, Disturbed U-Th-Pb systematics of young zircons and uranorhites: The case of Miocene Aegean granitoids, Greece: *Chemical Geology*, v. 73, p. 125–145.
- Hetzl, R., Echter, H.P., Seifert, W., Schulte, B.A., and Ivanov, K.S., 1998, Subduction- and exhumation-related fabrics in the Paleozoic high-pressure-low-temperature Maksyutov Complex, Anting area, southern Urals, Russia: *Geological Society of America Bulletin*, v. 110, p. 916–930, doi:10.1130/0016-7606(1998)110<0916:SAERFI>2.3.CO;2.
- Hollenstein, C., Müller, M.D., Geiger, A., and Kahle, H.G., 2008, Crustal motion and deformation in Greece from a decade of GPS measurements, 1993–2003: *Tectonophysics*, v. 449, p. 17–40, doi:10.1016/j.tecto.2007.12.006.
- Höpfer, N., and Schumacher, J.C., 1997, New field work and interpretations of the sedimentary sequence, the position of ophiolitic rocks and subsequent deformation on Syros, Cyclades, Greece: *Beihefte zum European Journal of Mineralogy*, v. 9, p. 162.
- Jacobshagen, V., ed., 1986, *Geologie von Griechenland*: Berlin and Stuttgart, Beiträge zur Regionalen Geologie der Erde, v. 19, Borntraeger, 363 p.
- Jansen, J.B.H., and Schuiling, R.D., 1976, Metamorphism on Naxos: Petrology and geothermal gradients: *American Journal of Science*, v. 276, p. 1225–1253, doi:10.2475/ajs.276.10.1225.
- Jolivet, L., 2001, A comparison of geodetic and finite strain pattern in the Aegean, geodynamic implications: *Earth and Planetary Science Letters*, v. 187, p. 95–104, doi:10.1016/S0012-821X(01)00277-1.
- Jolivet, L., and Brun, J.P., 2010, Cenozoic geodynamic evolution of the Aegean: *International Journal of Earth Sciences*, v. 99, p. 109–138, doi:10.1007/s00531-008-0366-4.
- Jolivet, L., and Patriat, M., 1999, Ductile extension and the formation of the Aegean Sea, in Durand, B., Jolivet, L., Horváth, F., and Séranne, M., eds., *The Mediterranean Basins: Tertiary Extension within the Alpine Orogen*: The Geological Society of London Special Publications, v. 156, p. 427–456.
- Jolivet, L., Facenna, C., Goffe, B., Burov, E., and Agard, P., 2003, Subduction tectonics and exhumation of high-pressure metamorphic rocks in the Mediterranean orogens: *American Journal of Science*, v. 303, p. 353–409, doi:10.2475/ajs.303.5.353.
- Jolivet, L., Rimmelé, G., Oberhänsli, R., Goffé, B., and Candan, O., 2004, Correlation of syn-orogenic tectonic and metamorphic events in the Cyclades, the Lycian nappes, and the Menderes massif: Geodynamic implications: *Bulletin de la Société Géologique de France*, v. 175, p. 217–238, doi:10.2113/175.3.217.
- Jolivet, L., Lecomte, E., Huet, B., Denele, Y., Lacombe, O., Labrousse, L., Le Pourhiet, L., and Mehl, C., 2009, The north Cycladic detachment system: *Earth and Planetary Science Letters*, v. 289, p. 87–104, doi:10.1016/j.epsl.2009.10.032.
- Kahle, H.-G., Straub, C., Reilinger, R., McClusky, S., King, R., Hurst, K., Veis, G., Kastens, K., and Cross, P., 1998, The strain field in the eastern Mediterranean region, estimated by repeated GPS measurements: *Tectonophysics*, v. 294, p. 237–252, doi:10.1016/S0040-1951(98)00102-4.
- Katzir, Y., Matthews, A., Garfunkel, Z., Schliestedt, M., and Avigad, D., 1996, The tectono-metamorphic evolution of a dismembered ophiolite (Tinos, Cyclades, Greece): *Geological Magazine*, v. 133, p. 237–254, doi:10.1017/S0016756800008992.
- Katzir, Y., Garfunkel, Z., Avigad, D., and Matthews, A., 2007, The geodynamic evolution of the Alpine orogen in the Cyclades (Aegean Sea, Greece): Insights from diverse origins and modes of emplacement of ultramafic rocks, in Taymaz, T., Yilmaz, Y., and Dilek, Y., eds., *The geodynamics of the Aegean and Anatolia*: The Geological Society of London Special Publications, v. 291, p. 17–40.
- Keay, S., 1998, *The geological evolution of the Cyclades, Greece: Constraints from SHRIMP U-Pb geochronology* [Ph.D. thesis]: Canberra, Australian National University, 337 p.
- Keay, S., Lister, G.S., and Buick, I., 2001, The timing of partial melting, Barrovian metamorphism and granite intrusion in the Naxos metamorphic core complex, Cyclades, Aegean Sea, Greece: *Tectonophysics*, v. 342, p. 275–312, doi:10.1016/S0040-1951(01)00168-8.
- Keiter, M., Piepjohn, K., Ballhaus, C., Lagos, M., and Bode, M., 2004a, Structural development of high-pressure metamorphic rocks on Syros island (Cyclades, Greece): *Journal of Structural Geology*, v. 26, p. 1433–1445, doi:10.1016/j.jsg.2003.11.027.
- Keiter, M., Piepjohn, K., and Ballhaus, C., 2004b, The young structural evolution of Syros (Cyclades, Greece)—Indications for late Miocene–Pliocene brittle fold and thrust tectonics: *Beihefte zum European Journal of Mineralogy*, v. 16, p. 66.
- Keiter, M., Tomaschek, F., and Ballhaus, C., 2008a, The structural inventory of Kythnos Island (Cyclades, Greece)—A reconnaissance: *Zeitschrift der deutschen Gesellschaft für Geowissenschaften*, v. 159, p. 513–520.
- Keiter, M., Tomaschek, F., Schmid-Beurmann, P., Ballhaus, C., and Löns, J., 2008b, Calcite needles in marbles on Syros (Cyclades, Greece)—Indicators for an obscured aragonite foliation and static exhumation: *Geotectonic Research*, v. 95, no. 01, p. 81–82.

- Klein, T., Reichhardt, H., Klinger, L., Grigull, S., Wostal, G., Kowalczyk, G., and Zulauf, G., 2008, Reverse slip along the contact phyllite-quartzite unit–Tripolitsa unit in eastern Crete: Implications for the geodynamic evolution of the External Hellenides: *Zeitschrift der deutschen Gesellschaft für Geowissenschaften*, v. 159, p. 375–398.
- Kokkalas, S., Xypolias, P., Koukouvelas, I., and Doutsos, T., 2006, Postcollisional contractional and extensional deformation in the Aegean region, *in* Dilek, Y., and Pavlides, S., eds., *Postcollisional tectonics and magmatism in the Mediterranean region and Asia*: Geological Society of America Special Paper 409, p. 97–123.
- Koukouvelas, I., and Kokkalas, S., 2003, Emplacement of the Miocene west Naxos pluton (Aegean Sea, Greece): A structural study: *Geological Magazine*, v. 140, p. 45–61, doi:10.1017/S0016756802007094.
- Kumerics, C., Ring, U., Brichau, S., Glodny, J., and Monie, P., 2005, The extensional Messaria shear zone and associated brittle detachment faults, Aegean Sea, Greece: *Journal of the Geological Society, London*, v. 162, p. 701–702.
- Lagos, M., Munker, C., Tomaschek, F., and Ballhaus, C., 2002, Geochemistry and Lu-Hf geochronology of the metavolcanic Grizzas sequence in northern Syros (Cyclades, Greece): *Beihefte zum European Journal of Mineralogy*, v. 14, no. 1, p. 97.
- Lagos, M., Scherer, E.E., Tomaschek, F., Munker, C., Keiter, M., Berndt, J., and Ballhaus, C., 2007, High precision Lu-Hf geochronology of Eocene eclogite-facies rocks from Syros, Cyclades, Greece: *Chemical Geology*, v. 243, p. 16–35, doi:10.1016/j.chemgeo.2007.04.008.
- Lazarus, E., 2004, Characterization of high-angle faults on the island of Syros, Greece [B.A. thesis]: Williamstown, Massachusetts, Williams College, 96 p.
- Lee, J., and Lister, G.S., 1992, Late Miocene ductile extension and detachment faulting, Mykonos, Greece: *Geology*, v. 20, p. 121–124, doi:10.1130/0091-7613(1992)020<0121:LMDEAD>2.3.CO;2.
- Le Pichon, X., and Angelier, J., 1979, The Hellenic arc and trench system: A key to the neotectonic evolution of the eastern Mediterranean area: *Tectonophysics*, v. 60, p. 1–42, doi:10.1016/0040-1951(79)90131-8.
- Lister, G.S., and Forster, M.A., 2009, Tectonic mode switches and the nature of orogenesis: *Lithos*, v. 113, p. 274–291, doi:10.1016/j.lithos.2008.10.024.
- Lister, G.S., and Raouzaïos, A., 1996, The tectonic significance of a porphyroblastic blueschist facies overprint during Alpine orogenesis: Sifnos, Aegean Sea, Greece: *Journal of Structural Geology*, v. 18, p. 1417–1435, doi:10.1016/S0191-8141(96)00072-7.
- Lister, G.S., Banga, G., and Feenstra, A., 1984, Metamorphic core complexes of Cordilleran type in the Cyclades, Aegean Sea, Greece: *Geology*, v. 12, p. 221–225, doi:10.1130/0091-7613(1984)12<221:MCCOCT>2.0.CO;2.
- Makris, J., 1978, The crust and upper mantle of the Aegean region from deep seismic soundings: *Tectonophysics*, v. 46, p. 269–284, doi:10.1016/0040-1951(78)90207-X.
- Malavieille, J., 2010, Impact of erosion, sedimentation and structural heritage on the structure and kinematics of orogenic wedges: Analog models and case studies: *GSA Today*, v. 20, p. 4–10, doi:10.1130/GSATG48A.1.
- Maluski H., Bonneau M. and Kienast J.-R., 1987, Dating the metamorphic events in the Cycladic area: <sup>39</sup>Ar/<sup>40</sup>Ar data from metamorphic rocks of the island of Syros (Greece): *Bulletin de la Société Géologique de France, Série 8*, v. 3, p. 833–842.
- Marschall, H.R., Altherr, R., and Ruepke, L., 2007, Squeezing out the slab—Modelling the release of Li, Be and B during progressive high-pressure metamorphism: *Chemical Geology*, v. 239, p. 323–335, doi:10.1016/j.chemgeo.2006.08.008.
- Marschall, H.R., Altherr, R., Kalt, A., and Ludwig, T., 2008, Detrital, metamorphic and metasomatic tourmaline in high-pressure metasediments from Syros (Greece): Intra-grain boron isotope patterns determined by secondary-ion mass spectrometry: *Contributions to Mineralogy and Petrology*, v. 155, p. 703–717, doi:10.1007/s00410-007-0266-9.
- McClusky, S., Balassanian, S., Barka, A., Demir, C., Ergintav, S., Georgiev, I., Gurkan, O., Hamburger, M., Hurst, K., Kahle, H., Kastens, K., Kekelidze, G., King, R., Kotzev, V., Lenk, O., Mahmoud, S., Mishin, A., Nadariya, M., Ouzounis, A., Paradissis, D., Peter, Y., Prilepin, M., Reilinger, R., Sanli, I., Seeger, H., Tealeb, A., Toksoz, M.N., and Veis, G., 2000, Global Positioning System constraints on plate kinematics and dynamics in the eastern Mediterranean and Caucasus: *Journal of Geophysical Research. Solid Earth*, v. 105, p. 5695–5719.
- McKenzie, D.P., 1970, Plate tectonics of the Mediterranean region: *Nature*, v. 226, p. 239–243, doi:10.1038/226239a0.
- Melidonis, N.G., and Constantinides, D.C., 1983, The stratabound sulphide mineralisation of Syros (Cyclades, Greece): *Zeitschrift der Deutschen Geologischen Gesellschaft*, v. 134, p. 555–575.
- Miller, D.P., Marschall, H.R., and Schumacher, J.C., 2009, Metasomatic formation and petrology of blueschist-facies hybrid rocks from Syros (Greece): Implications for reactions at the slab-mantle interface: *Lithos*, v. 107, p. 53–67, doi:10.1016/j.lithos.2008.07.015.
- Mocek, B., 2001, Geochemical evidence for arc-type volcanism in the Aegean Sea: The blueschist unit of Siphnos, Cyclades (Greece): *Lithos*, v. 57, p. 263–289, doi:10.1016/S0024-4937(01)00043-3.
- Mountrakis, D., 2006, Tertiary and Quaternary tectonics of Greece, *in* Dilek, Y., and Pavlides, S., eds., *Postcollisional Tectonics and Magmatism in the Mediterranean Region and Asia*: Geological Society of America Special Paper 409, p. 125–136.
- Neubauer, F., Frisch, W., Schermer, R., and Schlöser, H., 1989, Metamorphosed and dismembered ophiolite suites in the basement units of the Eastern Alps: *Tectonophysics*, v. 164, p. 49–62, doi:10.1016/0040-1951(89)90233-3.
- Okay, A.I., 2001, Stratigraphic and metamorphic inversions in the central Menderes Massif: A new structural model: *International Journal of Earth Sciences*, v. 89, p. 709–727, doi:10.1007/s005310000098.
- Okrusch, M., and Bröcker, M., 1990, Eclogites associated with high-grade blueschists in the Cycladic archipelago, Greece: A review: *European Journal of Mineralogy*, v. 2, p. 451–478.
- Papanikolaou, D.J., 1978, Contribution to the geology of the Aegean sea: The island of Andros: *Annales géologiques des Pays Helléniques*, v. 29, p. 477–553.
- Papanikolaou, D.J., 1987, Tectonic evolution of the Cycladic blueschist belt (Aegean Sea, Greece), *in* Helgeson, H.C., ed., *Chemical Transport in Metasomatic Processes*: North Atlantic Treaty Organization Advanced Science Institutes Series C, v. 218, p. 489–501.
- Papanikolaou, D., Bargathi, H., Dabovski, C., Dimitriu, R., El-Hawat, A., Ioane, D., Kranis, H., Obeidi, A., Oaie, C., Seghedi, A., and Zagorchev, I., 2004, Transect VIII, *in* Cavazza, W., Roure, F., Spakmann, W., Stampfli, G.M., and Ziegler, P.A., eds., *The TRANSMED Atlas—The Mediterranean Region from Crust to Mantle. Part Two*: Heidelberg, Springer, CD-ROM.
- Park, R.G., 1989, *Foundations of Structural Geology*, Second edition: Glasgow, Blackie, 148 p.
- Patzak, M.L., Okrusch, M., and Kreuzer, H., 1994, The Akrotiri unit on the island of Tinos, Cyclades, Greece: Witness to a lost terrane of Late Cretaceous age: *Neues Jahrbuch für Geologie und Paläontologie, Abhandlungen*, v. 194, p. 211–252.
- Pe-Piper, G., and Piper, D.J.W., 2002, The igneous rocks of Greece: The anatomy of an orogen: Berlin and Stuttgart, *Beiträge zur regionalen Geologie der Erde*, v. 30, Borntraeger, 573 p.
- Philippon, M., Brun, J.P., and Gueydan, F., 2010, From subduction to back arc extension in Syros (Cyclades; Greece): *Geophysical Research Abstracts*, v. 12.
- Philippon, A., 1901, *Beiträge zur Kenntnis der griechischen Inselwelt*: Petermanns Mitteilungen, v. 134, Gotha, Justus Perthes, 172 p.
- Putlitz, B., Matthews, A., and Valley, J.W., 2000, Oxygen and hydrogen isotope study of high-pressure metagabbros and metabasalts (Cyclades, Greece): Implications for the subduction of oceanic crust: *Contributions to Mineralogy and Petrology*, v. 138, p. 114–126, doi:10.1007/s004100050012.
- Putlitz, B., Cosca, M.A., and Schumacher, J.C., 2005, Prograde mica <sup>40</sup>Ar/<sup>39</sup>Ar growth ages recorded in high-pressure rocks (Syros, Cyclades, Greece): *Chemical Geology*, v. 214, p. 79–98, doi:10.1016/j.chemgeo.2004.08.056.
- Reinecke, T., Altherr, R., Hartung, B., Hatzipanagiotou, K., Kreuzer, H., Harre, W., Klein, H., Keller, J., Geenen, E., and Böger, H., 1982, Remnants of a Late Cretaceous high-temperature belt on the island of Anafi (Cyclades, Greece): *Neues Jahrbuch für Mineralogie-Abhandlungen*, v. 145, p. 157–182.
- Ridley, J., 1982a, Tectonic style, strain history, and fabric development in a blueschist terrain, Syros, Greece [Ph.D. thesis]: Edinburgh, University of Edinburgh, 283 p.
- Ridley, J., 1982b, Arcuate lineation trends in a deep level, ductile thrust belt, Syros, Greece: *Tectonophysics*, v. 88, p. 347–360, doi:10.1016/0040-1951(82)90246-3.
- Ridley, J., 1984, Evidence of a temperature-dependent “blueschist” to “eclogite” transformation in high-pressure metamorphism of metabasic rocks: *Journal of Petrology*, v. 25, p. 852–870.

- Ridley, J., and Dixon, J.E., 1984, Reaction pathways during the progressive deformation of a blueschist metabasite: The role of chemical disequilibrium and restricted range equilibrium: *Journal of Metamorphic Geology*, v. 2, p. 115–128, doi:10.1111/j.1525-1314.1984.tb00291.x.
- Ring, U., and Glodny, J., 2010, No need for lithospheric extension for exhuming (U)HP rocks by normal faulting: *Journal of the Geological Society of London*, v. 167, p. 225–228, doi:10.1144/0016-76492009-134.
- Ring, U., and Kassem, O.M.K., 2007, The nappe rule: Why does it work?: *Journal of the Geological Society of London*, v. 164, p. 1109–1112, doi:10.1144/0016-76492007-020.
- Ring, U., and Kumerics, C., 2008, Vertical ductile thinning and its contribution to the exhumation of high-pressure rocks: The Cycladic Blueschist Unit in the Aegean: *Journal of the Geological Society of London*, v. 165, p. 1019–1030, doi:10.1144/0016-76492008-010.
- Ring, U., and Layer, P.W., 2003, High-pressure metamorphism in the Aegean, eastern Mediterranean: Underplating and exhumation from the Late Cretaceous until the Miocene to Recent above the retreating Hellenic subduction zone: *Tectonics*, v. 22, 1022, doi:10.1029/2001TC001350, 23 p.
- Ring, U., and Reischmann, T., 2002, The weak and superfast Cretan detachment, Greece: Exhumation at subduction rates in extruding wedges: *Journal of the Geological Society*, v. 159, p. 225–228, doi:10.1144/0016-764901-150.
- Ring, U., Thomson, S.N., and Bröcker, M., 2003, Fast extension but little exhumation: The Vari detachment in the Cyclades, Greece: *Geological Magazine*, v. 140, p. 245–252, doi:10.1017/S0016756803007799.
- Ring, U., Will, T., Glodny, J., Kumerics, C., Gessner, K., Thomson, S., Güngör, T., Monié, P., Okrusch, M., and Drüppel, K., 2007, Early exhumation of high-pressure rocks in extrusion wedges: The Cycladic Blueschist Unit in the eastern Aegean, Greece and Turkey: *Tectonics*, v. 26, TC2001, doi:10.1029/2005TC001872, 23 p.
- Ring, U., Glodny, J., Will, T., and Thomson, S., 2010, The Hellenic subduction system: High-pressure metamorphism, exhumation, normal faulting, and large-scale extension: *Annual Review of Earth and Planetary Sciences*, v. 38, p. 45–76, doi:10.1146/annurev.earth.050708.170910.
- Rosenbaum, G., Avigad, D., and Sánchez-Gómez, M., 2002, Coaxial flattening at deep levels of orogenic belts: Evidence from blueschists and eclogites on Syros and Sifnos (Cyclades, Greece): *Journal of Structural Geology*, v. 24, p. 1451–1462, doi:10.1016/S0191-8141(01)00143-2.
- Sanchez-Gomez, J., Avigad, D., and Heimann, A., 2002, Geochronology of clasts in allochthonous Miocene sedimentary sequences on Mykonos and Paros Islands: Implications for backarc extension in the Aegean Sea: *Journal of the Geological Society London*, v. 159, p. 45–60.
- Schliestedt, M., and Matthews, A., 1987, Transformation of blueschist to greenschist facies rocks as a consequence of fluid infiltration, Sifnos (Cyclades), Greece: *Contributions to Mineralogy and Petrology*, v. 97, p. 237–250, doi:10.1007/BF00371243.
- Schliestedt, M., Altherr, R., and Matthews, A., 1987, Evolution of the Cycladic crystalline complex: *Petrology, isotope geochemistry, and geochronology*, in Helgeson, H.C., ed., *Chemical Transport in Metasomatic Processes*: North Atlantic Treaty Organization Advanced Science Institutes Series C, v. 218, p. 389–428.
- Schumacher, J.C., Brady, J.B., Cheney, J.T., and Tonnsen, R.R., 2008, Glaucophane-bearing marbles on Syros, Greece: *Journal of Petrology*, v. 49, p. 1667–1686, doi:10.1093/petrology/egn042.
- Seck, H.A., Kötz, J., Okrusch, M., Seidel, E., and Stosch, H.G., 1996, Geochemistry of a meta-ophiolite suite: An association of metagabbros, eclogites, and glaucophanites on the island of Syros, Greece: *European Journal of Mineralogy*, v. 8, p. 607–623.
- Skarpelis, N., Tsikouras, B., and Pe-Piper, G., 2007, The Miocene igneous rocks in the Basal Unit of Lavrion (SE Attica, Greece): *Petrology and geodynamic implications*: *Geological Magazine*, v. 145, p. 1–15.
- Sölva, H., Thöni, M., Grasemann, B., and Linner, M., 2001, Emplacement of eo-Alpine high-pressure rocks in the Austroalpine Ötztal complex (Texel group, Italy/Austria): *Geodinamica Acta*, v. 14, p. 345–360, doi:10.1016/S0985-3111(01)01072-5.
- Tirel, C., Gueydan, F., Tiberi, C., and Brun, J.P., 2004, Aegean crustal thickness inferred from gravity inversion: *Geodynamical implications*: *Earth and Planetary Science Letters*, v. 228, p. 267–280, doi:10.1016/j.epsl.2004.10.023.
- Tomaschek, F., 2010, *Praktische Aspekte der Mischkristallphase Zirkon: Reequilibrierungsprozess, Zirkon-Xenotim Mischungslücke, geochronologische Anwendungen in einem polymetamorphen Kristallinkomplex (Syros, Kykladen, Griechenland)* [Ph.D. thesis]: Münster, Westfälische Wilhelms-Universität Münster, 431 p.
- Tomaschek, F., Kennedy, A., Keay, S., and Ballhaus, C., 2000a, U/Pb-SHRIMP results for zircons from Syros, Greece: Geochronological constraints on Carboniferous and Triassic magmatic episodes in the Cyclades: *Terra Nostra*, v. 2000, no. 5, p. 58.
- Tomaschek, F., Baumann, A., Villa, I.M., Kennedy, A., and Ballhaus, C., 2000b, Geochronological constraints on a Cretaceous metamorphic event from the Vari Unit (Syros, Cyclades, Greece): *Beihefte zum European Journal of Mineralogy*, v. 12, no. 1, p. 214.
- Tomaschek, F., Kennedy, A.K., Villa, I.M., Lagos, M., and Ballhaus, C., 2003, Zircons from Syros, Cyclades, Greece—Recrystallization and mobilization of zircon during high-pressure metamorphism: *Journal of Petrology*, v. 44, p. 1977–2002, doi:10.1093/petrology/egg067.
- Tomaschek, F., Keiter, M., Kennedy, A.K., and Ballhaus, C., 2008, Pre-Alpine basement within the northern Cycladic Blueschist Unit on Syros Island, Greece: *Zeitschrift der Deutschen Gesellschaft für Geowissenschaften*, v. 159, p. 521–532, doi:10.1127/1860-1804/2008/0159-0521.
- Trotet, F., Jolivet, L., and Vidal, O., 2001a, Tectono-metamorphic evolution of Syros and Sifnos islands (Cyclades, Greece): *Tectonophysics*, v. 338, p. 179–206, doi:10.1016/S0040-1951(01)00138-X.
- Trotet, F., Vidal, O., and Jolivet, L., 2001b, Exhumation of Syros and Sifnos metamorphic rocks (Cyclades, Greece): New constraints on the P-T paths: *European Journal of Mineralogy*, v. 13, p. 901–920, doi:10.1127/0935-1221/2001/0013/0901.
- van Hinsbergen, D.J.J., Langeris, C.G., and Meulenkamp, J.E., 2005, Revision of the timing, magnitude, and distribution of Neogene rotations in the western Aegean region: *Tectonophysics*, v. 396, p. 1–34, doi:10.1016/j.tecto.2004.10.001.
- van Hinsbergen, D.J.J., Dupont-Nivet, G., Nakov, R., Oud, K., and Panaiotu, C., 2008, No significant post-Eocene rotation of the Moesian Platform and Rhodope (Bulgaria): Implications for the kinematic evolution of the Carpathian and Aegean arcs: *Earth and Planetary Science Letters*, v. 273, p. 345–358, doi:10.1016/j.epsl.2008.06.051.
- van Hinsbergen, D.J.J., Dekkers, M.J., Bozkurt, E., and Koopman, M., 2010, Exhumation with a twist: Paleomagnetic constraints on the evolution of the Menderes metamorphic core complex (western Turkey): *Tectonics*, v. 29, TC3009, doi:10.1029/2009TC002596, 33 p.
- von Follon, H., and Goldschmidt, V., 1887, Über die geologischen Verhältnisse der Inseln Syra, Syphnos und Tinos: *Jahrbuch der Geologischen Reichsanstalt Wien*, v. 37, p. 1–34.
- Walcott, C.R., and White, S.H., 1998, Constraints on the kinematics of post-orogenic extension imposed by stretching lineations in the Aegean region: *Tectonophysics*, v. 298, p. 155–175, doi:10.1016/S0040-1951(98)00182-6.
- Whitney, D.L., and Evans, B.W., 2010, Abbreviations for names of rock-forming minerals: *The American Mineralogist*, v. 95, p. 185–187, doi:10.2138/am.2010.3371.
- Wijbrans, J.R., and McDougall, I., 1986, <sup>40</sup>Ar/<sup>39</sup>Ar dating of white micas from an Alpine high-pressure metamorphic belt on Naxos (Greece): The resetting of the argon isotopic system: *Contributions to Mineralogy and Petrology*, v. 93, p. 187–194, doi:10.1007/BF00371320.
- Wijbrans, J.R., Schliestedt, M., and York, D., 1990, Single grain argon laser probe dating of phengites from the blueschist to greenschist transition on Sifnos (Cyclades, Greece): *Contributions to Mineralogy and Petrology*, v. 104, p. 582–593, doi:10.1007/BF00306666.
- Xypolias, P., Kokkalas, S., and Skourlis, K., 2003, Upward extrusion and subsequent transpression as a possible mechanism for exhumation of HP/LT rocks in Evia Island (Aegean Sea, Greece): *Journal of Geodynamics*, v. 35, p. 303–332, doi:10.1016/S0264-3707(02)00131-X.
- Ziv, A., Katzir, Y., Avigad, D., and Garfunkel, Z., 2010, Strain development and kinematic significance of the Alpine folding on Andros (western Cyclades, Greece): *Tectonophysics*, v. 488, p. 248–255, doi:10.1016/j.tecto.2009.07.002.



*Syros Island, in the heart of the Cycladic archipelago, has been a key area for the study of high-pressure rocks throughout the last decades. Excellently preserved blueschist- to eclogite-facies lithologies offer a unique opportunity to study processes of burial and exhumation in a young orogen. The authors present a new, highly detailed geological map of Syros and review the current state of research concerning this interesting island.*

## Contents

*Acknowledgments*

*Abstract*

*Chapter 1: Introduction*

*Chapter 2: General Petrography  
of Mapped Lithological Units*

*Chapter 3: Lithostratigraphy and Indications  
for Primary Associations in the  
Cycladic Blueschist Unit on Syros*

*Chapter 4: Structural Evolution of  
the Cycladic Blueschist Unit—  
The Example of Syros*

*Chapter 5: Concluding Remarks*

*References Cited*



3300 Penrose Place ■ P.O. Box 9140  
Boulder, CO 80301-9140, USA

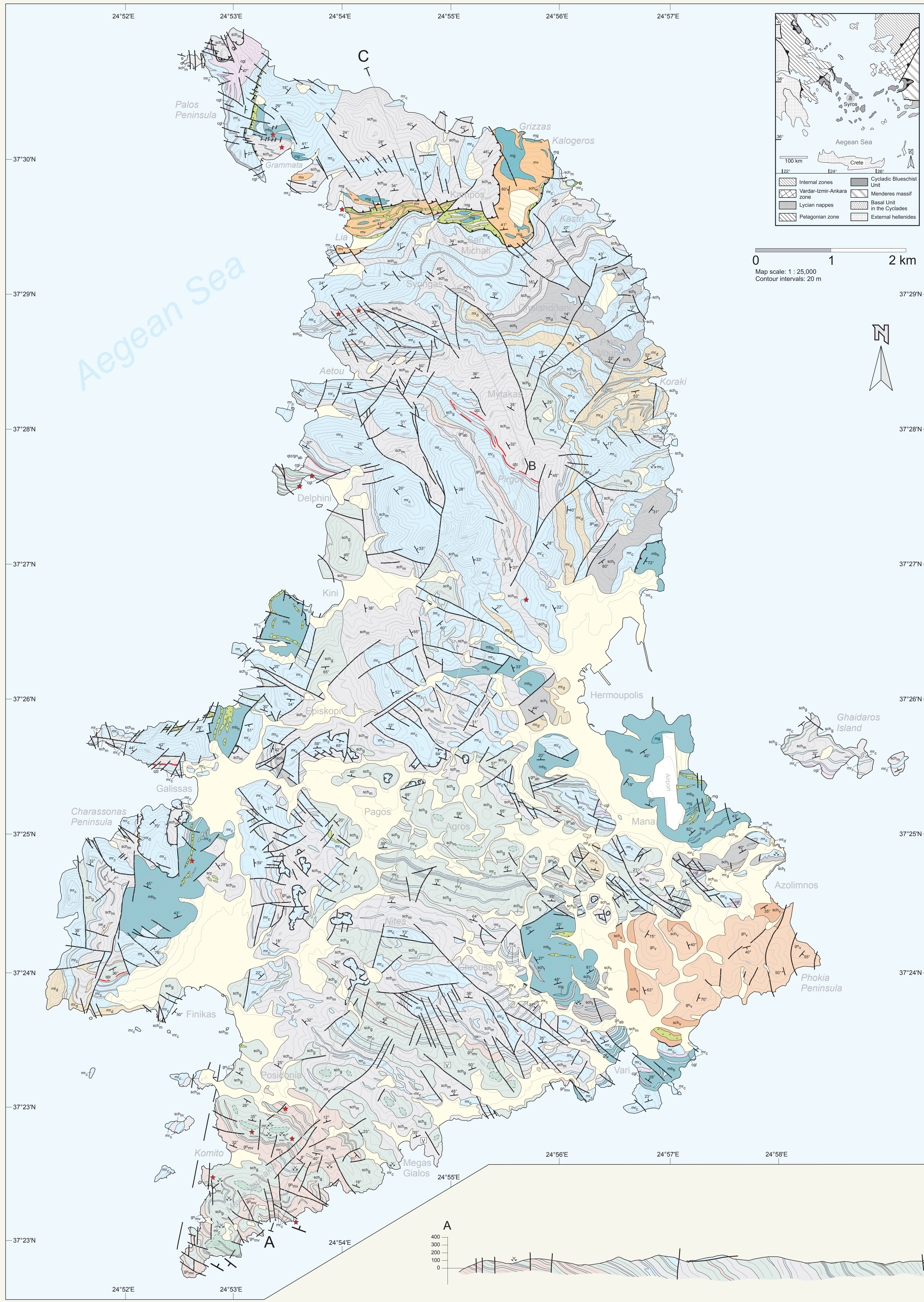
ISBN 978-0-8137-2481-2



9 780813 724812

# Geological map of Syros Island (Cyclades, Greece)

## 1:25,000

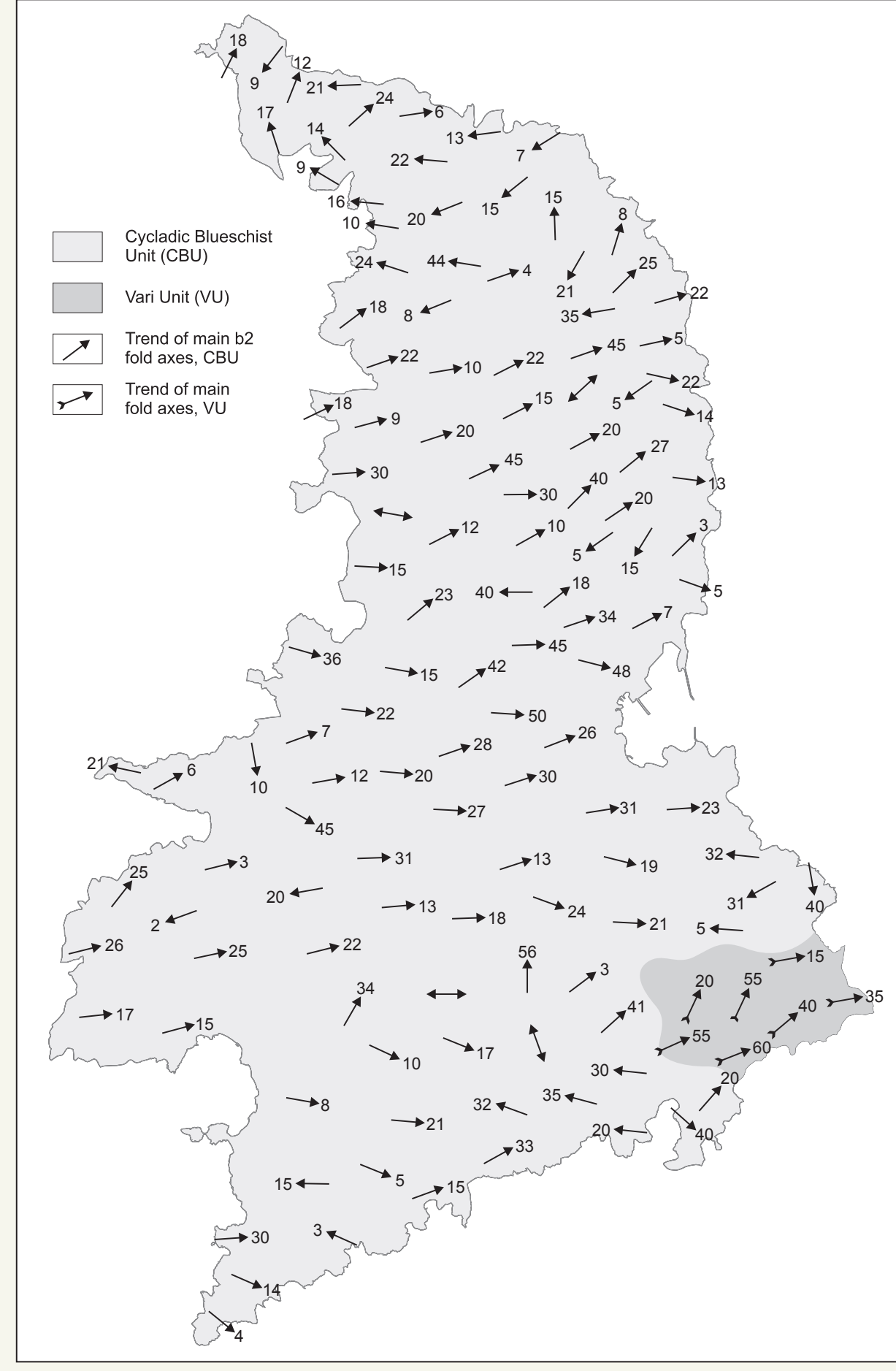
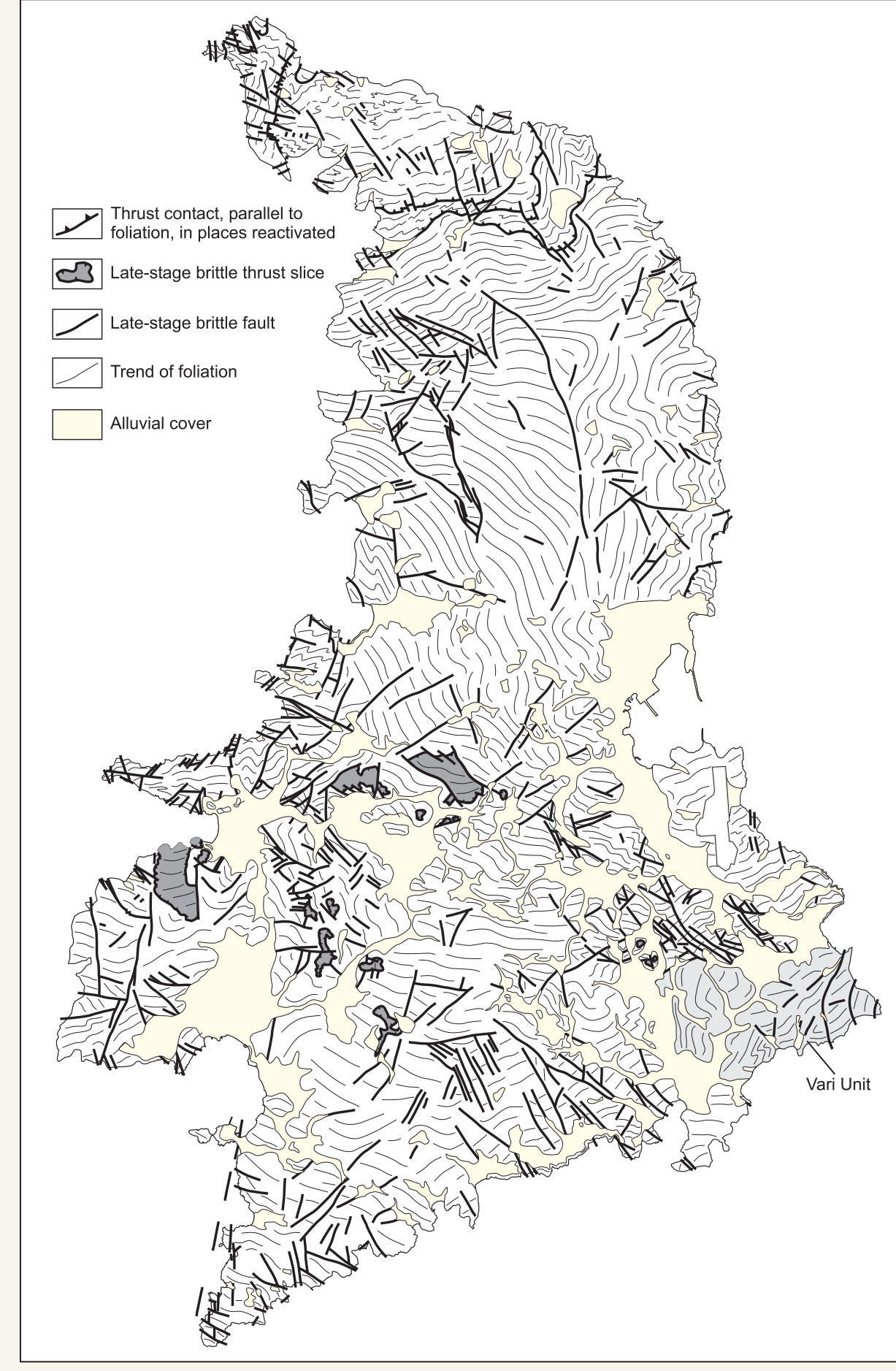
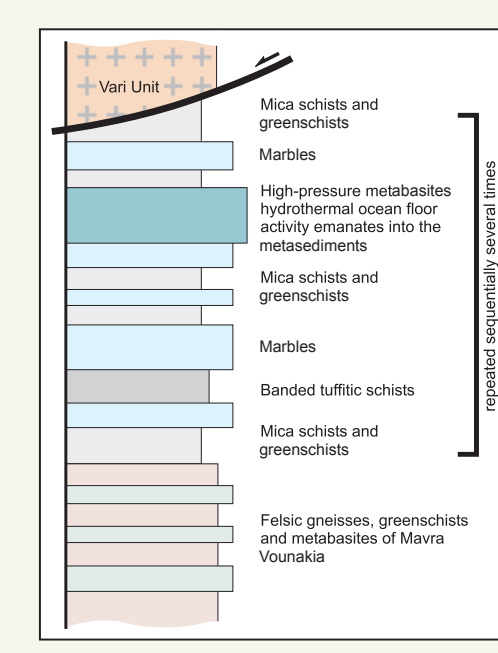


### Cycladic Blueschist Unit

- mc<sub>1</sub>** **Calcite marble.** Laminated to massive, medium- to coarse-grained light gray to blue-gray, with frequent intercalations of impure phengite-glaucophane-clinozoisite-quartz-bearing marbles, locally calcilicatic. In places matrix-supported mononitic conglomerate horizons with calcite clasts in carbonatic matrix, becoming frequent near contacts with schist units. Frequency and thickness of marble units decrease toward the south. Intrafolial folds on the dm- to m-scale and retrograde columnar calcite pseudomorphs after aragonite are in places well preserved. Surficial karst is common, sometimes so intense that interal fabrics are obscured.
- mc<sub>2</sub>** **Dolomitic marble.** Brownish-gray to yellowish dolomite alternating with calcite marble on the cm- to dm-scale, mapped as dolomitic marble where dolomite component exceeds an estimated 20 percent. More massive dolomite units lack internal foliation and tend to form s-parallel megaboudins in ductile calcite marble up to several hundred m in length.
- sch<sub>1</sub>** **Metasedimentary mica schist.** Foliated phengite-paragonite-quartz-glaucophane-garnet-epidote gray to bluish gray clastic metasediments, with frequent quartz segregations parallel to the s<sub>2</sub> cleavage. Minor intercalations of mafic glaucophane-paragonite-epidote-sphene-calcite blueschists, locally with static epidote-phengite-chlorite/garnet-calcite-quartz pseudomorphs after lawsonite. Toward the south, static selective to pervasive retrograde chlorite-actinolite-albite greenschist facies overprint becomes more common. Likely protoliths were graywackes and psammites with occasional mafic tuffitic intercalations. Genuine metapelite compositions appear to be rare or obscured by sodic metasomatism.
- mp** **Metaconglomerate.** Mostly mononitic conglomeratic layers with matrix-supported calcite clasts in a foliated impure calcite to calcilicatic (calcite-phengite-quartz) matrix. Clasts range in size from mm up to several cm. Metaconglomerate units form a few m thick, laterally discontinuous layers and lenses, situated preferentially at the base of marble units in contact with mica schists, indicating possible primary stratigraphic relations. On Palos peninsula, distinctly polymict metaconglomerates several hundred m in thickness, with clasts of calcite, phengitic schist, metabasite, and occasional Mn-rich piemontite (former hydrothermal ocean-floor sediment) occur. Locally, metaconglomerates grade into massive, poorly foliated and highly resistant clast-free calcite-quartz epidote-phengite calcilicatic felses.
- sch<sub>2</sub>** **Banded tuffitic schists.** Mafic glaucophane-garnet-omphacite-clinozoisite-ankerite layers alternating on a cm- to dm-scale with felsic layers composed of paragonite-quartz-clinozoisite-glaucophane-garnet and albite-actinolite-hornblende pseudomorphs after omphacite and jadeite. Occurrences at Azolimnos and Hermoupolis show well preserved blueschist-facies assemblages, while near Chalandriani and Galissas retrograde overprint is stronger.
- sp<sub>1</sub>** **Albitic garnet-bearing paragneiss.** Light gray to white, coarse-grained, foliated quartz-albite-paragonite-clinozoisite lithologies with gneissic fabric, in places with cm-sized garnet porphyroblasts. Lateral and vertical gradations into quartzite. Likely protoliths are psammitic arkosic layers in graywacke units.
- qtz** **Quartzite.** Resistant, up to several m thick albite-bearing quartzite, locally with reddish or greenish colour, cm-sized garnet porphyroblasts, and frequent, dm-sized intrafolial folds. Quartzite layers occur both inside schist and albitic gneiss units, and occasionally with metabasite. Lateral continuity typically no more than a few tens of m, in some instances (e.g., Mytakas) up to a few hundred m. Laterally grading into albitic gneiss.
- sch<sub>3</sub>** **Greenschists and epidote schists.** Schists more strongly overprinted by greenschist-facies metamorphism show the assemblage epidote-glaucophane and/or chlorite-albite, depending on the grade of overprint. Darker green shading indicates possible metavolcanics, i.e., epidotes with pillowlike structures.

**Petrological history of the Cycladic Blueschist Unit:**  
 Protolith age of oceanic fragments: ~80 Ma.  
 Age of blueschist- to eclogite facies metamorphism (M1): ~52 Ma.  
 Age of greenschist overprint (M2): 25-18 Ma.

**Petrological history of the Vari Unit:**  
 Protolith age of orthogneiss: 244-240 Ma.  
 Age of epidote-amphibolite facies metamorphism: 100-95 Ma.  
 Peripheral schists of the Vari Unit probably represent a Miocene shear zone.



### Vari Unit

- sp<sub>1</sub>** **Gneisses of Vari.** Predominantly albite+phengite+epidote+quartz (magnetite-ilmenite-titanite-potassic feldspar) trondhjemitic orthogneisses, locally with apatite veins. A granulite variety (e.g., on Phokia Peninsula, shows the assemblage hornblende (paragite) hornblende+albite+epidote+phengite+quartz (ilmenite-ilmenite)). A steep cleavage, superimposing on the gneiss an L-tectonic fabric. Peripheral parts of the gneiss are in places intercalated with slices of mica schist, amphibolite, and carbonate up to a few m in length (possible relicts of original country rocks). Possible intrusive contacts, i.e., apatite veins interfolded with amphibolite, are preserved south of Azolimnos. Along fractures, faults, and toward its margins, the gneiss may be retrogressed to greenschist-chlorite-epidote-actinolite-bearing varieties.
- sch<sub>3</sub>** **Mylonitic chlorite schists of the Vari Unit.** Mafic mylonitic schists and phyllites. Main assemblage is chlorite, actinolite, albite, clinozoisite and white mica. In places, with intercalations of massive or cumulated serpentinite.

The Vari unit, i.e., gneiss proper and its mylonitic margin, is likely to form part of the Cycladic Upper Unit. Amphibole chemistry suggests epidote-amphibolite facies metamorphism, with the paragneiss hornblende+albite+epidote+garnet in mafic lithologies within the gneiss. Evidence that the gneiss was affected by the Eocene high-pressure metamorphism, i.e., jadeite relicts or albite pseudomorphs after jadeite-quartz (common in felsic lithologies of the high-pressure units), is lacking. Contacts with high-pressure units are covered by alluvium or controlled by steep, late-stage brittle faults.

### Unmetamorphosed rocks

- iv** **Andesitic intrusives.** Unmetamorphosed, fine-grained andesitic or latitic dikes.
- ac** **Alluvial cover.** Undifferentiated; coastal deposits, sands, gravel, caliche and debris.
- gb** Geological boundary
- fd** Strike and dip of foliation
- ft** Late-stage brittle fault
- fto** Prograde, foliation-parallel thrust fault, in places showing brittle overprint
- ftt** Late-stage brittle thrust fault
- abp** Abandoned ore pit

